T&J

THAI GEOSCIENCE JOURNAL

THAI
GEOSCIENCE
JOURNAL

FIRST ISSUE

THAI GEOSCIENCE JOURNAL

MISTLETOE

TURNBERRY

570

1660000 mN

J3

B1

J6

J1

J4

J7

On the cover

1. A) *Thailandium solum* Kobayashi,1957 cranidia from Ko Tarutao at Ao Mo Lae (*Shelly J. Wernette* et al., p.72)
   B) Landmark Scheme of *Prosaukia* and *Thailandium* (*Shelly J. Wernette* et al., p.68)
2. Quartzofeldspathic garnet mica schist showing foliated texture (*Sirot Salyapongse* et al., p.34)
3. Field photograph of the Hua Na Kham Formation and the Khao Pa Khi Limestone (*Shikeki Hada* et al., p.10)
4. ASTER regolith-landform map of the Gnaweeda Greenstone Belt, Western Australia (*Siriporn Soongpankhao*, p.87)
5. Location and topography of study area, Banrai, Uthai Thani (*Apsorn Sardsud* et al., p.18)

THAI GEOSCIENCE JOURNAL

Vol.1 No.1 (First Issue)
July-December 2020

Preface

On behalf of the Department of Mineral Resources and the Geological Society of Thailand, it is my pleasure to support and publish the Thai Geoscience Journal (TGJ). The Thai Geoscience Journal (TGJ) is established by cooperation between the Department of Mineral Resources of Thailand and the Geological Society of Thailand in order to enhance research in all the many areas of geoscience. Thai Geoscience Journal (TGJ) continues publication from the former Journal of the Geological Society of Thailand (GST) the last volume of which was published in 2015. I congratulate TGJ for the First Issue to be released in July 2020.

This TGJ publication is an international peer reviewed, open access and online journal publishing original research articles in English and Thai that focuses in various subjects in geosciences, geo-environments, geo-hazards, and their related research in every area in the world. We warmly welcome all Thai and foreign scientists, geoscience and related researchers, to publish their valuable articles in the Journal free of charge.

We sincerely hope that this first issue will provide valuable geoscience knowledge and information, and will inspire readers and researchers to produce highly valued research in the future. Finally, we are pleased to invite geologists, scientists and researchers to publish in our TGJ.

Thank you very much.

(Dr. Sommai Techawan)
Director-General of Department of Mineral Resources
President of Geological Society of Thailand

From the editor

Welcome to the Thai Geoscience Journal (TGJ). This an online and print-off journal that discusses topics related to all areas of geoscience focusing on sedimentology and geomorphology, palaeontology, quaternary geology and environmental change, geological hazards, environmental geosciences, geophysics, mineral and petroleum geology, tectonics and structural geology, geochemistry and geochronology, metamorphic geology and volcanic and igneous geology. Articles in TGJ are peer-reviewed by geoscience specialists and academics from worldwide organizations. The success of the first issue of TGJ clearly reveals the international cooperation of geoscience society.

As the Editor-in-Chief of the TGJ, I would like to express our sincere thanks to authors who have chosen TGJ to publish their researches. Furthermore, the first issue would not have been possible without the great support from honorary editors, advisory editors, associate editors, and other editorial secretary teams for their work supporting the success of the first issue. We hope to receive more valuable articles from geologists, scientists, researchers, scholars, and practitioners for publication in the next issue in January 2021.

Finally, I would like to dedicate the first issue of TGJ and express deep condolences for the passing away of Department of Mineral Resources' former geologists, Dr. Sangad Bunopas (in July 2020), who is the most famous and important Thai geologist who established Shan-Thai and Indochina micro-continents for tectonics and the geology of Thailand and Dr. Somboon Khosithanont (in September 2019), one of our executive advisors and one of the authors in this first issue.

Thank you very much.

(Dr. Apsorn Sardsud)
Editor-in-Chief
Thai Geoscience Journal

LIST OF CONTENTS

A remarkable end-Permian boulder bed of conglomeratic limestone at Nam Nao in NE Thailand: its biostratigraphical and environmental significance

Shigeki Hada[1*], Somboon Khosithanont[2] and Hiroya Goto[3]
[1]Soemon-cho 1-8, Chuo-ku, Osaka 542-0084, Japan.
[2]Department of Mineral Resources of Thailand, RamaVI Rd.,
Ratchathewi, Bangkok, 10400, Thailand.
[3]Domoto 380-4, Tatsuno-cho, Tatsuno 679-4129, Hyogo, Japan.
*Corresponding author: s.hada@aloha.zaq.jp

Abstract

Litho- and bio-stratigraphic analyses on the Lower Permian Khao Pa Khi and Middle-Upper Permian Khao Tham Yai limestones, and the siliciclastic Hua Na Kham Formation on clastic-dominant continental shelves in the western margin of the Indochina Block record important aspects of the extinction-related Guadalupian-Lopingian (G-LB) interval, and a large-scale sea-level drop of a global environmental change in the low-latitudes of the East Paleo-Tethys. Fusulinid and foraminifer species within the Khao Tham Yai Limestone record the abrupt disappearance of large-tested fusulines. The Khao Tham Yai Limestone above the G-LB is characterized by the sudden flourishing of a diverse range of smaller fusulinid and foraminifer species, together with the occurrence of a large number of broken fragments of diverse large-tested fusulinids. The second disappearance of smaller foraminifers occurred during the Wuchiapingian in the upper part of the Khao Tham Yai Limestone. These two phases of disappearance of fusulinid and foraminifer species on the continental margin of the Indochina Block likely appeared a little late compared to similar phases in the paleo-atolls of the mid-Panthalassa. The Wuchiapingian Hua Na Kham Formation unconformably onlaps the Khao Tham Yai Limestone replacing previous carbonate formation. These carbonate and siliciclastic formations are largely heteropic facies and possibly interfinger with each other. A remarkable boulder bed of fusulinids and conglomeratic limestones occurs on the top of the Hua Na Kham Formation. Fusulinid and foraminifer species in boulders indicate that they were eroded off the Khao Tham Yai barrier reef and transported by submarine debris flows that brought them to sites on the continental shelf where the Hua Na Kham Formation deposited. Such catastrophic events may have been caused by large-scale eustatic sea-level drop. The effects of this global environmental change on the continental margin of the Indochina Block may have occurred a little later in the Wuchiapingian compared with subaerial exposure and erosion reported from the G-LB interval in mid-oceanic seamounts that occur in mid-Panthalassa.

Key words: boulder bed of limestone, foraminifer species, Indochina Block, sea level drop, Upper Permian

1. Introduction

Since 2005, we have been carrying out geological and paleontological studies on a karstic mountain in Khao Tham Yai (Hill of the Large Cave), about 30 km NW of Nam Nao in eastern Phetchabun Province, NE Thailand in collaboration with the Department of Mineral Resources, Thailand. From a regional tectonic perspective, our research area is located along the western margin of the Indochina Block (Fig. 1). We have already published parts of a biostratigraphic investigation concentrating on the evolution and extinction of a Middle and Upper Permian fusulinid and foraminifer fauna from a single limestone unit named the Khao Tham Yai Limestone in the Nam Nao district (Hada et al., 2015). We have clarified the following aspects of evolutionary and extinction patterns of fusulinid species in the shallow-water Paleo-Tethyan shelf area in the western margin of the Indochina Block.
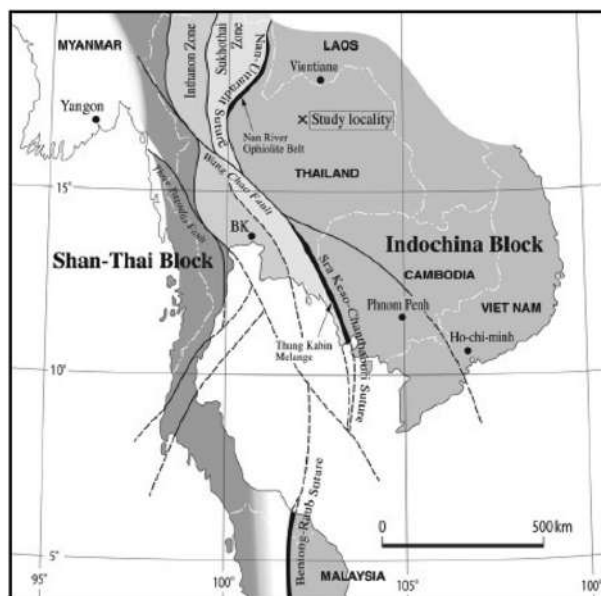
Figure 1: Index map showing the study locality and the tectonic subdivisions of Thailand and adjacent regions (Hada et al., 2015).

(1) The Khao Tham Yai Limestone ranges from the Wordian (middle Middle Permian) up to the Wuchiapingian (lower Upper Permian). The existence of the Wuchiapingian within a single continuous limestone section rangingfrom Middle to Upper Permian is confirmed for the first time in Thailand.

(2) Three fusulinid zones are differentiated in the Khao Tham Yai Limestone namely; *Colania, Lepidolina* and *Codonofusiella* zones in ascending order.

(3) Shell sizes of the fusulinid species in the *Lepidolina* Zone display continuous rapid morphological change along a one-way evolutionary path from small, primitive species with simple structure to large, highly evolved species having a complicated wall structure.

(4) The G-LB between the Guadalupian (Middle Permian) and Lopingian (Upper Permian) within the Khao Tham Yai Limestone is clearly defined as the boundary of the abrupt change in the fusulinid assemblages from the elimination of large-tested Verbeekinids and Schwagerinids to the domination of small-shelled Schubertellids with simple wall structure that underwent slower evolutionary morphological change than earlier fusulinids and persisted and expanded in the Wuchiapingian.

(5) Even smaller fusulinids abruptly become extinct near the top of the Khao Tham Yai Limestone during the Wuchiapingian.

(6) Eventually, clastic sediments unconformably onlap (abut) the Khao Tham Yai Limestone characterized by algae-foraminifera biota.

In this paper, we particularly provide details of our recent study on the Upper Permian siliciclastic formation onlapping the Khao Tham Yai Limestone and on a newly found boulder bed of fossiliferous and conglomeratic limestones on the top of the siliciclastic sequence focusing on a great variety of the fusulinid and foraminifer species identified from boulders, and their characteristic occurrence. In relation to this new data, the aim of this paper is also to reanalyze the biostratigraphic investigation of the smaller fusulinid and foraminifer species above the G-LB with special reference to remarkable facies change in the Khao Tham Yai Limestone.

2. Tectonic and geologic setting

Recently, Ridd et al. (2011) presented the widely available book entitled The Geology of Thailand in the English language that attempts to cover the wide range of Thai Geology. In this book Ueno and Charoentitirat (2011) provide an especially useful attempt to comprehensively review the Carboniferous and Permian systems of Thailand. They make great efforts to sort out the informal naming of many stratigraphic units based on available paleontological data that provide critical chronostratigraphic constraints. Following their synthesis, we firstly attempt to readjust the stratigraphic and geotectonic data presented by Hada et al. (2015), then move to the main issue.

Since the epoch-making proposal by Bunopas (1981), Thailand has come to be understood as being fundamentally comprised of two distinct continental blocks; the Indochina Block, which is regarded as a Cathaysian domain to the east and the Shan-Thai Block, which is a Gondwana-derived block associated with the eastern Cimmerian Continent to the west (Fig. 1).

The Indochina Continental Block is delineated to the west by the Nan Suture Zone (Nan-Uttaradit Suture in Fig.1) (Figs.1 and 2). The suture zone contains remnants of a now closed back-arc basin that once existed in the

western flank of the Indochina Block (Ueno and Hisada, 2001). Upper Triassic red beds with red chert pebbles that yield Middle Triassic radiolarians disconformably overlies the serpentinite mélange of the Nan Suture Zone in the Nan Mine, N Thailand. This indicates that the back-arc basin closed during Late Triassic time (Hada et al., 1999). Red chert is an important constituent element of the back-arc basin (marginal sea) that opened in the Permian and closed in the Triassic.

Another enigmatic aspect of the Indochina Block is the origins of the Nam Duk Basin. This basin along the western margin of the Indochina Block separates the Pha Nok Khao Platform to the east from the Khao Khwang Platform to the west (Fig. 2). It has been variously interpreted as the Indosinian collisional orogen, the Loei Fold Belt (Helmcke and Lindenberg, 1983; Helmcke, 1994) or a suture, the Loei Suture (Chutakosit-kanon et al., 1999; Charusiri et al., 2002). Charusiri et al., (2002) suggested that it represents a suture zone based on the existence of older rocks ranging from Upper Silurian to Cretaceous including radiolarian chert as well as basic and ultrabasic igneous rocks, which represent scraped-off ocean-floor rocks. It extends from Loei to the east of the Nam Duk Basin. However, the Loei Suture is still the subject of much debate.

The Nam Duk Formation in the Nam Duk Basin is composed of siliciclastic dominant strata and has also been the subject of many studies in the context of the geotectonic evolution of Thailand. It has long been believed that the formation represents a typical pelagic flysch-molasse succession corresponding to pre-, syn- and post-orogenic stages of an 'Indosinian' collisional orogeny based on the classic 'geosynclinal model' (Loei Fold Belt) (Helmcke and Lindenberg, 1983; Helmcke, 1994). However, it is hard to draw any conclusions in the context of the formation's orogenic development in the view of the incomplete understanding of the stratigraphy and stratigraphic relations between the Nam Duk Formation and surrounding formations (Ueno and Charoentitirat, 2011). Evidence for the existence of a molasse sequence is also questionable. Ueno and Charoentitirat (2011) interpreted the Nam Duk Basin as an intracra tonic depression between two shallow platform
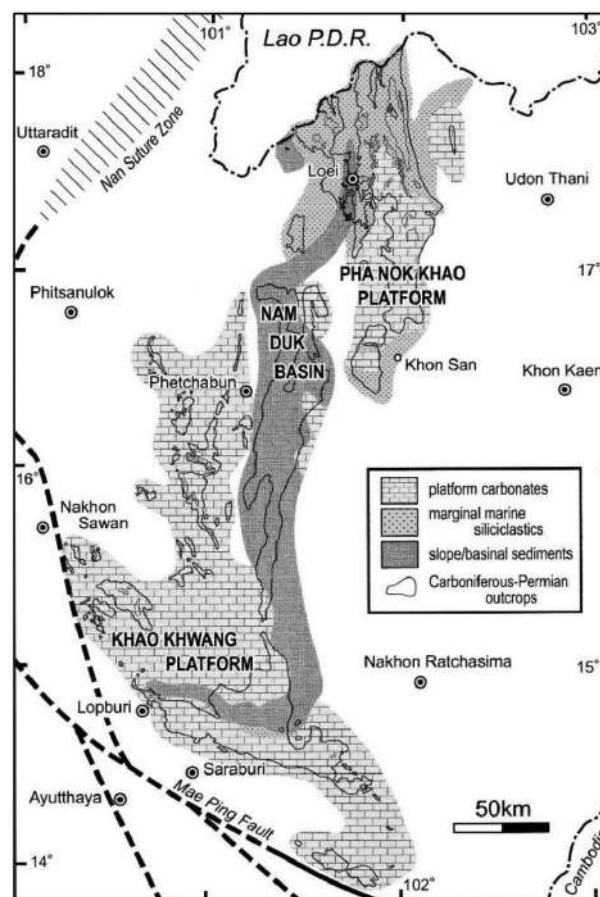
Figure 2: Major facies subdivisions for Late Paleozoic rocks on the western margin of the Indochina Block (Wielchowsky and Young, 1985; Ueno and Charoentitirat, 2011).

areas on the margin of the Indochina Block and reported that the strata of the Nam Duk Basin are dominated by Permian slope-to-basin sediments and pre-dominantly consist of turbidites. We suggest that the Loei Suture is not a suture between two microcontinents inside the Indo china Block, nor is Loei Fold Belt a collisional orogeny. Rather it possibly originated as an intraplate strike-slip deformation belt, and the Nam Duk Basin is a basin related to intraplate strike-slip deformation. The northern extension of the Loei Suture or the Nam Duk Basin is largely concealed by Mesozoic sediments thus relations to the Nan Suture Zone remain unclear (Fig. 2).

Ueno and Charoentitirat (2011) formally introduced the term Loei Group for a succession of carbonate and siliciclastic Pennsylvanian-Permian strata associated with the Pha Nok Khao Platform on the eastern side of the Nam Duk Basin. In the southern part of Loei, this group is composed of the siliciclastic Huai Som

(mostly Pennsylvanian), carbonate Pha Nok Khao (mainly Lower-Middle Permian) and siliciclastic Hua Na Kham (younger Permian) formations (Chonglakmani and Sattayarak, 1984).

The Khao Tham Yai Limestone (Hada et al., 2015) is extensively exposed in the Nam Nao district in NE Thailand and is assigned to the carbonate Pha Nok Khao Formation of the Loei Group on the Pha Nok Khao Platform. Fontaine and Salyapongse (2001) and Fontaine et al. (2002) first showed that the Khao Tham Yai Limestone ranges from Murgabian (middle Middle Permian) to the top of Median (upper Middle Permian). Later Hada et al. (2015) proved the age of the Khao Tham Yai Limestone extends to the Upper Permian (Wuchiapingian).

Fontaine and Salyapongse (2001) and Fontaine et al. (2002) reported a siliciclastic succession in the valley on the eastern side of the Khao Tham Yai Limestone. It appears to stratigraphically overlie the Khao Tham Yai Limestone. Although, it was previously assigned to the Nam Duk Formation, it bears similarity to the siliciclastic Hua Na Kham Formation of the Loei Group as noted by Ueno and Charoentitirat (2011).

Fontaine and Salyapongse (2001) also made a reference to the Khao Pa Khi Limestone that is in direct contact with the Hua Na Kham Formation. It is sparsely fossiliferous and was once regarded as Triassic, whereas Fontaine et al. (2002) later tentatively considered a Permian age. We recently found Lower Permian fusulinid species in the massive Khao Pa Khi Limestone and it is confirmed as Lower Permian (see below).

In the following, we describe the fusulinid and foraminifer species, and the relevant facies change of the Khao Tham Yai and Khao Pa Khi limestones of the Pha Nok Khao Formation of the Loei Group, and the boulder bed of fossiliferous and conglomeratic limestones at the top of the siliciclastic Hua Na Kham Formation of the Loei Group, which are distributed in the Pha Nok Khao Platform on the eastern side of the Nam Duk Basin on the western flank of the Indochina Block.

3. Lithology and fossils below the G-LB within the Khao Tham Yai Limestone of the Pha Nok Khao Formation, Loei Group

This limestone sequence which is exposed extensively in the Nam Nao district, which has been regionally included in the Lower to Middle Permian Pha Nok Khao Formation of the Loei Group and is termed the Khao Tham Yai Limestone (Hada et al., 2015). We previously redefined the range of the Pha Nok Khao Formation from the Lower to Upper Permian on the basis of biostratigraphic data (Hada et al., 2015). Strata of the formation include carbonate materials that accumulated *in situ* on the shallow-water, low-latitude Paleo-Tethyan shelf area within the western margin of the Indochina Block.

The Khao Tham Yai Limestone crops out as a very large, elongated, N-S trending limestone hill about 10 km long in the Nam Nao National Park in NE Thailand. It is well exposed on steep slopes, cliffs and the crest of the limestone hill in the Nam Nao district, and forms a continuous, near homoclinal section estimated to be ca. 1700 m thick (Fig. 3). It strikes NNW-SSE to NW-SE and dips moderately to the east (Fig. 4). We subdivided the Khao Tham Yai Limestone into the Lower, Middle and Upper members (Hada et al., 2015). Figure 5 shows a composite stratigraphic column and fusuline distribution of the upper part of the Lower Member and the Middle and Upper members of the Khao Tham Yai Limestone (Hada et al., 2015). Fontaine et al. (2002) has divided the Khao Tham Yai Limestone into 8 horizons from the western side (base) to the eastern side (top) of the hill. Lower, Middle and Upper members of the Khao Tham Yai Limestone approximately correspond to their horizons 1 to 4, 5 to 7 and 8, respectively.

First, provide a summary of the limestone focusing on the evolutionary and extinction patterns of the larger fusulinid species of the Lower and Middle members of the Khao Tham Yai Limestone based on the findings of Hada et al. (2015)

3.1 Lower Member

The Lower Member is further subdivided into Units 1 and 2 in ascending order that correspond to the horizons 1 and 2, and 3 and 4 of Fontaine et al. (2002). Unit 1 is difficult to study because of widespread and dense tropical vegetation. Horizon 1 is also not rich in fossils and contains scattered corals that are not well preserved and commonly destroyed by recrystallization. The limestone of Horizon 2 is packstone containing algae, smaller

Figure 3: Field photograph of the Khao Tham Yai Limestone. The Limestone forms a continuous, near homoclinal section striking NNW-SSE to NW-SE and moderately dipping eastward.
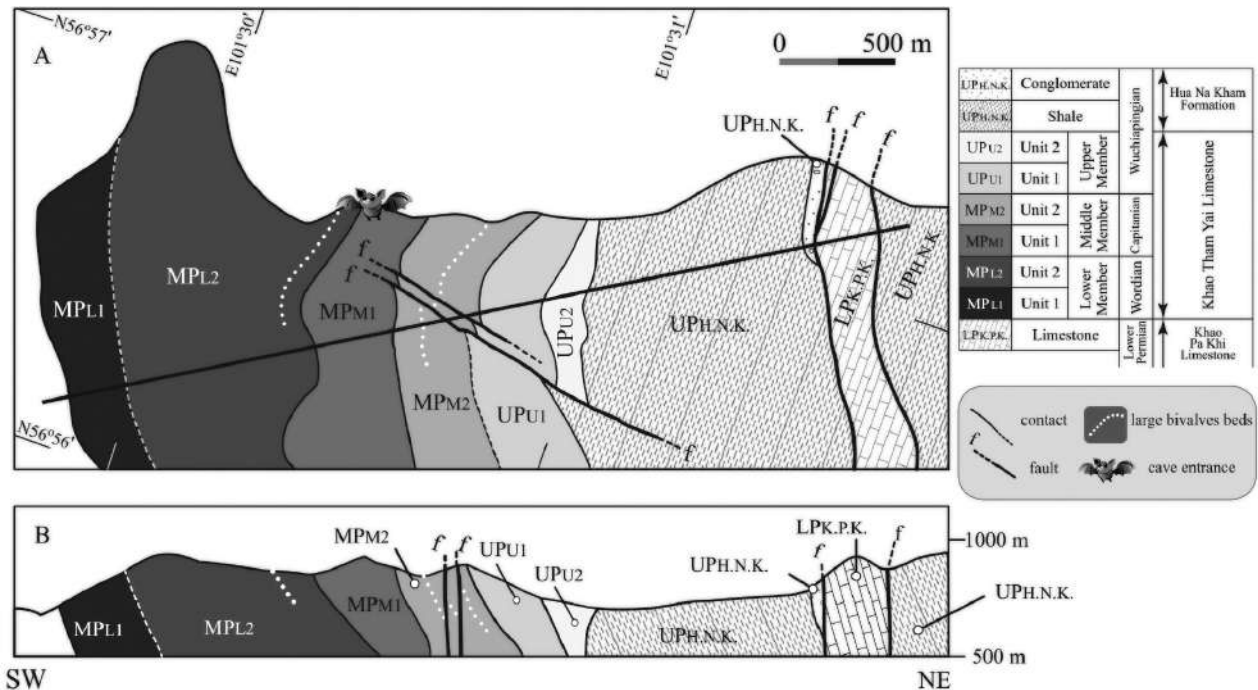
Figure 4. Geologic map (A) and structural cross-section (B) across the Khao Tham Yai Limestone, Hua Na Kham Formation and Khao Pa Khi Limestone in the Nam Nao district, NE Thailand.

foraminifers, abundant massive corals, bryozoans, and rarely brachiopod. Fusulinid fossils are extremely rare (Fontaine et al., 2002).

Unit 2 consists of mostly massive, dark gray limestone, commonly packstone rich in diverse fossils such as large fusulinids like *Colania douvillei* (Ozawa), smaller foraminifers, algae, and large bivalves (Alatconchidae), but corals are rare (Fontaine et al., 2002; Hada et al., 2015). *Colania douvillei,* which is prolific in some beds constitutes a transitional group between *Cancellina* and *Lepidolina* in phylogenic lineage; i.e., *Misellina-Cancellina-Colania-Lepidolina*

evolutionary lineage (Ozawa, 1970). It occurs widely across SE Asia embracing Laos, Viet Nam, Thailand and Peninsula Malaysia. It is a typical fusulinid species of the Wordian (middle Middle Permian) of the *Colania* Zone in the Tethyan Province (e.g. Ozawa, 1970; Ota, 1977; Ingavat et al., 1980).

3.2. Middle Member

The Middle Member consists of massive to poorly bedded, black limestone and thick-bedded dark gray limestone, commonly packstone and grainstone. It locally contains nodular or layered

chert. This member is further subdivided into Units 1 and 2 in ascending order (Hada et al., 2015) that approximately correspond to the horizons 5 and 6, and 7 of Fontaine at al. (2002), respectively. The limestone contains abundant, diverse fossils consisting of fusulinids including abundant large fusulinid species, smaller foraminifers, calcareous algae, crinoids, brachiopods, bivalves that include extraordinarily large bivalves (Alatoconchidae), bryozoans and rare fragments of corals.

Unit 1 of the Middle Member is particularly characterized by *Lepidolina asiatica* (Ishii) and *L. columbian*a (Dawson). *L. asiatica* occurs in SE Asia including eastern Peninsular Malaysia (Jengka Pass and Pahang) and western Cambodia (Sisophon). It belongs to the primitive species of the genus *Lepidolina* that may most likely be evolved directly from *Colania douvillei* (Ishii, 1966). Although *L. columbiana* was originally reported as the genus *Yabeina* from the Cache Creek Terrane of British Columbia, Canada (Ross, 1995). Goto et al., (1986) have described it under the genus *Lepidolina* on the basis of a statistical study of specimens. Limestones of the Cache Creek Terrane formed at low-latitude in mid-Panthalassa and were later tectonically accreted to North America (Ross, 1995). *L. columbiana* is sometimes included in *L. asiatica* (ex. Rui, 1983), our specimens in Unit 1 are here referred to as more evolved, larger forms of *L. asiatica* on the basis of prolocular diameter as described by Goto et al. (1986). *L. columbiana* has been found in eastern Thailand, western Cambodia and eastern Peninsular Malaysia in SE Asia.

Unit 2 of the Middle Member is specifically characterized by *L. multiseptata shiraiwensis* (Ozawa) in the lower part, *L. multiseptata multiseptata* (Deprat) in the upper part, and *Lepidolina kumaensis* Kanmera in the top (Fig. 5). These fusulinids of the genus *Lepidolina* widely occur in the Middle Permian limestones of SE Asia including eastern Thailand, western Cambodia, Viet Nam, Laos and eastern Peninsular Malaysia. These are the characteristic species of limestones not only in the continental blocks like the Indochina and South China blocks, which were distributed in low-latitudes of the eastern Paleo-Tethys in Middle Permian time (Domeier and Torsvik, 2014) (Fig. 6), but also those of the circum-Pacific region. The latter are species occurring in the accretionary complexes

originated on paleo-atolls surrounding paleo-seamounts in mid-Panthalassa such as the Cache Creek Terrane of British Columbia, Canada (Ross, 1995) and the Akiyoshi Terrane of Japan (Sano and Kanmera, 1991). Based on this evidence, Hada et al. (1996) proposed the mid-Permian *Colania-Lepidolina* Territory of the *Colania-Lepidolina* lineage in the paleo-equatorial area of East Paleo-Tethys and mid-Panthalassa. It is worth noting that distribution of *Colania* and *Lepidolina* is limited to the East Paleo-Tethys and Pan-thalassa region. Hada et al. (1996) also proposed another territory the mid-Permian *Neoschwagerina-Yabeina* Territory of the *Neoschwagerina-Yabeina* lineage on the southern side of the *Colania-Lepidolina* Territory at low-latitudes in the East Paleo-Tethys and mid-Panthalassa in the Southern Hemisphere. The habitat of *Neoschwagerina-Yabeina* stock characterizing the Sibumasu (Shan-Thai) Block is apparently different from that of the *Colania - Lepidolina* lineage (Ishii et al., 1985).

Unit 2 of the Middle Member also includes a layer with broken fragments of extra-ordinarily large Alatoconchidae bivalves. Isozaki and Aljinovic (2009) confirmed that Alatoconchidae are characterized by their co-occurrence with typical Tethyan faunal assemblages that include large-tested fusulinids. They also concluded that the distribution of Alatoconchidae was restricted to low-latitude (tropical) domains both in Paleo-Tethys and Panthalassa. Alatoconchidae started and evolved in the Early to Middle Permian and became extinct in the late Middle Permian. The stratigraphic range, their intimate association with large-tested fusulinids and timing of extinction of Alatoconchids are applicable to the example of the Nam Nao district in the western margin of the Indochina Block in East Paleo-Tethys.

To sum up, the Middle Member of the Khao Tham Yai Limestone records a remarkable example of the phyletic evolution in the genus *Lepidolina*. Notably, the genus *Lepidolina* apparently displays continuous and rapid morphological change along many one-way evolutionary trends from small, primitive species with simple structure to large, highly evolved species having a complicated wall structure at stratigraphically higher horizon levels (e.g. Ozawa, 1975; Kanmera et al., 1976; Hada et al., 2015). *Lepidolina kumaensis* is one of the most
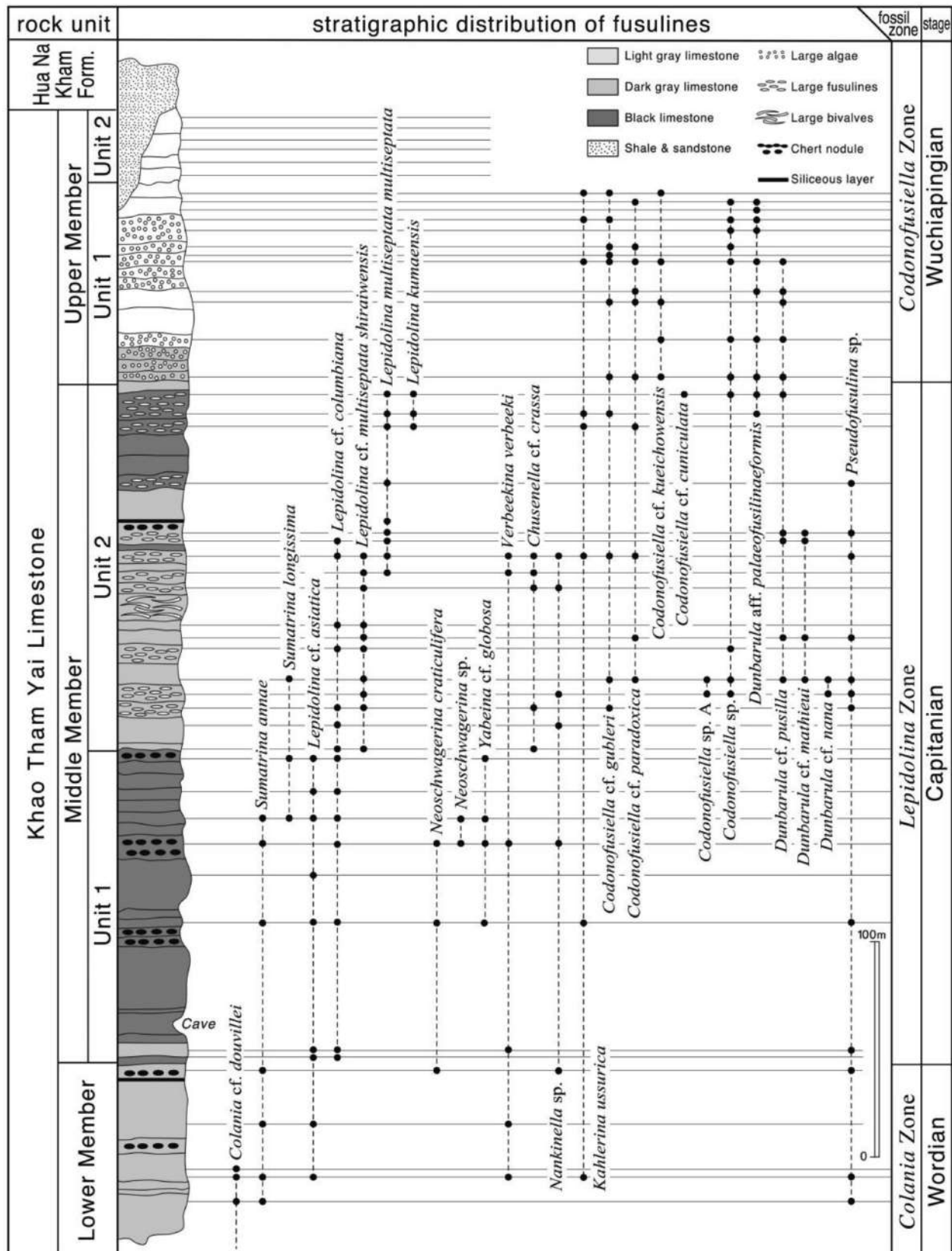
Figure 5: Composite stratigraphic column and fusuline distribution of the upper part of the Lower Member and Middle and Upper members of the Khao Tham Yai Limestone (slightly modified from Hada et al., 2015).
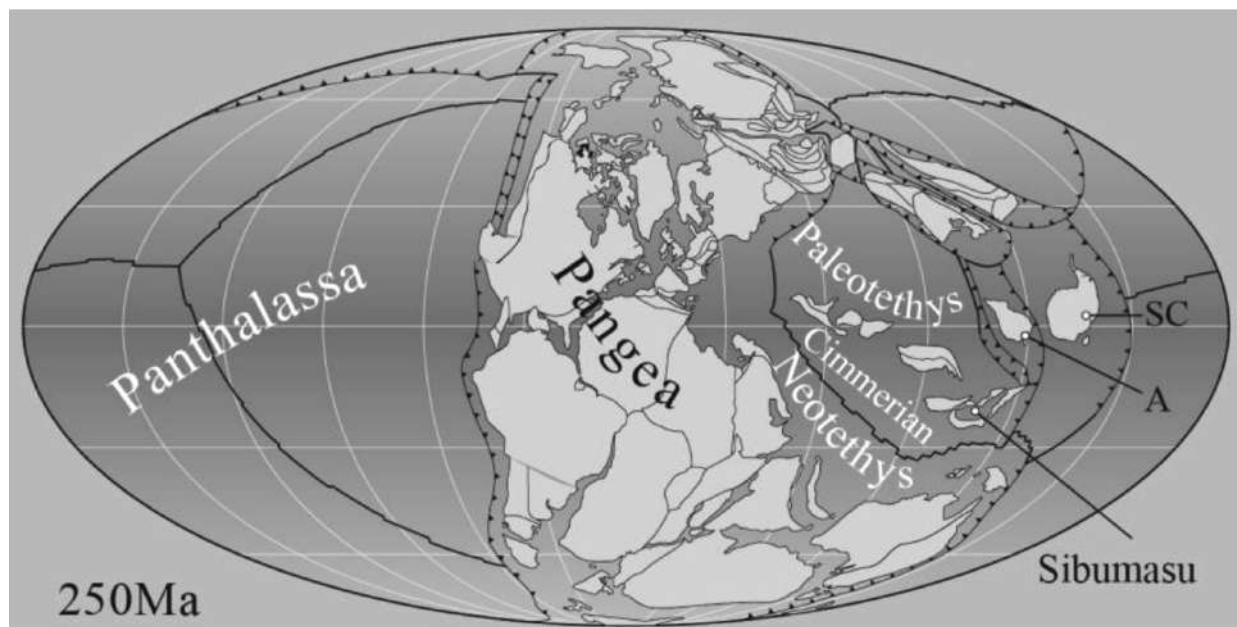
Figure 6: 250 Ma (Permo-Triassic) paleogeographic reconstruction showing simplified plate boundaries and with some major features labeled (modified from Domeier and Torsvik, 2014): A, Annamia (Indochina); SC, South China; Sibumasu constituted part of the eastern Cimmerian Continent.

advanced forms of Verbeekinidae and, recently, Kasuya et al. (2012) confirmed its termination by the end of the Capitanian (late Middle Permian). Our study of fusulinid faunas confirms that the Middle Member covers the Lepidolina Zone and can be assigned to the Capitanian (upper Maokoan) in South China (Sheng, 1963).

In conclusion, after marking the ultimate phase of their phyletic evolution of Permian fusulinid faunas in the top of Unit 2 of the Middle Member, the fusulinid assemblage characterized by long-ranging, large-tested Verbeekinids and Schwagerinids abruptly became totally extinct below the Guadalupian (Middle Permian)-Lopingian (Upper Permian) boundary (G-LB). Our study documents a remarkable horizon where the abrupt disappearance of large-tested fusulinids together with large bivalves occurred at the G-LB. The so-called end-Paleozoic mass extinction is the largest in Phanerozoic and has been considered to have occurred in two-phases (Jin et al., 1994): first, extinction at the Guadalupian-Lopingian boundary (G-LB; ca. 260 Ma) and second, at the Permo-Triassic boundary (P-TB; ca. 252 Ma). The importance of the most remarkable mass extinctions at the G-LB rather than the P-TB is emphasized repeatedly (e.g. Isozaki and Ota, 2001; Isozaki, 2007; Kofukuda et al., 2014).

4. Lithology and fossils above the G-LB with in the Khao Tham Yai Limestone of the Pha Nok Khao Formation, Loei Group

First, we provide a summary and re-examination of the smaller fusulinid and foraminifer species of the Upper Member of the Khao Tham Yai Limestone based on the findings of Hada et al. (2015) focusing in particular on their occurrence in relation to lithological change.

The boundary between the Middle and Upper members is clearly located between black limestones in the Middle Member and an overlying light gray limestone in the Upper Member. It is also clearly defined as the boundary of the abrupt change in the fusulinid assemblage from large-tested Verbeekinids and Schwagerinids to the small-shelled Schubertellids as mentioned above. The Upper Member is divided into Units 1 and 2 in ascending order, and the former approximately corresponds to the horizon 8 of Fontaine et al. (2002). Unit 2 is newly distinguished as a unit separated from the horizon 8 of Fontaine et al. (2002) and it forms the uppermost unit of the Khao Tham Yai Limestone.

Unit 1 of the Upper Member is mainly composed of thick-bedded, light gray limestone, commonly grainstone that characteristically contains small-shelled fusulinids and smaller foraminifers, abundant green algae, and totally

lacks in situ (autochthonous) large-tested fusulinids (see below). The abrupt domination of small-shelled fusulinids, smaller foraminifers and green algae is accompanied by a remarkable lithological change from black carbonaceous limestone to light gray crystalline, dolomitic limestone.

The lower half of Unit 1 is characterized by a sudden flourishing of diverse species of *Codonofusiella* and *Dunbarula,* such as *Codono-fusiella* cf. *gubleri* (Tien), *C. kuwangsiana* Sheng, *C. kueichowensis* Sheng, *C. paradoxica* Dunbar and Skinner, *Dunbarula paleofusilinae-formis* Sheng, *D.* cf. *pusilla* Skinner, *Colaniella minima* Wang, *Reichelina* cf. *media* Maclay, *R.* sp., *Sichotenella orientalis* Toumanskaya, *Nanlingella* cf. *meridionalis* Rui and Sheng, *N.* sp., *Kahlerina* cf. *ussurica* Sosnina, *K.* sp., and abundant green algae.

In contrast, the upper half of Unit 1 is particularly notable for the occurrence of a large number of broken fragments of diverse large-tested fusulinids having abraded outer volutions with iron-oxide-stained zones and abundant green algae accompanied by smaller foraminifers the same as those in the lower part of Unit 1. Fusulinid bioclasts contained in this lithofacies are of the same genus, *Lepidolina,* but include species at different stages of phyletic evolution, such as *Lepidolina asiatica, L. multiseptata, L. multiseptata multiseptata* or *L. kumaensis.* Their sizes are remarkably smaller than typical sizes of the species because of abrasion. Other broken fusulinid fossils include *Pseudofusulina* sp., *Sumatrina* sp., etc. It is noteworthy that the limestones appear to contain bioclasts exhibiting different degree of diagenesis (S. Mizutani, personal communication). Moreover, fossils of the Khao Tham Yai Limestone are more or less broken reflecting an energetic environment. The facies rich in elongated-type of *Dunbarula* have also been considered reflecting an energetic environment. Broken fragments of large-tested fusulinids undeniably represent a reworked fauna based on the mode of occurrence of large-shelled fusulinids together with the small-shelled fusulinids and green algae.

Unit 1 of the Upper Member is replete with diverse species of *Codonofusiella* and *Dunbarula.* Specifically, *Codonofusiella* cf. *kueichowensis, C. paradoxica* Dunbar and Skinner and *Dunba-rula paleofusulinaeformis* that characterize the Wuchiaping Limestone in low-latitudes of Tethyan domains in Kwangsi, Kueichou and Szechuan in South China (Sheng, 1963) occur in Unit 1. Based upon these observations, Unit 1 most likely corresponds to the *Codonofusiella* Zone of Sheng (1963) in South China. Thus, the age of Unit 1 of the Upper Member is considered to be Wuchiapingian. In our recent investigation of Unit 1, we found additional small fusulinid species as *Nanlingella* cf. *meridiionalis* Rui and Sheng, and *Reichelina* cf. *media* Maclay. Those fusulinids appear in the upper part of the *Codonofusiella* Zone and flourished in the lower and middle part of the *Paleofusulina* Zone. So, it is possible that the age of the upper part of Unit 1 and Unit 2 of the Upper Member extends to the *Changhsingian* although no typical *Changhsingian* (uppermost Permian) *Paleofusu lina-Reichelina* assemblage has been recognized from the Khao Tham Yai Limestone. Existence of the Wuchiapingian within a single continuous limestone section ranging from Middle to Upper Permian is confirmed for the first time in Thailand (Hada et al., 2015).

The newly differentiated Unit 2 of the Upper Member is the stratigraphically highest unit of the Khao Tham Yai Limestone. It is mainly composed of massive, crystalline light gray limestone commonly grainstone in which large algae are locally abundant, and fusulinid faunas are totally absent. Small foraminifers are all broken, fragmented species of *Codonofusiella, Reichelina* and *Colaniella.* The age of Unit 2 seems most likely to be Wuchiapingian based on its stratigraphic position. Unit 2 of the Upper Member is possibly comparable to a "barren interval" reported by Ota and Isozaki (2006) and assigned to shallow marine limestone in mid-Panthalassa below the G-LB. In more detail, Kofukuda et al. (2014) documented that the disappearance of major taxa at the end of the Capitanian occur in two steps in the barren interval in mid-Panthalassa; i.e., first the disappearance of large-tested fusulines in the upper Capitanian, and then a second episode involving smaller foraminifers also in the upper Capitanian, although smaller foraminifers reappeared above the GL-B. On the other hand, in the Nam Nao district, the abrupt disappearance of large-tested fusulines and a sudden flourishing of smaller fusulinid and foraminifer species clearly occurred across the G-LB, and the second disappearance of smaller foraminifers was

registered during the Wuchiapingian in Unit 1 of the Upper Member of the Khao Tham Yai Limestone. Kofukuda et al. (2014) also reported the subaerial exposure and erosion of mid-oceanic seamounts that occurred in the topmost barren interval across the G-LB in mid-Panthalassa. While, in the Nam Nao district, Unit 1 and the topmost barren interval of the Khao Tham Yai Limestone is disconformably overlain by the siliciclastic Hua Na Kham Formation and the top bed of the Hua Na Kham Formation is characterized by remarkable boulder bed of fusulinid and conglomeratic limestones derived from the Khao Tham Yai Limestone (see below). Namely, the two phases of the disappearance of major taxa and a large-scale sea-level drop started above the G-LB and occurred a little later during the Wuchiapingian on the continental margin of the Indochina Block. Large-scale sea-level drop at the end of Capitanian has been globally recognized through analyses of continental shelf areas around Tethys. The sea-level drop detected around Paleo-Tethys and mid-Panthalassa during the late Middle to early Late Permian likely reflected a global cooling, which caused a large-scale eustatic regression (e.g. Haq and Schutter, 2008). Although the possible cause of a global cooling is still not definite, Isozaki (2009) recently proposed that a change in the core's geodynamo might have played an important role in determining the course of the Earth's surface climate and biotic extinction/ evolution.

5. The Hua Na Kham Formation of the Loei Group with special reference to the boulder bed of conglomeratic limestone

In the valley on the eastern side of the Khao Tham Yai Limestone, Fontaine and Salyapongse, (2001) and Fontaine et al. (2002) reported a siliciclastic succession consisting of shale, cleaved siltstone, minor sandstone and rare thin beds of argillaceous limestone approximately 1000 m thick, and stratigraphically overlying the Khao Tham Yai Limestone. Although the succession is intensely weathered and exposed only in scattered small outcrops, it is attributed to the Upper Permian Hua Na Kham Formation of the Loei Group (Ueno and Charoentitirat, 2011). Little has been known about the fossil content of the Hua Na Kham Formation, but Fontaine et al. (2002) reported poorly preserved fusulinaceans as *Codonofusiella, Dunbarula, Reichelina* and *Lepidolina* from loose blocks of argillaceous limestone. This assemblage is similar to some beds in the eastern part of the Khao Tham Yai Limestone and they suggested a Midian (upper Middle Permian) age.

Hada et al. (2015) demonstrated that onlap of the clastic formation onto the Khao Tham Yai Limestone occurred on a larger scale replacing previous carbonate formation characterized by algae-foraminiferal biotas. In detail, the onlap of siliciclastic rocks onto Unit 1 of the Upper Member of the Khao Tham Yai Limestone to the south of the fault identified by a marker bed of Alatocon-

Figure 7: Field photograph of the Hua Na Kham Formation and the Khao Pa Khi Limestone. A: A distance view. Boulders dispersed at the foot of the Khao Pa Ki Limestone hill just like loose blocks are outcrops of the boulder bed at the top of the Hua Na Kham Formation. B: Close-up view of the boulder bed of the Hua Na Kham Formation.
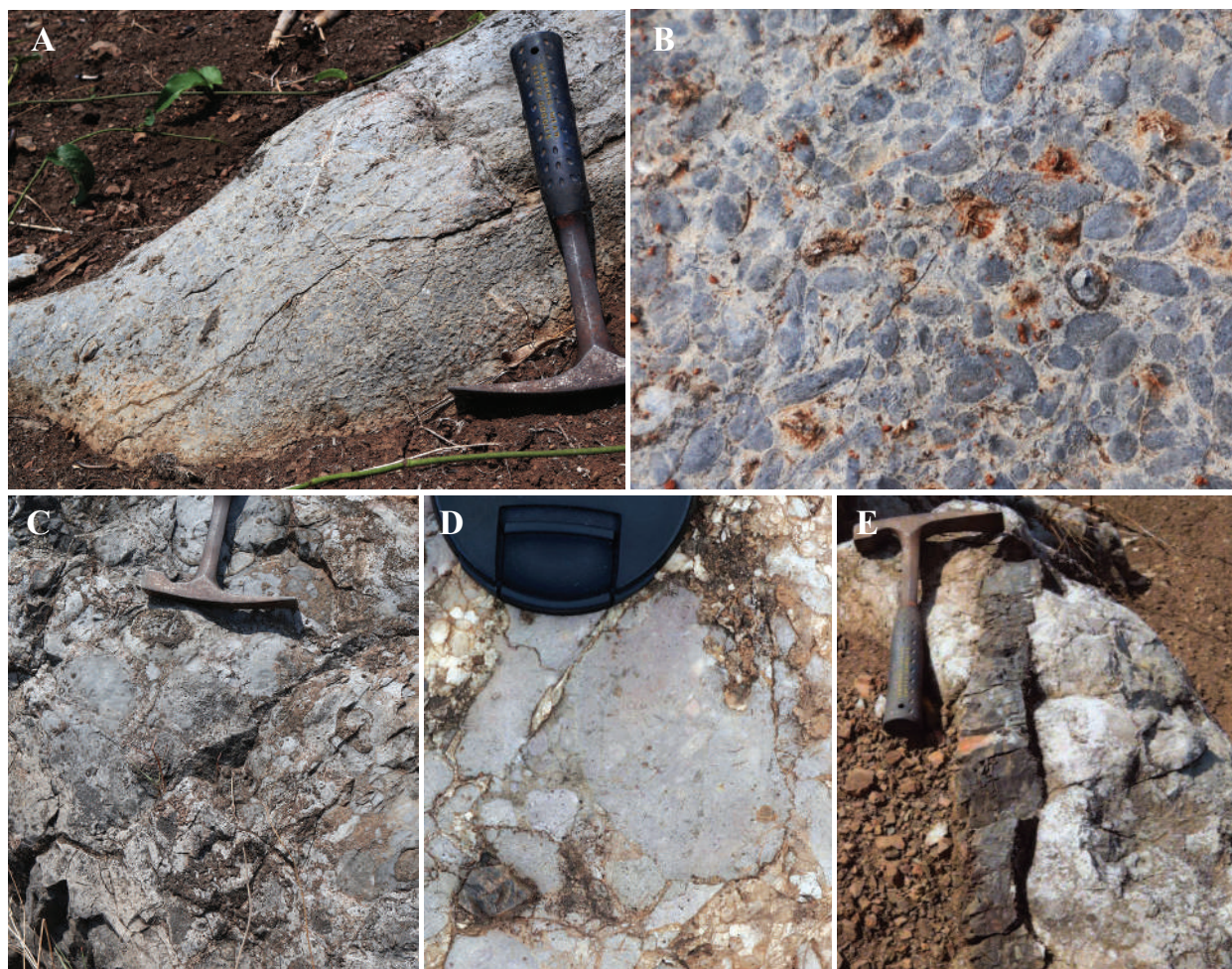
Figure 8: Field occurrence of boulders of fusulinids and conglomeratic limestone at the top of the Hua Na Kham Formation. (A) Fusulinid limestone. (B) An enlarged view of the fusulinid boulder. (C) Bioclastic limestone (rudstone) (D) Brecciated limestone. (E) Bioclastic limestone accompaning chert band.

chidae and onto its Unit 2 (barren interval) to the north of the fault is regionally recognized (Fig. 4). The strike of siliciclastic Hua Na Kham Formation is NW-SE and is the same as the Khao Tham Yai Limestone, but steeply dipping towards the west. As repeatedly emphasized by Ueno and Charoentitirat (2011), siliciclastic formations and carbonate formations having similar ages in some areas are largely heteropic facies and possibly interfinger with each other. The relationship between the Khao Tham Yai Limestone and the siliciclastic Hua Na Kham Formation of the Loei Group in the Nam Nao district shows that both formations are heteropic and the latter finally overlies the Khao Tham Yai Limestone.

Recently, we discovered a remarkable boulder bed of fossiliferous and conglomeratic limestones at the top of the Hua Na Kham Formation. Large boulders of a large-tested fusulinid limestone and a remarkable conglomeratic limestone having various lithologies have been dispersed at the top of a rather steep slope under the Khao Pa Khi Limestone hill just like loose blocks on the slope. Siltstones surrounding boulders are so strongly weathered that it is remarkably difficult to judge in the field whether boulders are loose blocks or lie within a siltstone matrix of the Hua Na Kham Formation. Fossils yielded from boulders match those of the Upper Member of the Khao Tham Yai Limestone, whereas totally different fossils characterize the Lower Permian Khao Pa Khi Limestone in direct contact to the east with the Hua Na Kham Formation (see below). At the same time, it is regarded as most unlikely that boulders were accumulated by farmers working in cornfields in the valley considering its topographic position, their number and size. In conclusion, the large boulders of fossiliferous conglomeratic limestones that appear to be loose blocks are interpreted as

constituent rocks of the uppermost strata of the Hua Na Kham Formation (Fig. 7A and B). Boulders are composed of a brecciated limestone with or without fusulinid fossils, large-tested fusulinid limestone, and bio-clastic limestone (rudstone). Those boulders are sometimes accompanied by chert nodules and bands. All these conglomeratic limestones are regarded as part of an intraformational conglomerate and breccia in origin. The shape of boulders is subangular, tabular and disc-shaped, and the sizes of major axes of most boulders are approximately 1-3 m (Fig. 8A, B, C, D and E). Boulders of fusulinacean limestone contain *Lepidolina* cf. *multiseptata, Verbeekina verbeeki, Sumatrina* sp., *Pseudofusulina* sp., and conglomeratic limestone boulders yield abundant broken or fragmented and abraded fusulinid species such as *Lepidolina multiseptata mulutiseptata, L. asiatica, L.* sp., *Colania douvillei, Sumatrina* sp., *Pseudofusulina crassa, P. padangensis, P.* sp., *Neoschwagerina* sp. and *Verbeekina verbeeki,* and fusulinacean species such as *Pseudofusulina* sp., *Sichotenella* sp., *Codonofusiella* sp., *Dunbarula* sp., *Kahllerina* sp., and *Reichelina* sp. These fusulinid and fusulinacean species are surprisingly similar to those of the Khao Tham Yai Limestone.

In conclusion, boulders of fossiliferous and conglomeratic limestones are interpreted to have eroded off from the Khao Tham Yai Limestone and brought to the Hua Na Kham Formation based on the fusulinids and foraminiferal fauna they contain. Boulders may be transported by large-scale submarine debris flow from a

Khao Tham Yai barrier reef developed on clastic-dominant continental shelves (Fig. 9). The occurrence of conglomeratic limestone boulders in a siliciclastic matrix indicates that the carbonate sediments were lithified before they were enveloped by the flow of terrigenous mud. This is a reason that the limestones appear to contain bioclasts showing different degree of diagenesis mentioned above.

Similar large boulders beds of limestone are known within the uppermost Jurassic-lowermost Cretaceous Torinosu Group on Shikoku Island of southwest Japan. The presence of limestone boulders derived from the mounds has been interpreted as indicating that cessation of carbonate deposition may have been associated with catastrophic events (Kano, 1988). Terrigenous sediments flowed over the carbonate deposits, killing the colonial organisms and stopping carbonate sedimentation possibly indicating that the cessation of the carbonate deposition may have been associated with a large-scale eustatic sea-level drop. The Ordovician Cow Head Breccia in the Appalachian Orogen in Canada is also an example of mixed angular breccia and softly deformed tabular blocks of limestone showing different degrees of diagenesis and typically developed off the edge of the carbonate bank at the ancient continental margin (James and Stevens, 1986). Similar coarse carbonate Upper Devonian debris was deposited along the base of a steep-walled platform as talus breccias (via rockfall) and debris-flow breccias in the Napier Range of the Canning Basin of NW
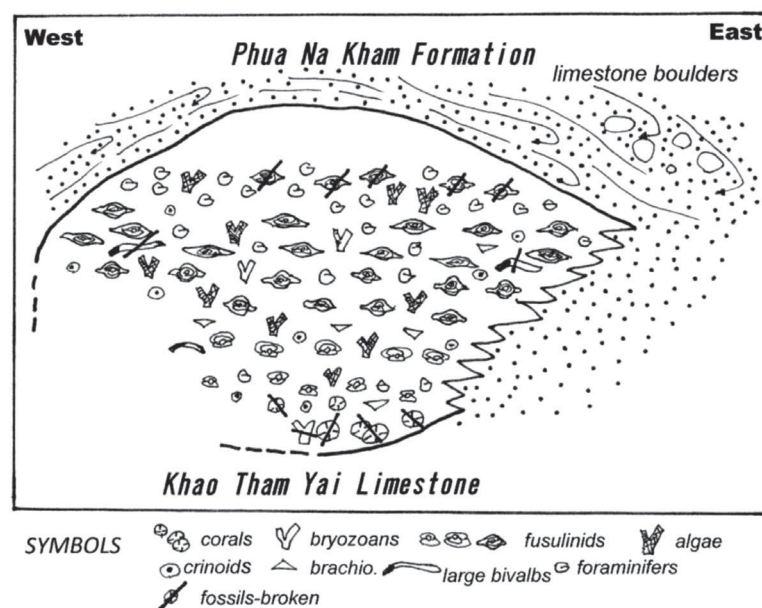
Figure 9: Model illustrating possible development of the Khao Tham Yai barrier reef (transverse section) on the continental shelf of the western margin of the Indochina Block. Limestone boulders were transported by submarine debris flow from the Khao Tham Yai barrier reef to sites on the continental shelf where the Hua Na Kham Formation was deposited (modified after Kano, 1988).
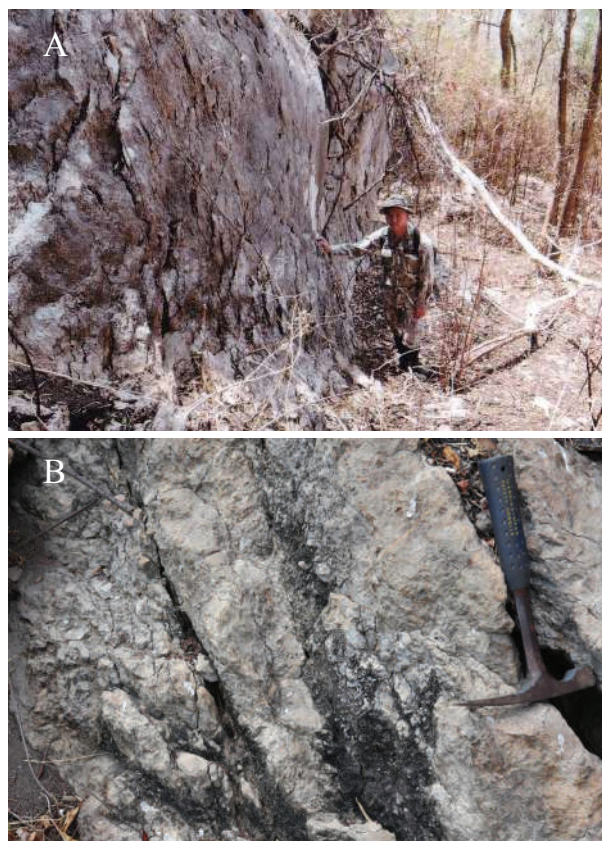
Figure 10. Field photographs of a fault scarp between the Khao Pa Khi Limestone and the Hua Na Kham Formation (A) and Riedel shear in its fault breccia indicate a reverse sense of slip (B).

Australia. Changes in sedimentary style on the slope, reflecting differing rates of carbonate production on the platform, are linked to relative sea-level fluctuations (George et al., 1997). The broken limestone and limestone breccias have been also reported from the reef-capped Akiyoshi seamount in the accretionary complex of Japan. In this case, large-scale collapse of the seamount and limestone cap was caused as the result of the encroachment of the seamount into a trench area (Sano and Kanmera, 1991).

The age of the Hua Na Kham Formation in the Loei Group can be defined as Wuchiapingian and possibly extends to Changhsingian considering its stratigraphic relation with the Khao Tham Yai Limestone, fossils of conglomeratic limestone boulders and argillaceous limestone.

6. The age of the Khao Pa Khi Limestone of the Pha Nok Khao Formation, Loei Group

The Khao Pa Khi Limestone is a continuous succession of narrow hills aligned in a north-south direction. The limestone is pale gray or whitish gray, massive, vertically dipping, approximately 250 m thick (Fig. 8A). Stylolites commonly observed in the limestone occur as single low amplitude suture planes. It is in direct contact to the west with the siliciclastic Hua Na Kham Formation. It is sparsely fossiliferous and was once regarded as Triassic (Fontaine and Salyapongse, 2001). Fontaine et al. (2002) later suggested a Permian age for the Khao Pa Khi Limestone based on foraminifers, and corals (from loose blocks). Fontaine et al. (2002) commented that if the corals belong to the Khao Pa Khi Limestone, they show that an inconsistent Upper Permian or Triassic age and also suggested the existence of fault between the Khao Pa Khi Limestone and the siliciclastic Hua Na Kham Formation. Recently, we found fusulinid fossils in outcrops of the Khao Pa Khi Limestone. Those are *Misellina* cf. *otai, Sakaguchi* and *Sugano, M.* sp. and *Para-schwagerina* cf. *fosteri* (Thompson and Miller). *Misellina otai* is the most primitive representative of the genus (Sakagami and Sugano, 1966). In late Early Permian time *Misellina* spread throughout Paleo-Tethys, although the occurrence of localities, yielding this genus, are sporadic (Ishii et al., 1985). *Misellina* gave rise to the *Misellina-Cancellina-Colania-Lepidolina* and the *Misellina-Maklaya–Neoschwagerina-Yabeina* evolutionary lineages (Ozawa, 1970). The Khao Tham Yai Limestone that is supposed to be developed in the same continental shelves as the Khao Pa Khi Limestone on the western margin of the Indochina Block is characterized by the former evolutionary lineage.

Our study of the fusulinid fauna confirms the *Misellina* Zone of the Lower Permian for the Khao Pa Khi Limestone of the Pha Nok Khao Formation. The fault between the Khao Pa Khi Limestone and the Hua Na Kham Formation is confirmed at the bottom of the Khao Pa Khi Limestone. It is N-S trending and dips steeply east to vertical. Discontinuous shear plane and foliation plane Riedel shear indicate a reverse sense of slip consistent with uplift of the Khao Pa Khi Limestone against the Hua Na Kham Formation (Fig. 10A and B).

7. Concluding remarks

Litho- and bio-stratigraphic analyses of the Lower Permian Khao Pa Khi and Middle-Upper

Permian Khao Tham Yai limestones, and the heteropic siliciclastic Hua Na Kham Formation indicate they accumulated on a clastic-dominant continental shelf at low-latitude on the western margin of the Indochina Block. We have clarified the following matters. (1) The abrupt disappearance of large-tested fusulines with large bivalves clearly occurred at G-LB within the Khao Tham Yai Limestone, and they never returned. (2) The Khao Tham Yai Limestone above the G-LB is characterized by sudden proliferation of a diverse range of species of smaller foraminifers and the occurrence of a large number of broken fragments of diverse large-tested fusulinids and abundant green algae. Broken fragments of large-tested fusulinids undeniably represent a reworked fauna from (3) The first disappearance of large-tested fusulines and the proliferation of smaller fusulinid and foraminifer species clearly occurred across the G-LB, and the second disappearance of smaller foraminifers was registered during the Wuchiapingian. These two phases of dis-appearance of fusulinid and foraminifer species on the continental margin of the Indochina Block have likely occurred a little later comparing to the phases on the paleo-atoll in mid-Panthalassa. (4) The Wuchia-pingian siliciclastic Hua Na Kham Formation unconformably onlaps the Khao Tham Yai Limestone replacing previous carbonate formation characterized by algae-foraminiferal biotas. A remarkable boulder bed of fusulinids and conglomer atic limestones occurs at the top of the Hua Na Kham Formation. The fusulinacean assemblage yielded within boulders undoubtedly compares to that of the Middle and Upper members of the Khao Tham Yai Limestone. Therefore, it is reasonable to consider that these boulders were eroded from the Khao Tham Yai Limestone and brought to the Hua Na Kham Formation. Boulders may be transported by large-scale submarine debris flow originating from the Khao Tham Yai barrier reef and developed on a clastic-dominant continental shelf. Terrigenous sediments flowed over the carbonate deposits, possibly indicating that the cessation of the carbonate deposition may have been associated with catastrophic events like a large-scale eustatic sea-level drop. (5) Although the subaerial exposure and erosion reported from mid-oceanic seamounts occurred across the G-LB in the uppermost barren interval in mid-Panthalassa, a large-scale sea-level drop associated with global environmental change inside the continental margin of the Indochina Block occurred a little later during the Wuchiapingian. (6) Our recent study of the fusulinid fauna confirms the Misellina Zone of the Lower Permian for the Khao Pa Khi Limestone of the Pha Nok Khao Formation.

Acknowledgements

References

Bunopas, S. (1981). *Paleogeographic history of western Thailand and adjacent parts of Southeast Asia A plate tectonic interpretation* (Ph. D. Thesis). Victoria University of Wellington. New Zealand.

Charusiri, P., Daorerk, V., Archibald, D., Hisada, K., & Ampaiwan, T. (2002). Geotectonic evolution of Thailand: New synthesis. *Journal of the Geological Society of Thailand, 1,* 1-20.

Chonglakmani, C., & Sattayarak, N. (Cartographer). (1984). *Geological Map of Changwat Phetchabun (Sheet NE 47-16,)* [map]. 1:250,000. Bangkok: Survey Division, Department of Mineral Resources.

Chutakositkanon, V., Hisada, K., Charusiri, P., & Arai, S. (1999). Detrital chromian spinels from the Nam Duk Formation: a key to elucidate the tectonic evolution of central mainland Southeast Asia and the Loei Suture Zone in Thailand. In: Rathanasthien, B. and Rieb, S.L. (Eds.) *Proceedings of International Symposium on Shallow Tethys (ST9 5)* (pp. 450-456). Chiang Mai.

Domeier, M., & Torsvik, T.H. (2014). Plate tectonics in the late Paleozoic. *Geoscience Frontiers, 5,* 303-350.

Fontaine, H., & Salyapongse, S. (2001). A Murgabian to Lower Triassic sequence exposed from Khao Tham Yai to Khao Pa Khi, Northeast Thailand: A preliminary report. *Journal of the Geological Society of Thailand, 1*, 43-47.

Fontaine, H., Salyapongse, S., Nguyen Duc Tien, & Vachard, D. (2002). The Permian of Khao Tham Yai area in Northeast Thailand. *The Symposium on Geology of Thailand, Bangkok, Thailand* (pp. 26-31).

George, A.D., Playford, P.E., & Powell, M. C. (1997). Lithofacies and sequence development on an Upper Devonian mixed carbonate-siliciclastic fore-reef slope, Canning Basin, Western Australia. *Sedimentology*, *44,* 843-867.

Goto, H., Maruoka, K., & Ishii, K. (1986). Lepidolina columbiana (Permian Fusulinid) from British Columbia, Canada. Tran-saction *Proceedings of the Palaeontological Society of Japan* (pp. 422-434).

Hada, S., Bunopas, S., Ishii, K., & Yoshikura, S. (1999). Rift-drift history and the amalgamation of Shan-Thai and Indochina/East Malaya Blocks. In: Metcalfe, I., Ren Jishun, Charvet, J., & Hada, S. (Eds.), *Gondwana Dispersion and Asian Accretion, Final Results Volume for IGCP Project 321* (pp. 67-87). Rotterdam: A.A. Balkema Publishers.

Hada, S., Ishii, K., Landis, C.A., & Aitchison, J. (1996). Mid Permian Fusulinacean territories and identity of the Kurosegawa Terrane in Southwest Japan (Geologic Development of the Asian-Pacific Region, with implication in evolution of Gondwanaland). *Japan Contribution to the IGCP, 1996 (IGCP National Committee of Japan)* (pp. 27-34).

Hada, S., Khosithanont, S., Goto, H., Fontaine, & H., Salyapongsa, S. (2015). Evolution and Extinction of Permian fusulinid fauna in the Khao Tham Yai Limestone in NE Thailand. *Journal of Asian Earth Sciences, 104,* 175-184.

Haq, B.U., & Schutter, S.R., (2008). A chlonology of Paleozoic sea-level changes. *Science, 322,* 64-68.

Helmcke, D. (1994). Distribution of Permian and Triassic syn-orogenic sediments in central mainland SE-Asia. In: Wongwanich, T., Tansathien, W., & Tulyatid, J. (Eds.), *Proceedings of the International Symposium on Stratigraphic Correlation of South east Asia (IGCP 306)* (pp.123-128). Bangkok.

Helmcke, D., & Lindenberg, H.G. (1983). New data on the Indochinan Orogeny from Central Thailand. *Geologishe Rundschau, 72,* 317-328.

Ingavat, R., Toriyama, R., & Pitakpaivan, K. (1980). Fusuline Zonation and Faunal characteristics of the Ratburi Limestone in Thailand and its Equivalents in Malaysia. *Geology and Palaeontology of Southeast Asia,* (21), 43-56.

Ishii, K. (1966). On some Fusulinids and other foraminifera from the Permian of Pahang, Malaya. *Journal of Geosciences, Osaka City University, 9,* Art 4-V, 131-136, pls. 5-6.

Ishii, K., Okimura, Y., & Ichikawa, K. (1985). Notes on Tethys biostratigraphy with reference to Middle Permian Fusulinaceans. In: Nakazawa, K., Dickins, J.M. (Eds.), *The Tethys, Her Paleogeography and Paleobiogeography from Paleozoic to Mesozoic, Tokai University Press, Tokyo* (pp. 677-692).

Isozaki, Y. (2007). Guadalupian-Lopingian boundary event in mid-Panthalassa: correlation of accreted deep-sea chert and mid-oceanic atoll carbonates. In: Wong, T. (Ed.), *Proceedings of the XVth International Congress of Carboniferous and Permian Stratigraphy* (pp. 111-124). Amsterdam: Royal Netherlands Academy of Arts and Science.

Isozaki, Y. (2009). Illawarra Reversal: The fingerprint of a superplume that triggered Pangean breakup and the end-Guadalupian (Permian) mass extinction. *Gondwana Research, 15,* 421-432.

Isozaki, Y., & Aljinovic, D. (2009). End-Guadalupian extinction of the Permian gigantic bivalve Alatconchidae: End of gigantism in tropical seas by cooling. *Palaeogeography, Palaeoclimatology, palaeoecology, 284,* 11-21.

Isozaki, Y., & Ota, A. (2001). Middle/Upper Permian (Maokouan/Wuchapingian) boundary in mid-oceanic atoll limestone in Kamura and Akasaka, Japan. *Proceedings of Japan Academy, 77B,* 104-109.

James, N. & Stevens, R.K. (1986). Stratigraphy and correlation of the Cow Head Group, western Newfoundland. *Bulletin of the Geological Survey of Canada., 336* (pp. 143).

Jin, Y., Zhang, J., & Shang, Q.H. (1994). Two phases of the end-Permian mass extinction. In: Embry, A.F., Beauchamp, B., & Glass, D.J. (Eds.), *Pangea: Global Environments and Resources. Canadian Society of Petroleum Geologists, Memoir, 17,* 813-822.

Kanmera, K., Ishii, K., & Toriyama, R. (1976). The evolution and extinction patterns of Permian Fusulinaceans. *Geology and Palaeontology of Southeast Asia,* (17), 129-154.

Kano, A. (1988). Facies and depositional conditions of a carbonate mound (Thithonian-Berriasian, SW-Japan). *Facies, 18,* 27-47.

Kasuya, A., Isozaki, I., & Igo, H. (2012). Constraining paleo-latitude of a biogeographic boundary in mid-Panthalassa: Fusuline province shift on the Late Guadalupian (Permian) migrating seamount. *Gondwana Research, 21,* 611-623.

Kofukuda, D., Isozaki, Y., & Igo, H. (2014). A remarkable sea-level drop and relevant biotic responses across the Guadalupian-Lopingian (Permian) boundary in low-latitude mid-Panthalassa: Irreversible changes recorded in accreted paleo-atoll limestones in Akasaka and Ishiyama, Japan. *Journal of Asian Earth Sciences, 82,* 47-65.

Ota, A., & Isozaki, Y. (2006). Fusuline biotic turnover across the Guadalupian-Lopingian (Middle-Upper Permian) boundary in mid-oceanic carbonate buildups: biostratigraphy of accreted limestone in Japan. *Journal of Asian Earth Sciences, 26,* 353-368.

Ota, M. (1977). Geological studies of Akiyoshi: A geosynclinals reef complex. *Bulletin of the Akiyoshidai Science Museum,* (5), 1-44, pls. 1-31.

Ozawa, T. (1970). Notes on the phylogeny and classification of the Superfamily Verbee-kinoidea. Memoir of the Faculty of Science Kyushu University, Series D, *Geol., 20,* 17-58.

Ozawa, T. (1975). Evolution of Lepidolina multiseptata (Permian Foraminifer) in East Asia. Memoirs of the Faculty of Science Kyushu University, Series D, *Geol., 23* (2), 117-164, plates 22-26.

Ridd, M. F., Barber, A. J., & Crow, M. J. (Eds.), (2011). *The Geology of Thailand. Geological Society, London* (pp. 626).

Ross, C.A. (1995). Permian fusulinaceans. In: Scholle, P.A., Peryt, T.M., Ulmer-Scholle, D.S. (Eds.), *The Permian of northern Pangea. 1, Springer-Verlag, Berlin* (pp. 167-185).

Sano, H., & Kanmera, K. (1991). Collapse of ancient oceanic reef complex-What happened during collision of Akiyoshi reef complex? - Sequence of collisional collapse and generation of collapse products. *Journal of the Geological Society of Japan, 97,* (8), 631-644.

Sheng, J.Z. (1963). Permian fusulinids of Kwangsi, Kueichow and Szechuan. *Palaeontological Sinica, N.S.B.,* (10), 1-247, plates 1-36.

Ueno, K., & Charoentitirat, T. (2011). Carboniferous and Permian. In: Ridd, M. F., Barber, A. J., Crow, M. J. (Eds.). *The Geology of Thailand. Geological Society* (pp. 71-136). London.

Ueno, K., & Hiasada, K. (2001). The Nan-Uttaradit-Sa Kaeo Suture as a Main Paleo-Tethyan Suture in Thailand: Is it real? *Gondwana Research,4,* 804-806.

Wielchowsky, C.C., & Young, J.D. (1985). Regional facies variations in Permian rocks of the Phetchabun fold and thrust belt, Thailand. In: Thanavarachorn, P., Hokjaroen, S., Youngme, W. (Eds.) *Conference on Geology and Mineral Resources Development of the Northeast Thailand 1985* (pp. 41-55). Khon Kaen.

Possible sources of elevated arsenic in surface and ground water, Amphoe Banrai, Changwat Uthai Thani, Thailand

Apsorn Sardsud[1], Onuma Khamphleang[1] and Jitisak Premmanee[2*]

[1]*Division of Mineral Resources Analysis and Identification, Department of Mineral Resources.*
[2]*An ex-official of the Department of Mineral Resources.*
∗*Corresponding author: gi.geosciences@gmail.com*

Abstract

This study is cooperation between the Division of Mineral Resources Analysis and Identification, Department of Mineral Resources and the Uthai Thani Provincial Public Health Office to help and verify elevated arsenic level at Tambol Nongjok/Nongbomklouy, Amphoe Banrai, Changwat Uthai Thani because the elevated arsenic level may pose health risk to local residents. Geochemical techniques were employed by collecting water and stream/lake sediments, and analyzing for arsenic covering the target and adjacent areas. A total of 371 water samples were compiled. Assay results of 281 surface water samples range from <2–2,713 ppb, average 97 ppb; and of 90 groundwater samples range from <2–505 ppb, average 47 ppb. Integrated spatial studies of these water assays with geography, water flow pattern and arsenopyrite mineralization outline 2 tiers of risk areas. Tier 1 arsenic assays ≥300 ppb, covers 2 areas in south of Ban Thapfaimai and at Wat Nongmaitai, Tambol Nongjok and Tier 2 arsenic assay ≥100 ppb, encompasses 14 villages in Tambol Nongjok/Nongbomkluay Changwat Uthai Thani; Tambol Wangkan Changwat Suphanburi and Tambol Sukduenha Changwat Chainat. A total of 88 stream/ lake sediments samples were compiled. Assay results range from <5–167 ppm, average 31 ppm. A group of high assays (75-167 ppm) are close to the expired tin-tungsten mining licenses at Ban Nongyaingern, Tambol Wangkan. Other high assays (≥50 ppm) are contained within the Tier 2 area. These findings indicate that water sampling is a more practical approach than sediment sampling in order to outline the arsenic risk areas and may identify the point sources. Four possible arsenic sources were identified: (1) Khao Koktungkung, (2) west of Ban Putakien (3) Wat Nongmaitai and (4) west of Ban Nongmaikean where it was later found altered granite with quartz veins and disseminated arsenic rich sulfide minerals at an under-construction water reservoir.

Key words: Arsenic, Banrai, geochemical exploration, sources, risk area, water sampling

Introduction

This project was initiated by the Uthai Thani Provincial Public Health Office (UTPHO). The Office has actively followed up the elevated arsenic level in surface water as well as in local residents since 2011. Even though, elevated arsenic level in water of the area was known for many years. The Division of Mineral Resources and Identification, Department of Mineral Resources (DMR), Ministry of Natural Resources and Environment filed the first records in 2006. Later, some records were available from a cooperative project between the DMR and the Department of Disease Control, Ministry of Health in 2009. Also, the DMR Hazardous Element Project sampled surface water and sediments in this area during 2012 and 2013.

Nevertheless, most of the mentioned records did not study throughout the area but rather concentrated on the known problematic sites. The data under the DMR Hazardous Element Project systematically cover parts of the area in Suphanburi and Uthai Thani, but no sampling in nearby Chainat provinces.

Therefore, the Division of Mineral Resources and Identification, DMR launched this project in early 2019 to systematically document elevated arsenic levels and hopefully identify the possible sources. Geochemical prospecting techniques were employed by collecting water and stream/lake sediments, and analyzing arsenic covering the target and adjacent areas.

Study Area

The initial study area consists of 5 villages (Ban[i] Tapfaimai, Maiphongan, Nongmaikean, Keanpetphailin and Nongmaitai) of Tambol[i] Nongjok and 1 village (B. Lanka) of T. Nongbomkluay, Amphoe[i] Banrai, Changwat[i] Uthai Thani (Fig. 1). However, after compilation of previous data, the study area was expanded to include the nearby villages of T. Nongjok / Nongbomkluay /Tapluang, A. Banrai, C. Uthai Thani, of T. Wangkan /Nongkratum, A. Danchang /Doembangnangbuat, C. Suphanburi, of T. Sukduenha /Kaboktia, A. Noenkham, C. Chainat. The final rectangle of entire study area covers about 16x20 km or 320 km².

Figure 1 shows the topography of the area which consists of broad and gentle slope with higher ground formed as an axis at the middle, like a turtle back. The axis orients almost north-south direction and divides water flow into east and west directions. To the east, water curves to southeast direction and drain into the Thachin River, C. Chainat. The west part, water runs into Krasiao stream, then to Krasiao reservoir, A. Danchang, C. Suphanburi. Khao[ii] Phuklang and Urkhwai exhibit karst topography in the north and mainly consist of Ordovician limestone.

A group of hills, K. Koktungkung, Puchi and Pongngam present in the south and consist of meta-sediments, limestone and granite of Silurian/Devonian, Ordovician and Triassic Periods respectively. Contacts of these meta-sediments and limestone with granite host tin-tungsten deposits. A few mines operated around 1987 in secondary elluvial and alluvial deposits at K. Koktungkung and at B. Tapfaimai. Jariyawat (1996) reported that the mineralization formed in 1-10 cm quartz veins oriented N45W and N60E within granitic rock.

Interestingly, those southern hills formed natural geographic boundaries of 7 Tambols (Nongjok, Nongbomkluay, Wangkan, Nongmakhamong, Nongkrathum, Sukduenha and Kaboktia), 4 Amphoes (Banrai, Danchang, Dermbangnangbuat and Noenkham) and 3 Changwats (Uthai thani, Suphanburi and Chainat).

Previous Data and Additional Sampling

Figure 2 shows sample points including previous and additional samples. The previous water and sediment samples (Fig. 2A) were compiled from many sources, such as DMR's reports, UTPHO, the DMR's Hazardous Elements
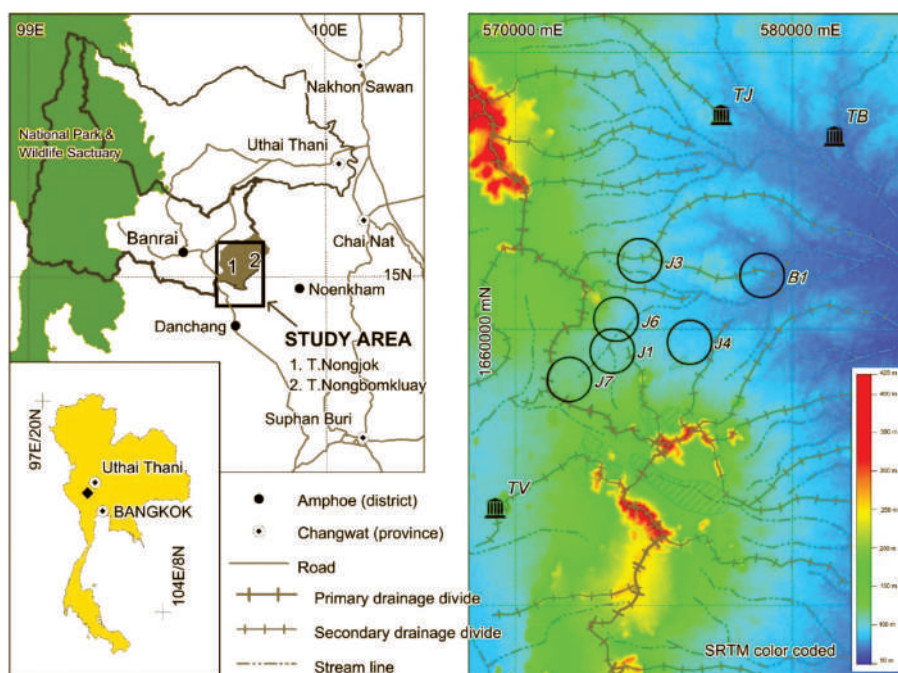
Figure 1: Location and topography of study area, Banrai, Uthai Thani

i - Ban, Tambol, Amphoe and Changwat are local administrative names and refer to village, sub-district, district and province respectively. In this report, they are abbreviated to B., T., A. and C. respectively.

ii- Khao refer to mountain or hill and in this report is abbreviate to K.

Project (Uthai Thani and Suphanburi provinces) and others, detailed in Premmanee (2019a). The samples consist of 32 streamsediments, 139 surface water, 50 ground water, and total 221 samples.

Figure 2b shows the additional samples collected in April 2019. The new sample set aim to fill-up spaces, create more density and verify some assays in the problematic areas. Additional samples consist of 56 stream/lake sediments, 142 surface water, 40 ground water, and total 238 samples. Note that these samples were collected, prepared and analyzed according to protocols in the Standard Method for Examination of Water and Waste Water no.3113 (2017) for water samples and the Hazardous Waste Test Methods no.SW-846 (2019) for solid samples.

These assays were combined into a single set, total 459 samples (Table 1). Arsenic contents in surface water, ground water and sediments average at 97 ppb[iii] 47 ppb and 31 ppm[iii] respectively. These averages lay about 20, 10 and 2 times higher than the averages in surface water (4 ppb) and stream sediments (12-15 ppm) under

the DMR Hazardous Element Project (Premmanee, 2019b). Note that World Health Organization (WHO, 2020) has suggested an arsenic safe content limit in drinking water of 10 ppb, while the Pollution Control Department (PCD, 2020) of Thailand has tabulated the standard arsenic values (refer to maximum permissible limit or MPL) in water and agricultural soil at 10-50 ppb and 3.9 ppm respectively.

Beside the water and sediments, UTPHO collected urine samples from local residents periodically every other year, since 2011 (Table 2) (Ms. Sukanya Pataisophon, personnel communication). The samples were in the 5 villages of T. Nongjok and 1 villages of T. Nongbomkluay (village J1, J3, J4, J6, J7 and B1 on Fig. 1). Results showed that 288 (55%) samples out of 520 samples are above acceptable levels[iv]

Arsenic Distribution

Figure 3 shows arsenic distribution in surface water (3A), ground water (3B) and sediments (3C). Elevated arsenic in surface water, ground water and sediments scatter around the tin-tungsten
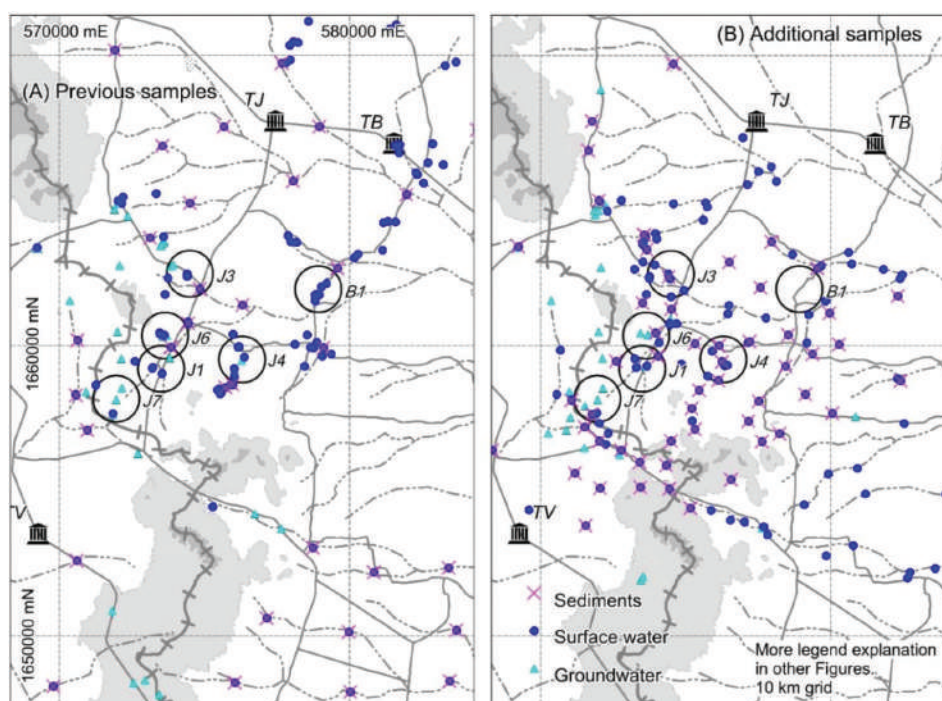
Figure 2: Samples location maps, (A) previous samples and (B) additional samples.

iii - ppb – part per billion or microgram per liter (μg/l) and ppm – part per million or milligram perliter (mg/l)

iv - Based on the Department of Desease Control (2019), the acceptable levels refer to 2 conditions. Urine sample collected from seafood consuming restricted of 48-72 hours is at <50 μg/l and from the unrestricted seafood consuming is at < 100 μg/dl.

Table 1. Statistics of arsenic assays in surface water, ground water and sediments.

Assay statistics	Surface water (ppb)	Ground water (ppb)	Combined water (ppb)	Sediments (ppm)
Number of samples	281	90	371	88
Minimum	<2	<2	<2	<5
Minimum	2713	447	2713	167
Average*	97.0	46.8	85.9	31.1
Standard deviation*	167.2	83.1	153.8	30.7
Detection limit (DL)	2	2	2	5
Number of <DL	8	27	35	3
Outlier	6 (2713,1589, 1350, 1295, 1206, 1170)	1 (505)	6 (2713,1589, 1350, 1295, 1206, 1170)	

Note: * If the assay is <DL, then DL/2 will use for calculation

Table 2. Urine arsenic levels in local residents.

Testing year		T. Nongjok	T. Nongbomkluay	Combined
2011	Total samples	202	-	202
	Anomaly (%)	73 (36%)	-	73 (36%)
2013	Total samples	86	-	86
	Anomaly (%)	49 (57%)	-	49 (57%)
2015	Total samples	101	-	101
	Anomaly (%)	86 (85%)	-	86 (85%)
2017	Total samples	96	75	171
	Anomaly (%)	38 (40%)	42 (56%)	80 (47%)
Total 520 samples with 288 (55%) anomalous values				

Figure 3: Arsenic distribution in (A) surface water, (B) groundwater and (C) stream/lake sediments.

prospective areas of K. Koktungkung and more densely to the north, especially at abandoned tin mining pits, south of B. Tapfaimai. The furthest north high arsenic assays distribute along water channels north of B. Maiphongam and Putakien.

The highest arsenic assay (2,713 ppb) in surface water was collected from a small water channel, south of B. Tapfaimai. 4 more high assays (>1,000 ppb) were detected at the tin mining pits in this area. The 6th high assay (1,170 ppb) is located at Wat Nongmaitai, B. Nongmaitai, about 3.5 km east of the Tapfaimai's tin pits. Interestingly, a group of high arsenic values (100-499 ppb) in surface water depicted at B. Maiphongam and further north which is located in different drainage catchment to the one of B. Tapfaimai. These show that arsenic sources may not only originated from the tin mining/prospective areas of K. Koktungkung but from unidentified natural sources northeast of B. Maiphongam as well.

High arsenic assays in ground water display similar patterns to surface water, but at B. Phutakien (Figs. 3A and 3B) where mixed of very low and high arsenic assays (≤50 to ≥100 ppb) detected in ground water. The highest assay (505 ppb) was found in 30 m water well here, but all surface water yield <50 ppb. In addition, the downstream assays of surface water gradually increase for about 5 km, i.e. 10, 22, 59, 72, 135 and 128 ppb, from the village. These findings are illustrated (Fig. 4) showing possible transport mechanism of arsenic in water of this area. It is estimated that arsenic may be mobilized as far as 10 km from the sources

High arsenic (≥75 ppm) in sediments distributed in 2 areas, east/northeast of K. Koktungkung and around B. Maiphongam and Phutakien. Medium high assays (25-74 ppm) located in those tin pits at B. Tapfaimai. These results do not quite agree with water assays. It seems that arsenic in sediments disperse irregularly around the sources. However, due to sampling period during the dry season, very limited stream sediments were collected, but the majority were lake/pond sediment which may not represent transported materials. So, sediments sampling may not be practical in this case.

Risk Areas and Possible Point Sources

Many spatial factors (such as topography, drainage system, arsenic mineralization style, geological environment and others) will help to outline the risk areas and to identify arsenic point sources. As mentioned, water assays will limit the risk areas compared to sediment assays. And yet, many authorities recommend MPL in consumable water at 10-50 ppb. So, the practical threshold arsenic assays in surface water should be higher than the MPL in order to separate the risk areas. In this study, arsenic in surface water average at 97 ppb while 47 ppb in ground water. Therefore, surface water assay at 100 ppb is selected for the practical threshold value.

The 100 ppb lines were manually drawn following drainage system and catchment areas, so as the 300 ppb lines (very high arsenic values). Figure 5 shows results of the 2 tiers of risk areas as follow.

Tier 1: arsenic assays ≥ 300 ppb in surface water, encompass 2 areas: (1) south of B. Tapfaimai where there are many abandoned tin mining pits and (2) Wat Nongmaitai, B. Nongmaitai; both at T.Nongjok A. Banrai C. Uthai Thani, covering approximately 4 square km or 2,500 rai.

Tier 2: arsenic assays ≥ 100 ppb in surface water, encompass 14 villages of B. Putakien, Maiphongam, Koksaard, Nongmaikean, Tapfaimai, Keanpetpilin, Nongmaitai, T. Nongjok; B. Lanka, T. Nongbomklouy, A. Banrai, C. Uthai Thani; B. Nongyaingern, Bungyang, Wangthong, Wangkan, Phunglouang, T. Wangkan, A. Danchang, C. Suphanburi; and B. Huaisong, T. Sukduenha, A. Noen Kham, C. Chainat; covering approximately 65 square km or 40,000 rai..

Note that the 100 ppb line is open at T. Wankan due to the fact that not enough samples in the area.

Point sources of arsenic are picked from distribution pattern of arsenic in water and sediment, topography, arsenic mineralization style as well as geological environment.

Although, initial fieldwork at the tin-tungsten prospective area of K. Koktungkung found no evidence of primary sulfide minerals such as pyrite or arsenopyrite, only some iron oxides are found on the surface. Still, K. Koktungkung

remains the most likely important point source of arsenic. Arsenic in this area radially distribute into water channels of 10 villages: Tapfaimai, Lanka, Huaisong, Bungyang, Wangthong, Wangkan, Phungluang, Nongyaingern, Nongmaitai and Keanpetpailin. Arsenic from this source is limited to the south-east side of the water channel running from B.Nongmaitai to Nongmaikean.

On the other north-west side of the water channel, west of B. Nongmaitai, Keanpetpailin, Nongmaikean, arsenic remains high in water indicating other sources beside from the K. Koktungkung. High arsenic assays were obtained around B. Putakien and Maiphongam which located in different catchment basin to the K. Koktungkung, so, the areas may hold some concealed arsenic sources. Very high arsenic in water (Tier 1 area) is present at Wat Nongmaitai; so an arsenic source should be in this area as well.

In summary, there are 4 possible point sources: (1) K. Koktungkung, (2) west of B. Putakien and Maiphongam, (3) Wat Nongmaitai, B. Nongmaitai, and (4) west of B. Nongmaikean (Fig. 5).

Luckily, later field work at an under-construction water reservoir of B. Nongmaikean in July 2019, has found outcrops of altered granite with thin (<5cm) quartz veins and arsenic rich sulfide minerals (Fig. 6). Rock chip samples of mixed altered granite with weathered sulfides minerals and altered granite gave 4,890 and 25 ppm arsenic respectively. This evidence confirms an arsenic source. However and inexplicably, 2 water assays at this reservoir gave 20 and 23 ppb arsenic which are in the normal range.

Conclusions and Remarks

1. Geochemical prospecting techniques are an effective tool to outline the risk areas and to identify the sources. It also demonstrates that elevated arsenic sources not only from known tin-tungsten mining areas but also from other concealed sources. In this case, water samples are more practical than sediment samples, but both should be concurrently conducted for confirmation. It is estimated that arsenic may be mobilized for 10 km from a source.
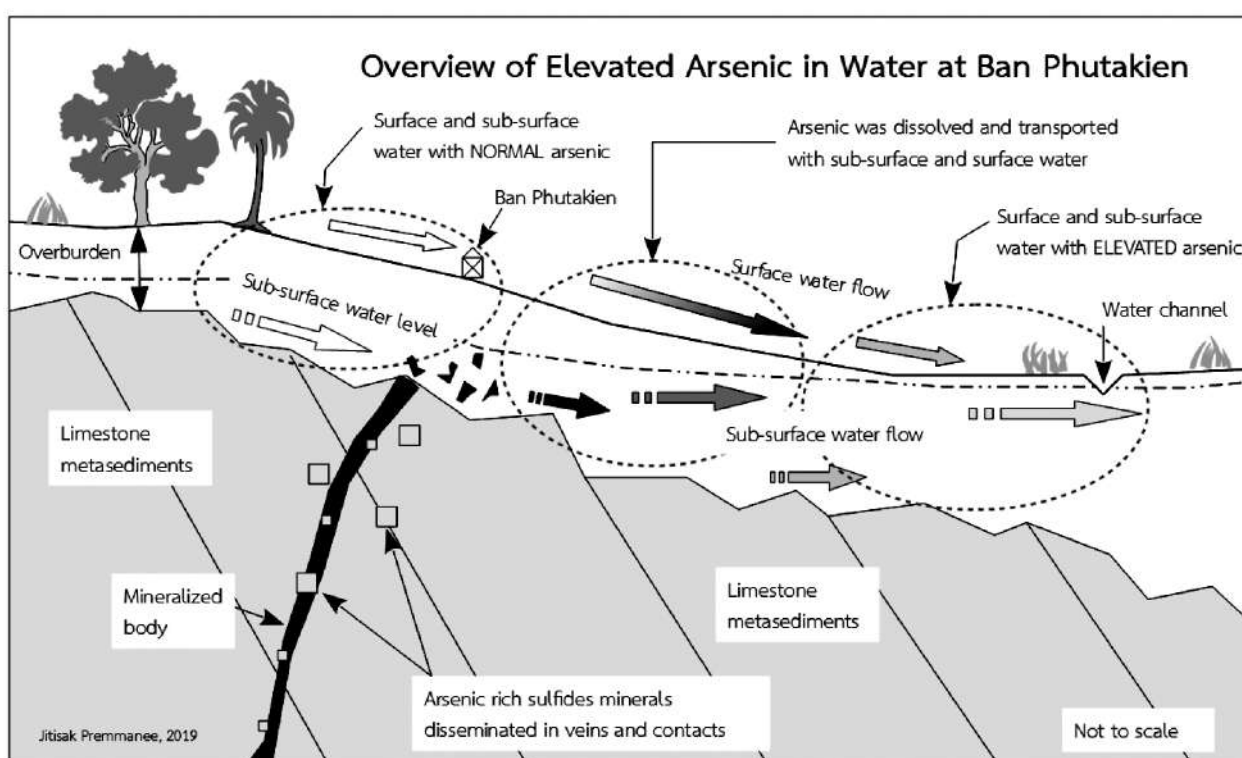
Figure 4: Possible transport mechanism of arsenic at Ban Phutakien, Banrai, Uthai Thani.
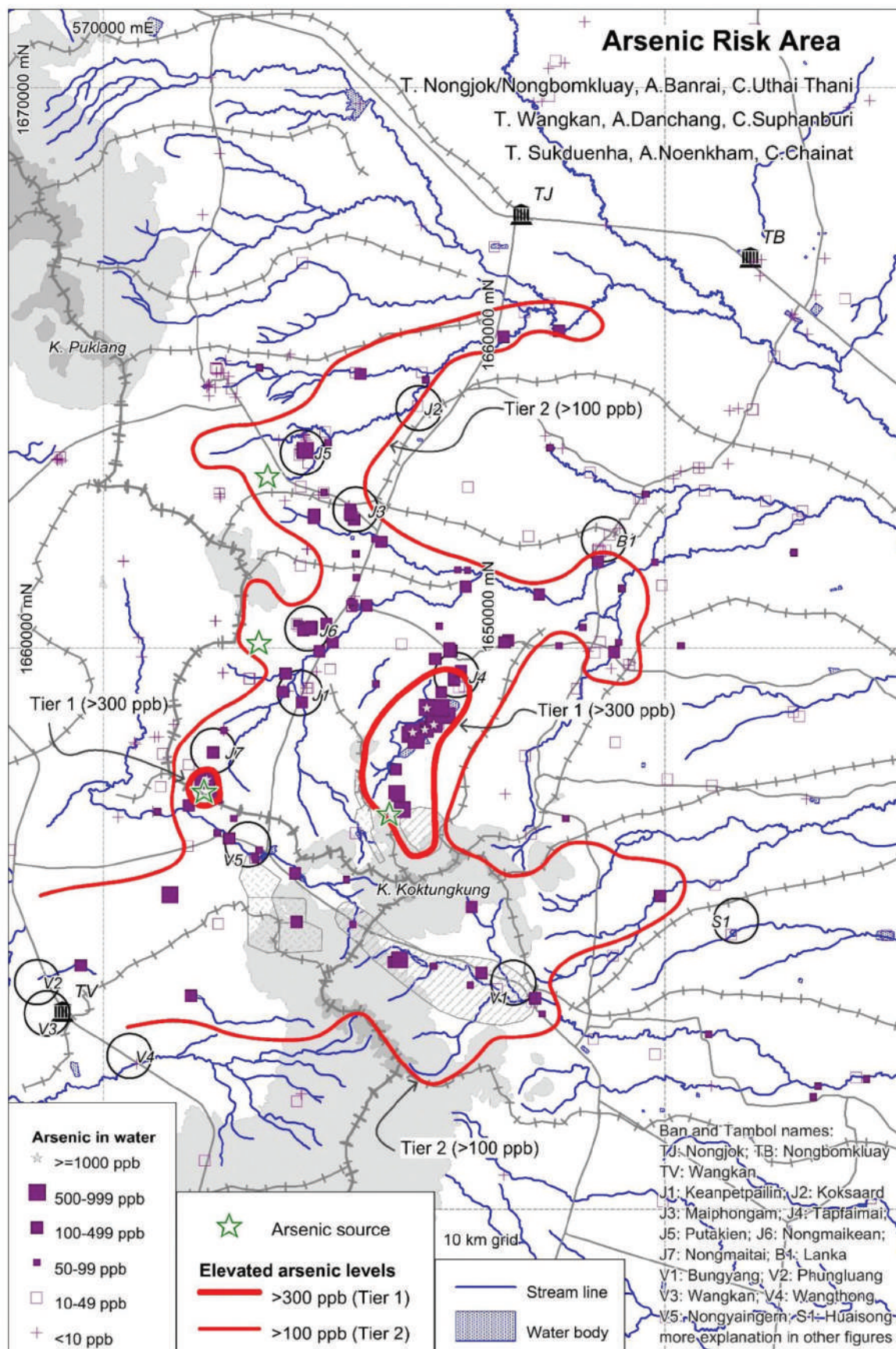
Figure 5: Arsenic risk areas, Banrai/Danchang/Noenkham, Uthai Thani/Suphanburi /Chainat.

Figure 6: Nongmaikean water reservoir showing quartz veins in altered granite with disseminated arsenic rich sulfide minerals.

2. The 100 ppb threshold value in surface water assay, a simple and rational figure, has separated the risk area in this study, but may not be effective in the others. However, the figure may be used for a quick evaluation basis beside the MPL values (10-50 ppb for drinking and consumable water).

3. Local residents in the risk and nearby areas should be mad aware of this elevated arsenic in surface water. Large water supply system should consider bringing from outside the risk area with acceptable arsenic level. Rain water is the best alternative for drinking water.

4. Any related government authorities should continue their rolls in the area, such as UTPHO, DMR, Local Administrative Offices, etc.

5. A few research type questions remain un-answered, such as low arsenic content in water at the reservoir where some rich arsenic sulfide minerals was identified, distribution pattern or behavior of arsenic in surface and ground water at B. Phutakien, or dispersion distance of arsenic from source into water system and surrounded area.

References

Department of Disease Control. (2019). *Disease Caused by Arsenic or Its Toxic Compound.* http://envocc.ddc.moph.go.th/contents/view/187 (in Thai)

Hazardous Waste Test Methods. (2019). *Hazardous Waste Test Methods / SW-846.* https://www.epa.gov/hw-sw846

Jariyawat, P. (1996). Tin Deposit in Central Thailand, *in Economic Geology Division Meeting Year 1996,* Department of Mineral Resources, Bangkok, p.132-143 (in Thai).

Pollution Control Department of Thailand. (2020). *Standard for Arsenic in Drinking Water.* http://www.pcd.go.th/info_serv/reg_std_water01.html#s3 (in Thai)

Pollution Control Department of Thailand. (2020). *Standard for Arsenic in Surface Water.* http://www.pcd.go.th/info_serv/reg_std_water 05.html#s3 (in Thai)

Pollution Control Department of Thailand. (2020). *Standard for Arsenic in Ground Water.* http://www.pcd.go.th/info_serv/reg_std_water 03.html (in Thai)

Pollution Control Department of Thailand. (2020). *Standard for Arsenic in Agricultural Soil.* http://www.pcd.go.th/info_serv/reg_std_soil01.html (in Thai)

Premmanee, J. (2019a). *Study on Possible Sources of Arsenic Distribution in Uthai Thani province,* Department of Mineral Resources, Bangkok, 79p. (in Thai)

Premmanee, J. (2019b). Arsenic and Cadmium: Under the DMR Hazardous Elements Project, *in Geothai 2562,* at The Berkley Hotel Pratunam, Bangkok, 16-17 September 2019, p. 3-5.

Standard Methods For the Examination of Water and Wastewater. (2017). 3113 Metals by Electrothermal Atomic Absorption Spectrometry. https://www.standardmethods.org/doi/10.2105/SMWW.2882.045

World Health Organization. (2020). *Arsenic.* https://www.who.int/news-room/fact-sheets/ detail/arsenic

Transition between the Thabsila metamorphic complex and the Lower Paleozoic formations and their sandstone provenance, Kanchanaburi, western Thailand

Sirot Salyapongse, Praipada Santadgarn, Panus Hong, Suwijai Jatupornkongchai, Ekkachak Chandon and Prinya Putthapiban*

Geoscience Program, School of Interdisciplinary Studies, Mahidol University,
Kanchanaburi Campus, 199 Moo 9, Sai Yok, Kanchanaburi, Thailand, 71150.
*Corresponding author: prinyapp@gmail.com

Abstract

In Kanchanaburi province of western Thailand, the oldest three rock units include the Thabsila regional metamorphic complex exposed side by side with the Cambrian Chao Nen and the Ordovician Tha Manao formations, possessing field relation, petrography and geochemistry strongly suggesting a transitional relationship. The latter two rock formations are equivalent to the Cambrian Tarutao Group and the Ordovician Thung Song Group from southern Thailand. They are characterized by alternating lithofacies of argillites, siliciclastics and carbonates. The gradational nature among them both in lithology and grade of metamorphism with only a single mode of foliation development indicates one episode of progressive regional metamorphism. Modal compositions of the Upper Thabsila and the Chao Nen meta-siliciclastic sandstones show them as original quartz arenite and subarkose to arkosic sandstones. Their provenances was from a continental block setting. The chemical discrimination diagrams indicate they have been deposited in a passive continental margin environment and have an asymmetrically cyclic sedimentation habit. This evidence implies that there is no unconformity between the Thabsila complex and the Lower Paleozoic formations. Although this terrain was subjected to a series of northwest dextral strike-slip fault movement, their gradational nature in grades of metamorphism is, in part of some sections, still preserved. Their sharing of the same provenance and the tectonic setting show that they were continuously deposited throughout the long history of the Shan-Thai terrane (up to as young as around Carboniferous, the timing of tectonically uplifting by the incoming of volcanism to this terrane). The underlying older Precambrian basement, the source rock of the Thabsila complex have never been observed. Probably have been re-melted to the common foliated Triassic S-type granite in western Thailand.

Key words: Cambrian, Ordovician, regional metamorphism, sandstone provenance

I. Introduction

The lithologic transition between the Thabsila complex and the lower Paleozoic rocks exposed in Kanchanaburi and northern Thailand areas have been questioned for many decades since the German Geological Mission to Thailand (1972) and Bunopas, (1981). The study area is along the road to Sri Sawat district, passing along the Khwae Yai river between Ban Tha Manao and Ban Mong Krathae, Kanchanaburi (Fig. 1). Nevertheless, most of the mentioned records did not study throughout the area but rather concentrated on the known problematic sites. The data under the DMR Hazardous Element Project systematically cover parts of the area in Suphanburi and Uthai Thani, but no sampling in nearby Chainat provinces.

This paper characterizes the apparent similarity between the quartz mica schist, quartz schist and the foliated feldspathic quartzite of the Upper Thabsila complex and the Cambrian Chao Nen feldspathic (-micaceous) quartzites, and shows a commonality in sedimentary, petrographic mode, provenance and geochemistry that constrains their transition.

II. Geological setting

In relation to the field relationship between the high grade Thabsila complex and the nearby Lower Paleozoic (Chao Nen and Tha Manao) formations, the conclusion has been drawn earlier since the time of the German Geological Mission (1972), and subsequently Bunopas (1981) who confirmed the German Mission's
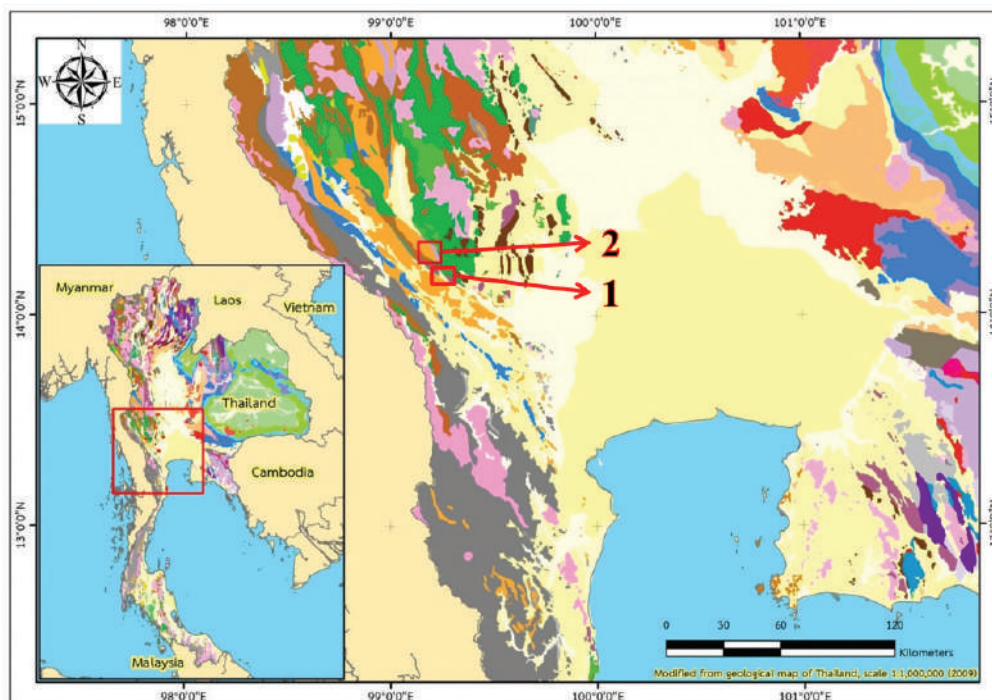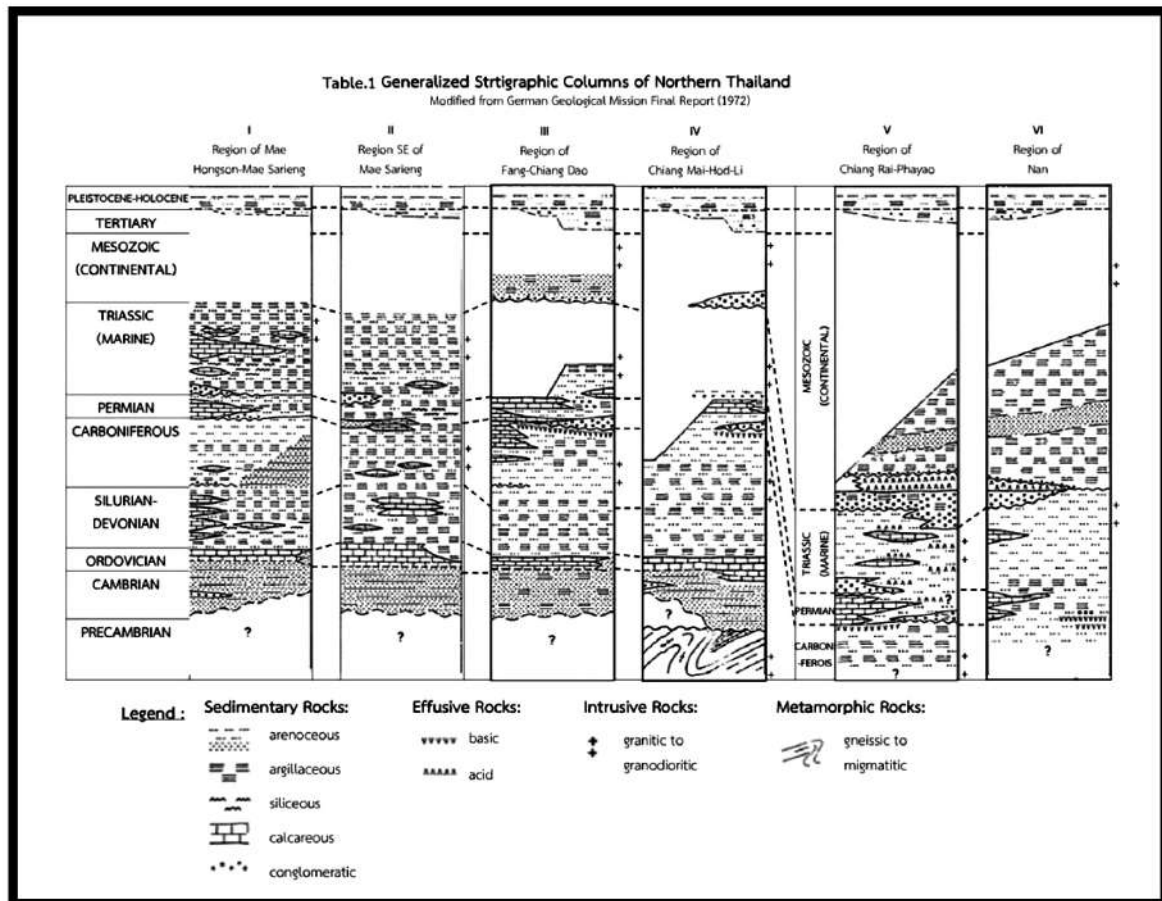
Figure 1: Index map showing the studied area of the Thabsila complex (1) and the Chao Nen-Tha Manao formations (2) adjacent to the Khwae Yai River, in Kanchanaburi.

conclusion that in most of the places, there is an obscured and questionable unconformity with subsequent slip movement. Bunopas (1981) noted that, there is a drastic change in metamorphic grade in many places between the higher grade Inferred Precambrian and the lower grade Lower Paleozoic rocks in Thailand. This contact relation is generally a fault contact.

In Kanchanaburi (table 2), the metamorphic nature of the lower Paleozoic rocks is quite clearly developed and distinctive cleavage is obvious. For the regional metamorphic rocks that have been subjected to only one episode of metamorphism and range in grades from higher Amphibolite facies progressively lowering to slate or cleaved rock of the lower Greenschist facies and faded away around the Upper Paleozoic rocks. The other kind of metamorphic rocks belonging to the occurrence from contact metamorphism by large body of foliated Triassic S-type, volatile rich granite which is common and widespread in isolated intrusions ranging from batholith to small satellitic and isolated bodies (pluton) but conjoined at depth forming a large batholith. This kind of foliated contact metamorphism is affected only to the lower grade part of the regional metamorphism. By the time of intrusion, the relative thermal control between the intruding and the intruded rocks must be the important

control on the occurrence of the foliated contact metamorphic rocks being generated (Salyapongse et al., 2015). Generally, once the originally regional lower grade country rocks have been upgraded to a higher grade and mimically imitated the original foliation and increasing grades up to even calc-silicate rocks and sillimanite mica schist originated from a commonly low-grade Cambrian to Siluro-Devonian rocks.

Nanthasin et. al, (2012) summarized the Thabsila metamorphic complex into four units based on lithology from younger to older units: (1) Unit A is composed of marble, mica schist and quartzite, (2) unit B comprises mylonites, (3) unit C is composed of calcsilicate, and (4) unit D comprises various gneisses. Their approximation has been based on geothermobarometric and pseudo section of the 4 Thabsila unit as indicating PT ranging from Lower T / intermediate P at 500-650 °C / 5-6.5 Kb up to 640-719 °C / 5.5-8 Kb, probably of Barrovian Facies Series conformably from top to bottom as a progressive sequence. The ages of metamorphic events in western Thailand is controversial. Nanthasin et. al, (2012) gave a metamorphic age of Eocene which contradicts the earlier interpretation on meta morphism age which quoted as Late Triassic (Hansen et al, 2014), and thought to represent a Barrovian Facies Series. Generally, the dislocated

Table.1 Generalized Strtigraphic Columns of Northern Thailand
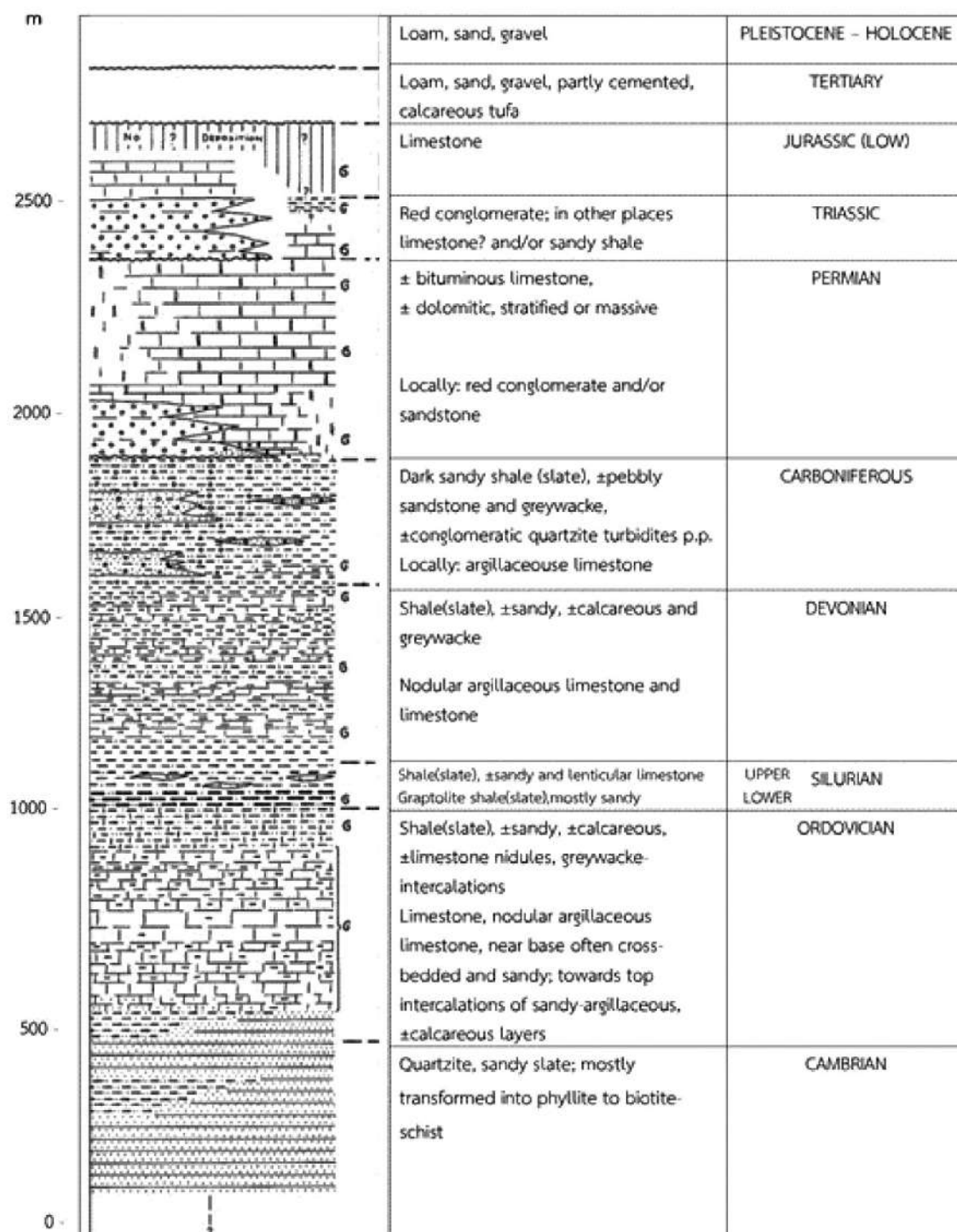Modified from German Geological Mission Final Report (1972)

metamorphism is restricted to a narrow fault zone which obviously from Nanthasin et. al's description of mylonite unit that seems to be restricted only in the zone B. On the other hand, it is doubtful that the cataclastic metamorphism is high grade enough for the recrystallization of the zircon and produced the Thabsila metamorphic complex which cover an area more than one thousand square kilometer. The commonly tourmaline rich accessory mineral in various kind of rock for example quartzite and quartz schist in Thabsila area is very common as the same as that commonly found in metamorphic pegmatite. A very interesting publication by Hay and Dempster (2009), presented a special kind of low temperature metamorphism which induced a zircon rimming indicating quite young event. Since the Zr age was derived at 55 my which is quite young and seems to relate to the Eocene collision between Asia and Eurasia since the last 55 Ma. However, a detailed survey by Musikarak (2019) reported the event of Eurasia–India collision is related to a dextral movement and only caused brittle deformation contrasting with the common ductile feature in this area which is sinistral and originated earlier.

III. The Upper Thabsila meta-siliciclastic sandstones

This unit, which is about 2400 m thick belonging to the upper part of the Thabsila is exposed just across the Khwae Yai River fault valley to the west around Ban Pong Pat near Tha Thung Na dam (Table 3 and Fig. 2). Generally, the transferring of the Upper Thabsila sequence to the Lower Paleozoic rocks frequently has been obscured by faulting and specifically around the Tha Thung Na area (Fig. 2). Observation along the Khwae Yai fault zone by traversing their geologic cross-section for many kilometers down south revealed an obviously through a unique key bed containing a characteristic metamorphic mineral allowing their equilibration very nicely along both side geology, and can be concluded as an early remark that, the Khwae Yai fault zone was a kind of horizontal strike-slip fault and having dextral offset around 15 km. Even though the lack of unconformity evidence, Bunopas (1981) has assigned the age of the Thabsila as inferred Precambrain basing on their apparent difference in grades of metamorphism as had been impressed at that time.
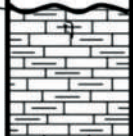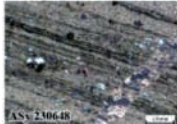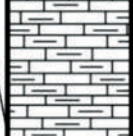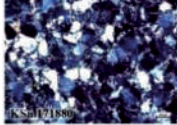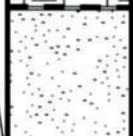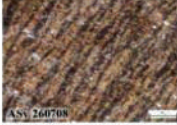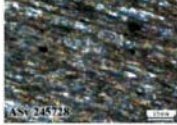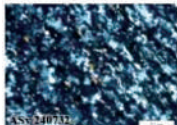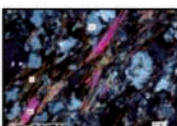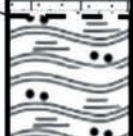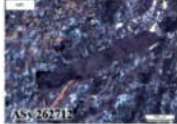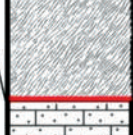
Table.2 Generalized Stratigraphical Column Region Sri Sawat -Thong Pha Phum – Sangklaburi Western Thailand

Modified from German Geological Mission Final Report (1972)

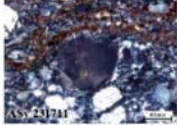| m	Lithology	Description	Age
		Loam, sand, gravel	PLEISTOCENE – HOLOCENE
		Loam, sand, gravel, partly cemented, calcareous tufa	TERTIARY
		Limestone	JURASSIC (LOW)
2500		Red conglomerate; in other places limestone? and/or sandy shale	TRIASSIC
2000		± bituminous limestone, ± dolomitic, stratified or massive Locally: red conglomerate and/or sandstone	PERMIAN
		Dark sandy shale (slate), ±pebbly sandstone and greywacke, ±conglomeratic quartzite turbidites p.p. Locally: argillaceouse limestone	CARBONIFEROUS
1500		Shale(slate), ±sandy, ±calcareous and greywacke Nodular argillaceous limestone and limestone	DEVONIAN
1000		Shale(slate), ±sandy and lenticular limestone Graptolite shale(slate),mostly sandy	UPPER SILURIAN LOWER
500		Shale(slate), ±sandy, ±calcareous, ±limestone nidules, greywacke-intercalations Limestone, nodular argillaceous limestone, near base often cross-bedded and sandy; towards top intercalations of sandy-argillaceous, ±calcareous layers	ORDOVICIAN
0		Quartzite, sandy slate; mostly transformed into phyllite to biotite-schist	CAMBRIAN

Table 3. Stratigraphic column of Thabsila metamorphic complex (reconstructed) and Chao Nen-Tha Manao formations in Kanchanaburi.

AGE	THICKNESS	STRATIGRAPHY	LITHOLOGY	ZONE	THIN SECTION	DESCRIBE
Quaternary	20 m		Gravel, sand, silt, clay			Alluvium and fluvial sedimentary deposits
Ordovician	900 m		Meta-argillaceous limestone	Tha Manao	ASy 230648	Thick beded meta-argillaceous limestone, grey color
Cambrian	600 m		Meta-sandstone	Chao Nen	ASy 718809	Thin beded meta-sandstone, medium to fine grained and moderately sorted
Upper Precambrian (Upper Thabsila)	312 m		Slate	Thabsila Zone D	ASy 260708	Grey-greenish slate, fine grained, intensively eroded
	249 m		Phyllite and schist interbeded with quartzite	Thabsila Zone C	ASy 245728	Grey phyllite, phylliticschist with kyanite and andalusite porphyroblast
	20 m		Meta-limestone			Banded quartzite, medium grained and well sorted, fused quartz grain and foliated
	515 m		Quartzite		ASy 240732	
	80 m		Calc-silicate, Marble			Thick quartzschist, coarse grained, shows schistosity, micaceous rich
	776 m		Quartz-mica schist	Thabsila Zone B	ASy 236730	
	400 m		Schist and fgr paragneiss		ASy 262712	Thin layer schist and shows schistosity with sillimanite and fibrolite.
Lower Precambrian (Lower Thabsila)	500 m		Calc-silicate		ASy 231715	Brownish green, coarse grained, show foliated silica and carbonate minerals
	250 m		Gneiss	Thabsila Zone A	ASy 231711	Coarse to med grained, alternated light and dark bands
	>300 m		Migmatite		ASy 214738	Dark grey-black, coarse grained with partly melted leucocratic vein and restite

Table3.1 Symbols of Stratigraphic column of Thabsila metamorphic complex and Chao Nen-Tha Manao formations in Kanchanaburi.

Figure 2: Geologic map of the Thabsila sequence.
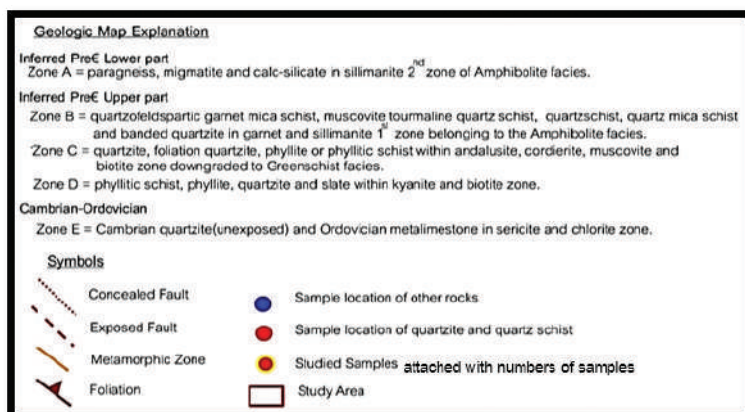
Figure 2.1: Explanation of Thabsila metamorphic complex.

The geologic map of the Thabsila meta morphic complex (Fig. 2) has been subdivided into the Lower and the Upper parts and in zones from A to E, as a revised version from Muang-phongoen and others (2015). Both the Lower and the Upper Thabsila units, have been subdivided into zones lithologically and structurally more or less coincident with the many insignificant fault lines (Fig. 2). The contrast in grades of metamorphism is noticeable also in the meta-siliciclastic sandstones, which alternate with other meta-pelitic rocks only in the Upper Thab-sila unit. However, the Upper unit exhibits a transition from a lower grade, finer-grained biotite paragneiss (Fig. 3) grading to a coarser-grained banded or augen biotite-horn-blende/quartzo feldspathic paragneiss with calc-silicate and migmatite in the lower part.

Figure 3: ASy 232731. Fine-grained paragneiss started segregation into many thin leucocratic threads, an indication of a lower grade paragneiss, which has been increased to a higher grade, rendering more thicker bandings and developing feldspathic augen when moving to the west. Ductile shearing is considered localized and not show consistent or extensive distribution.

Generally, all the northwestern strike-slip faults were horizontally dislocated parallel to the metamorphic layering, so that their consecutively transitioning nature are still preserved and can be recognizable along strike across their transitional zone (Fig. 4). This has been observed to establish throughout the stratigraphic column westwardly, although many fault lines have been detected (Fig. 2). The sequential evolution of the mineral assemblages in the Upper Thabsila complex

Figure 4: Horizontal slip fiber (slickenside fibers) in the meta-limestone cliff which developed on the bedding plane of Permian limestone exposed along a road-cut outcrop next to the nearby dextral movement strike-slip fault.

(Salyapongse, et. al., 2019), as well as an eastward decreasing in grades of metamorphism, have been described also from the intercalated pelitic horizons by Muangphongoen et al., (2015). Within the Upper Thabsila unit, however, there are many horizons of quartz-mica schist, quartz schist, and foliated quartzite which are here referred to as meta-siliciclastic sandstones alternating with other meta-pelitic rocks only in the Upper Thabsila complex. Correspondingly, both of the meta-siliciclastic horizons and the meta-pelitic horizons are exhibiting conformably and progressively decreasing in grades eastward in the same fashion and prograding further to the younging direction towards the Lower Paleozoic as well. Another important lithological type was found as alternating calc-silicate, marble and meta-limestone at least two lensoid bodies have been detected.

III-1. Petrographic analysis of the Upper Thabsila meta-siliciclastic sandstones

The Upper Thabsila sequence from high to low grade starts the alternating sequence with lower grade biotite paragneiss (Fig. 3), quartz-fibrolite-garnet mica schist, quartz schist, andalusite phyllitic schist, banded quartzite, andalusite quartzite, andalusite-kyanite phyllitic schist/phyllite, foliated quartzite and slate (See more detail in Fig. 2). These packages of rocks have strike-slip fault contact with the Lower Paleozoic rocks. In the lowest part overlying the fine-grained biotite paragneiss, a mica schist unit illustrates a foliated texture defined by mica and quartz with hardly recognized minor feldspar, localized red garnet, biotite, fibrolite and muscovite with accessories apatite and zircon

(sample no.1 in Table 4). Further in the younging horizons, particularly in the meta-siliciclastic sandstone, they are characterized by dominant muscovite over the biotite and the mineral grain sizes are sharply reduced. (Figs. 5-7). This textural feature shows a decrease in grain size along with a reduction in grade of metamorphism. Considering the whole Upper Thabsila complex, the original sedimentary protoliths show an increasing maturity toward the younger beds (sample no.5 and 6 see Fig. 2 and Fig. 18). To facilitate feldspar identification for point counting, it can be accomplished by etching the uncovered thin section with conc. HF for about 20 seconds (Figs. 12 and 13). By this method, the feldspar relief becomes more distinctive than quartz and turned extinct in XPL.
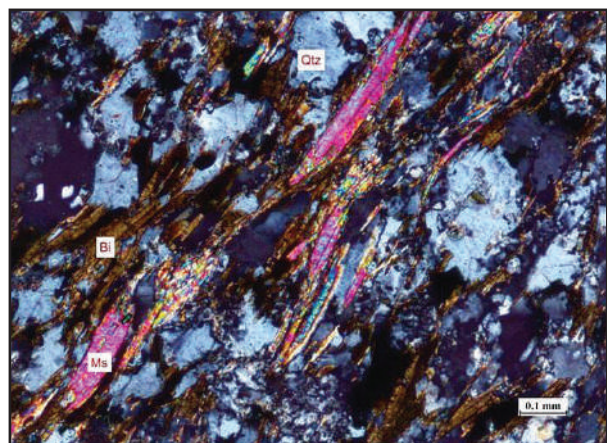
Figure 5: ASy 236730 (no. 1, Zone B) XPL Quartzofeld-spathic garnet mica schist showing foliated texture defined by biotite and a lesser amount of muscovite including with garnet and apatite. The availability of the feldspar is hardly identifiable if it lacks twinning. Comparatively the mica grains are distinctively larger grain sizes than the lower grade units to the east. (Abbrev: ASy = Amphoe Sai Yok 1:50,000 map sheet)
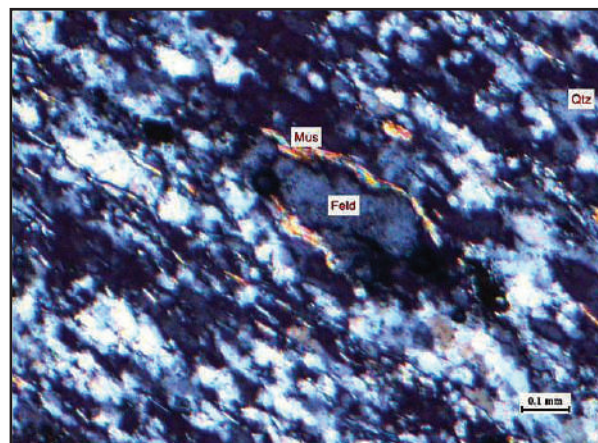
Figure 6: ASy 243730 (no.4, Zone C) XPL. Foliated quartzite in of lower grade, having foliated texture defined by elongated quartz aggregates with minor muscovite and opaque minerals. Tourmaline is quite common in the Upper Thabsila. Accessory zircon is usually detected. (Abbrev: ASy = Amphoe Sai Yok 1:50,000 map sheet)
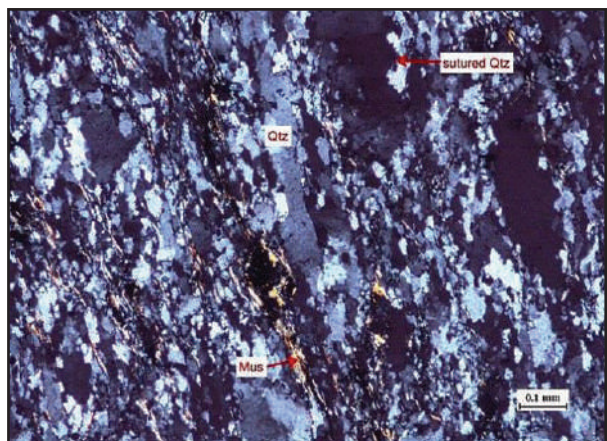
Figure 7: ASy 257720 (no. 6, Zone D) XPL. Foliated quartzite further eastward, exhibiting foliated texture defined by a very fine-grained flake of muscovite and an elongated quartz aggregate showing sutured grains caused by metamorphism and deformation with accessory zircon. (Abbrev: ASy = Amphoe Sai Yok 1:50,000 map sheet)

IV. The Chao Nen and the Tha Manao meta-siliciclastic sandstones

The Cambrian Chao Nen and the Ordovician Tha Manao rock sequences were formed as elongated bodies sub-parallel to the north-west-trending Si Sawat dextral strike-slip fault zone more or less running along the Khae Yai river valley. Upper Paleozoic and the Mesozoic continental red beds can be respectively observed to the west and far west. Whereas the marine Permian clastic rock units with the fusulinid *Monodiexodina* sp. in a small limestone lens, occurr in a dislocated fault-slab within the fault zone along the Khwae Yai river valley (Fig. 8). The Chao Nen and the Tha Manao formations (Fig. 8) exposing further north along the road, were proposed by Bunopas (1981) to be originally deposited as a continuous sequence from siliciclastic rich graded to calcareous sandstone, sandy limestone, limestone and argillaceous limestone characterizing upward facies change of the two rock units. The total thicknesses of these rock sequences are approximately 3,500 m.

Geologic map of the Chao Nen quartzite
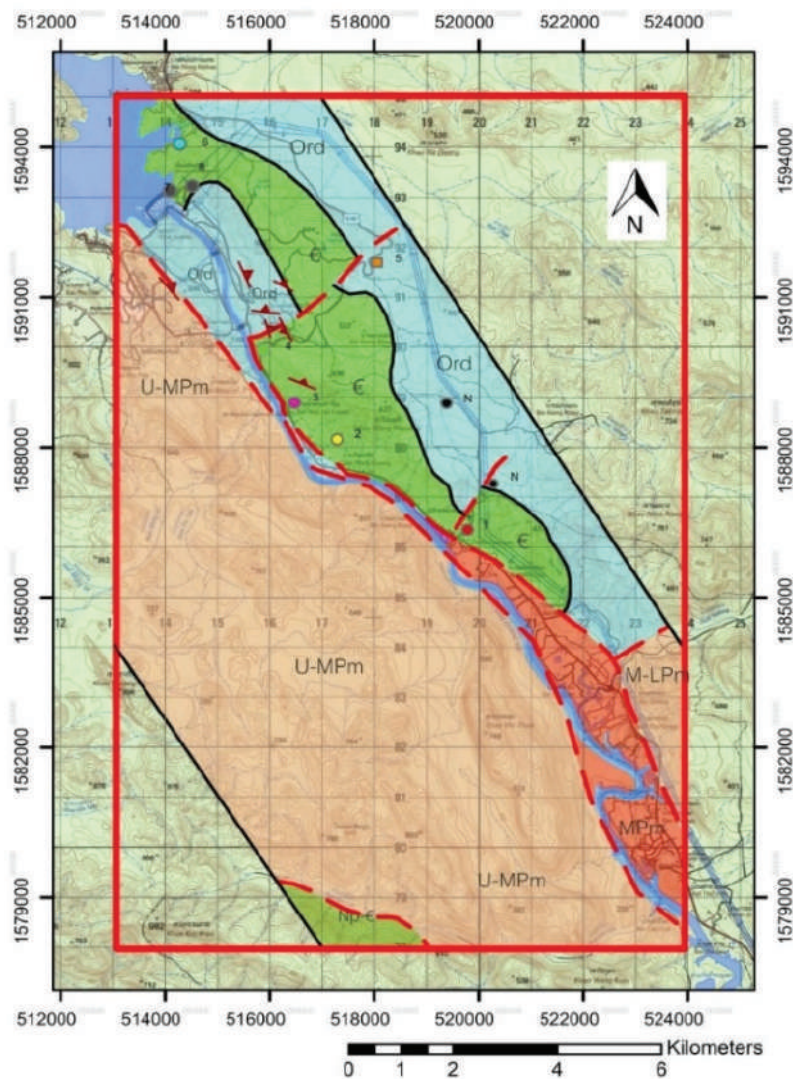
Figure 8: Geologic map of the Cambrian Chao Nen and the Ordovician Tha Manao.

Geologic map Explanations

U-MPm = Meta limestone graded to limestone with fusulinid
MPm   = Volcaniclastic sandstone, *Monodiexodina* sp. bearing calcareous sandstone and sandy limestone lense
M-L Pm = Volcaniclastic sandstone and meta banded limestone
Ord   = Meta-argillaceous limestone with Nautiloid
Є   = Meta-argillaceous arkosic to subarkosic sandstone and calcareous sandstone
Np-Є   = Paragneiss, schist and calc-silicate

Symbols

Contact
Fault
Attitude
●N Nautiloid fossil
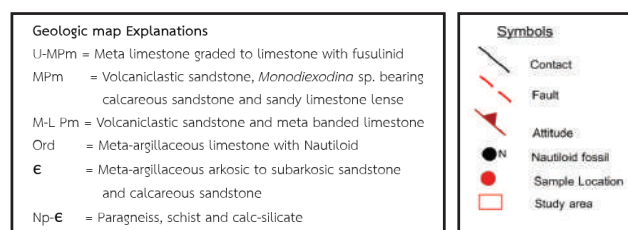● Sample Location
▢ Study area

Figure 8.1: Geologic map explanation and symbols of the Cambrian Chao Nen and the Ordovician Tha Manao formations.

The Cambrian-Ordovician rock sequence has been recognized for quite a long time being extended throughout the western part of the country or along the western Shan-Thai block. They characterize some transitional siliciclastic-carbonate facies of the Lower Paleozoic succession in Thailand. In most localities observed, they are underlain by the inferred Precambrian units and generally demarcated by detachment planes which orientated northwestward. The Chao Nen meta-sandstone and the Tha Manao meta-limestone units are well exposed along road-cut outcrops near to the Srinagarindra dam (Fig. 8) which situated in Khuen Srinagarindra 1:50,000 map sheet.

IV-1. Petrographic analysis of the Chao Nen and the Tha Manao siliciclastic sandstones

Petrographic examination of the Cambrian low-grade meta-feldspathic sandstones suggested that their differences in mineral compositions are basically related to the variation in argillaceous and carbonate or matrix/cement components relative to detrital quartz and feldspar (Figs. 9-13). Since it is a low grade and the generated rock foliation is directly related to the original content of the argillaceous material, the more it contains, the better the foliated texture (see modal comp. no. 1 and 3 in Table 5 and see Fig. 9 and Fig. 10) can be appreciated. In all of the samples, sedimentary relict texture and the original mineral phases are still recognizable although slightly modified by replacements or recrystallization of sericite after clay mineral/feldspar in noncarbonated sandstone and authigenic replacement of calcite after quartz and feldspars in calcareous sandstone (Fig. 13). The incipient low-grade regional metamorphism is locally indicated by the inconsistent development of the foliation as well. In terms of metamorphic zoning, the occurrence of sericite in the Chao Nen sandstones considered successively lower grade than the biotite-muscovite zone of the Upper Thabsila (Fig. 7 and Fig. 9).
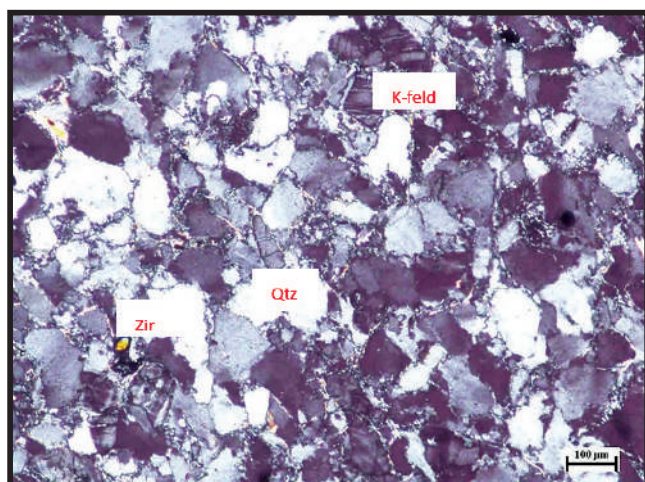
Figure 9: KSn 171880 (no. 2) XPL. The Cambrian Chao Nen meta-sericitized feldspathic sandstone showing faintly oriented texture defined by a smaller and minor amount of recrystallized sericite crystals which restricted to the grain boundaries. Note the grain supported with subangular shape nature and minor content of the very fine-grained silica cement plus a lesser amount of inter granular sericite crystals. Probably due to this specimen was originally relatively less argillaceous/clayey material and lower grade of metamorphism so that its foliation is not obvious. Accessory detrital zircon is frequently observed. (KSn = Khuean Srinagarindra 1:50,000 sheet).
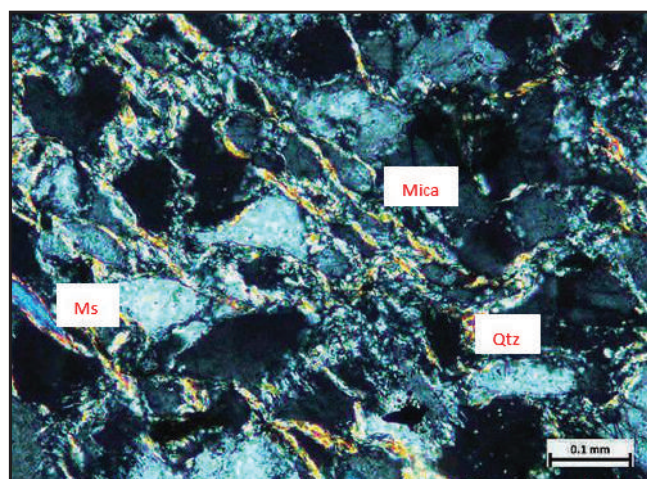
Figure 10: KSn 141932 (no. 7) XPL. Cambrian meta- sericiticitized feldspathic sandstone. It illustrates angular to irregular grains with very fine-grained matrix support and foliated texture defined by recrystallized white mica which in parts replaced after feldspar grains, possibly formed during the transition from diagenesis to low-grade regional metamorphism. A bigger muscovite grain is possibly detrital muscovite. Note the matrix-supported texture probably originally was argillaceous rich now has been recrystallized mainly to micro quartz and foliated white mica. (KSn = Khuean Srinagarindra 1:50,000 sheet)
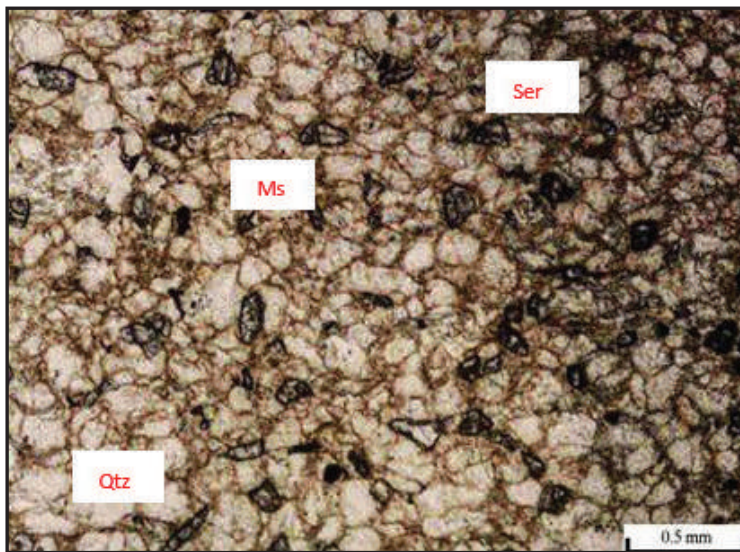
Figure 11: KSn 141931 (no. 3) PPL. Showing a Cambrian Chao Nen meta sericitized feldspathic sandst one compris es higher relief feldspar grains after HF etching to facilitate point counting. (KSn = Khuean Srinagarindra 1:50,000 sheet)
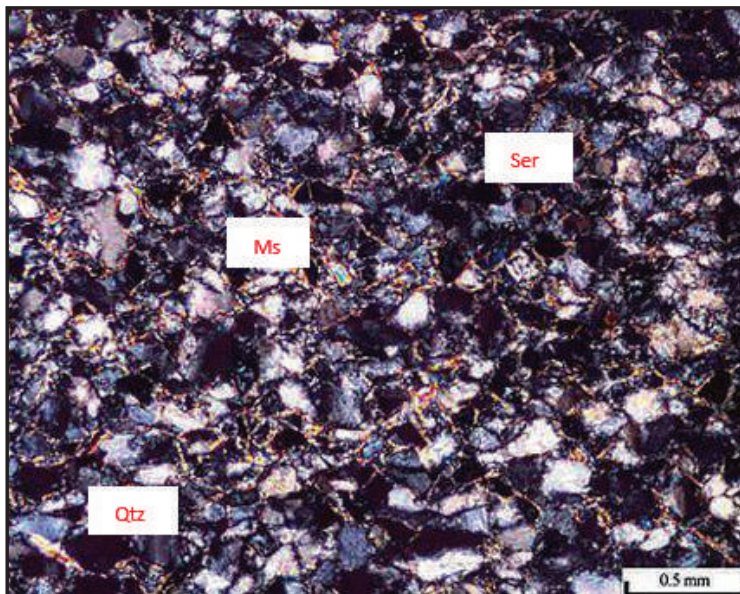
Figure 12: KSn 141931 (no. 3) XPL. At the same po sition. Note the development of sericite faintly oriented within the rare matrix part of the meta sericitized feldspathic subarkose. All the detrital feldspar became extinct. (KSn = Khuen Srinagarindra 1:50,000 sheet)
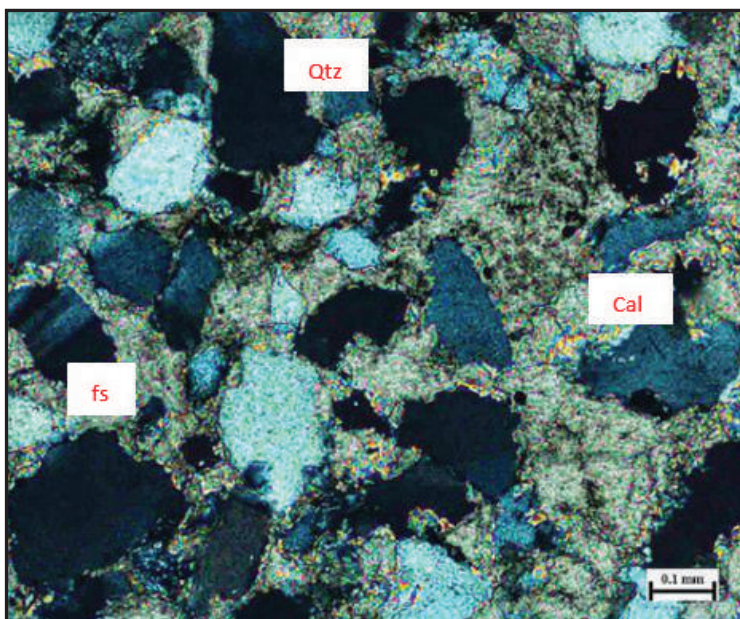
Figure 13: KSn 180918 (no. 5) XPL. Ordov ician calcareous feldspathic sandstone. It shows cement/matrix supported and non foliated texture probably due to carbonation and the rarity of argillaceous material. Note the replacement boundaries of feldspars and quartz (at extinction) by calcite caused the irregularity in grain shape and the reduction in grain size against the replacing calcite. Although calcite appears extensively replaced after quartz and feldspars, this sample will also be included for point counting for a comparison. (KSn = Khuean S rinagarindra 1:50,000 sheet)

V. Results and discussions
V-1. Modal classification and provenance of the Upper Thabsila, the Chao Nen and the Tha Manao meta-siliciclastic sandstones.

Table 4. Modal compositions of the Thabsila complex.

No.	Grain size	Sorting	Foliated	Quartz	Feldspar	Lithic	Others	Recalculated		
								Quartz	Feldspars	Lithic
1	coarse	mod.	yes	78.33	5	0	16.67 (bi,ms,gar,op)	94	6	0
2	med.	mod.	faintly	89.67	3.67	0	6.67 (bi)	96.07	3.93	0
3	fine	well	yes	84.33	0	0	15.67 (bi,mus,zr)	100	0	0
4	fine	well	yes	91	0.67	0	8.33 (ms,bi,tur,py, zr,op)	99.27	0.73	0
5	med.	mod.	yes	90.67	2.33	0	7 (bi,ms,zr,op)	97.49	2.51	0
6	med.	mod.	yes	87	2	0	11 (ms,bi,py, zr,op)	97.75	2.25	0

Abbrev.: ms = Muscovite, ser = Sericite, tur = Tourmaline, op = Opaque and Zr = Zircon

It can be mentioned shortly from the modal analyses (Table 4) that, the samples contain a significant amount of quartz while the lithics, if originally available, must have all been destroyed during the transportation. Feldspar is not high signifying these feldspars from the mode were the leftover from weathering and erosion of the protolith. The other significant constituent is the micaceous minerals, biotite and muscovite, which most of them represented the regional metamorphic origin (Table 4). Orientation and recrystallization of the metamorphic micaceous minerals are the product of regional metamorphism in the later period subsequence to diagenesis. Types of the micaceous mineral developed in both of the Thabsila and the Lower Paleozoic rocks can be equilibrated with the original content and chemistry of the clay matrix in the former siliciclastic sandstones studied.

Table 5. Modal compositions of the Chao Nen Cambrian meta-sandstones and the Tha Manao Ordovician calcareous sandstone (no.5), Kanchanaburi province.

No.	Grain size	Sorting	Foliated	Quartz	Feldspar	Lithic	Others	Recalculated		
								Quartz	Feldspars	Lithic
1	med.	mod.	yes	84.5	12.5	0	3 (ser,ms,op)	87.1	12.9	0
2	med.	well	faintly	89.0	10.0	0	1(ser,zr)	89.9	10.1	0
3	med.	mod.	yes	85.7	11.3	0	3 (ser,tur,op)	88.4	11.6	0
4	fine	mod.	yes	87.2	8.8	0	4 (ser,ms,op)	90.8	9.2	0
5	med.	well	None	72.0	8.0	0	20 (calcite cement)	86.3	13.7	0
6	fine	well.	None	77.0	22.0	0	1 (ser,ms,tur,zr)	77.8	22.2	0
7	fine	mod.	yes	71.5	25.5	0	3 (ser,ms,op)	97.75	2.25	0
8	med.	well	None	79.0	20.0	0	1 (ser,op)	79.8	20.2	0

Abbrev.: ms = Muscovite, ser = Sericite, tur = Tourmaline, op = Opaque and Zr = Zircon

Comparatively the same reading about the modal analysis result of the Lower Paleozoic rocks as that of the Upper Thabsila sequence can be apparent here as well. The percentage of quartz is more or less similar to the Upper Thabsila complex. Feldspar is significantly higher. Micaceous minerals are lesser. Tourmaline, considered to represent a metamorphic phase, is available in this Lower Paleozoic meta-siliciclastic sandstone as well as that was already noted from the Upper Thabsila. It may be useful as a support for a continuous depositional environment between the Upper Thabsila and the Lower Paleozoic sequence. Notably, all these meta-siliciclastic sandstones are devoid of any rock fragment.

The nonuniform foliation development and the textural remnants of a diagenetic process (Figs. 9 and 10) in the Chao Nen, may suggest lower grade metamorphism

V-2. Modal classification and provenance of the Upper Thabsila and the Lower Paleozoic meta-siliciclastic sandstones
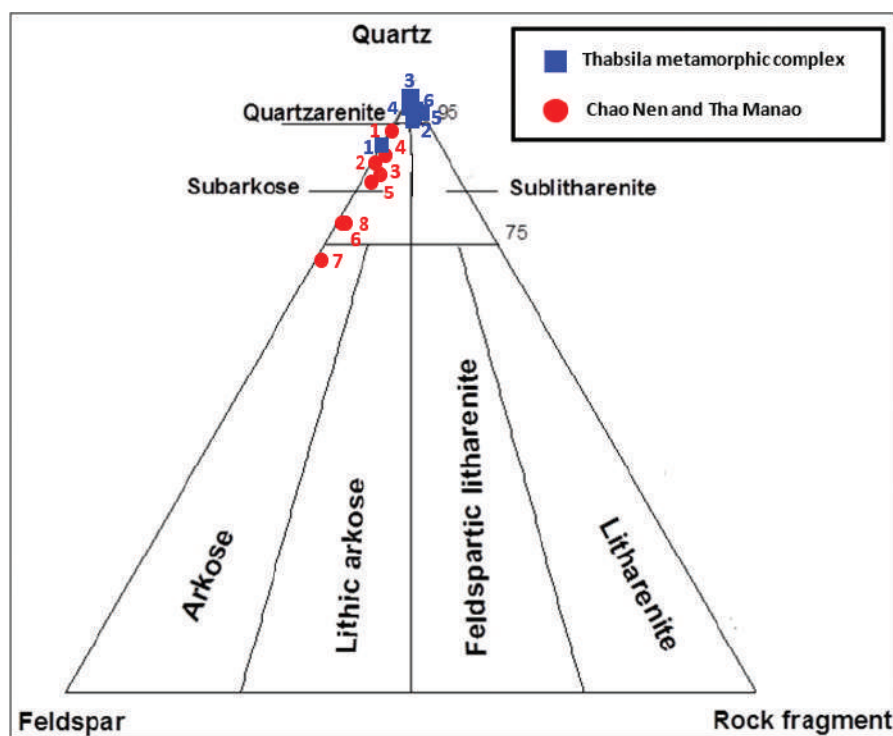
Figure 14: A Quartz-Feldspar-Lithic ternary diagram modally classified altogether the studied met-siliciclastic sandstones to show an evolution in modal composition relatively to their stratification (Folk,1980).

Modally the mineral volume percentages as counted and recorded as QFL percent suggest the compositional classification spanning from arkose to subarkose and quartz arenite. Considering in detail about the degree of maturity relative to lithology from the older to the younger beds, the Thabsila samples are starting mainly with a lesser mature composition, i.e. subarkose (no. 1, Fig. 14) probably with a higher percentage of feldspar and the least quartz content (the sample numbers are running consecutively from older to younger beds), then evolving further to quartz arenite, i.e., much more mature withlesser amount of the original clayey matrix (Figs. 6 and 7). Continuation to the Lower Paleozoic sequence, the sedimentation seems continuing from the more mature (sample no. 1), i.e. from subarkose toward the less mature, the arkose (sample no.7 in Fig. 14). Other than for the modal classification of all the meta-siliciclastic sandstones, the same modal plot can also be used as a provenance categori-zation of the source terrane. All of the meta-siliciclastic sandstones studied illustrate a continental block setting. They share the same provenance.
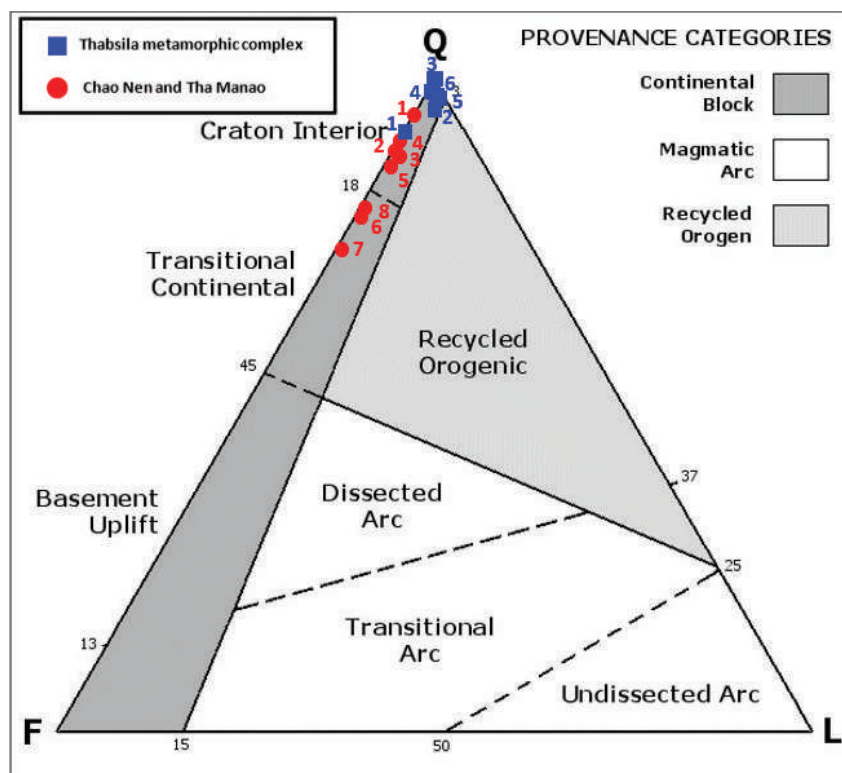
Figure 15: A Quartz-Feldspar-Lithic ternary diagram showing provenance classification basing on the same plot as that of Fig. 14 with the superimposed provenance categories of all the studied meta-siliciclastic sandstones (Dickinson et. al,1983).

V-2.1 Geochemical analyses by XRF of the Upper Thabsila, the Chao Nen and the Tha Manao meta-siliciclastic sandstones.

Table 6. XRF chemical analyses of major oxides from the Thabsila meta-siliciclastic.

Thabsila Sequence							
Oxide	**Samples**						**Aver.**
	1	2	3	4	5	6	
SiO_2	67.41	90.63	92.31	95.88	96.51	96.04	89.796667
Al_2O_3	14.90	4.822	4.446	2.149	2.266	2.37	5.1588333
TiO_2	0.49	0.2478	0.2088	0.2613	0.149	0.1657	0.2537667
CaO	0.5603	0.1157	0.04631	0.00	0.04371	0.00	0.12767
Fe_2O_3	6.072	1.236	0.9419	0.6015	0.5885	0.5474	1.66455
Na_2O	1.879	0.2304	0.7803	0.00	0.00	0.00	0.4816167
K_2O	7.499	2.283	0.9112	0.8313	0.3313	0.6726	2.0880667
FeO	0.00	0.00	0.00	0.00	0.00	0.00	0.00
MgO	0.779	0.2999	0.2003	0.00	0.00	0.08686	0.2276767
SO_3	0.00	0.01137	0.00	0.02368	0.00	0.00	0.0058417
ZrO_2	0.03182	0.03512	0.04323	0.03914	0.02482	0.02823	0.0337267
P_2O_5	0.1021	0.00	0.02383	0.00	0.00	0.00	0.0209883
Cr_2O_3	0.00	0.04028	0.03337	0.05394	0.04481	0.0429	0.0358833

Table 7. XRF chemical analyses from the Chao Nen and the Tha Manoa meta-siliciclastic.

Oxide	Chao Nen and Tha Manao						Aver.
	Samples						
	1	2	3	4	5	6	
SiO_2	90.98	91.74	87.23	89.43	72.97	87.04	85.74125
Al_2O_3	4.04	3.67	6.07	5.18	3.64	5.68	5.5325
TiO_2	0.18	0.2	3.67	0.32	0.19	0.18	0.63375
CaO	1.1	0.1	0.29	0.03	15.77	0.00	2.20375
Fe_2O_3	0.87	0.32	0.62	0.7	1.14	0.78	0.89
Na_2O	0.00	0.00	0.00	0.00	0.00	0.00	0
K_2O	1.97	1.74	2.69	1.91	1.8	3.51	2.71625
FeO	0.00	0.00	0.00	0.00	0.00	0.00	0
MgO	0	0.09	0.26	0.29	1.41	0.19	0.365
SO_3	0.00	0.00	0.00	0.00	0.00	0.00	0
ZrO_2	0.02	0.00	0.07	0.06	0.02	0.02	0.03
$P2O_5$	0	0.05	0.16	0.00	0.08	0.00	0.06
Cr_2O_3	0.00	0.00	0.00	0.00	0.00	0.00	0

When considering the inconsistency in a rock name between the different classification methods of the no.1 Thabsila meta-sandstone (Figs. 14 and 16), it tells subarkose in mode, while its chemical plot suggests wacke. This disagreement can be realized from the current availability of micas, garnet, fibrolite, and other accessories which have not been plotted in Figure 14. All these minerals considered to be a derivative from the original muddy sandstone (or wacke sandstone) before it was metamorphosed to sillimanite-garnet-micas schist. From the chemical analysis (Table 6 and 7), the Na_2O content is only available in the Thabsila no. 1 to 3 and never reappear again even in the Lower Paleozoic rocks. These features probably were related to both original source rock compositional control as well as nature of the transporting medium and the weather condition at the time. Another deviated plot has been observed also with the Lower Paleozoic rock sample of no.5. Its deviation (Fig. 19) is considered to be the result of the the presence of calcite replacement after quartz and feldspar and from its availability as the cementing non-silicate Ca bearing mineral (Fig. 13).

V-3. A chemical classification diagram of the Upper Thabsila, the Chao Nen and the Tha Manao meta-siliciclastic sandstones.
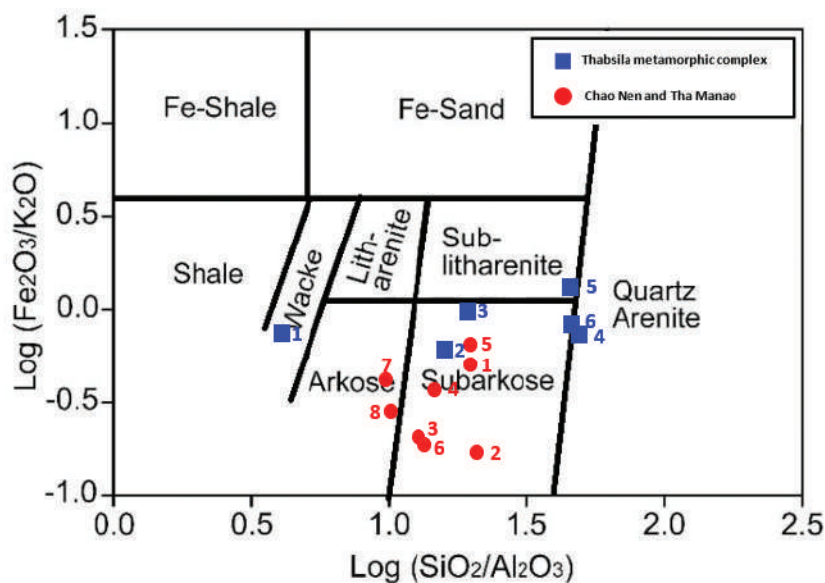

Figure 16: A geochemical classification diagram for the studied meta-siliciclastic sandstones. (after Herron, 1988)

All the sample populations of both the Thabsila complex and the Lower Paleozoic formations are compositionally separated in 2 superimposing asymmetric cycles both are striding the fields of chemical lithologies ranging from wacke to subarkose to quartz arenite for the Upper Thabsila. The Upper Thabsila rocks are compositionally richer in Fe_2O_3 as indicated by the occurrence of many iron-rich minerals such as biotite, garnet, and opaque iron ore. Compared to the plot of the Lower Paleozoic, they are lower in Fe_2O_3

content. The amount of biotite also reflects the Al_2O_3 and K_2O content in the analyses. Another important supplier of the Al_2O_3 is significantly from the feldspars but only K-feldspar will provide a significant amount of K_2O. All these are the variability between the amount of the mineral phases or mode, correspondingly reflected the amount of the major oxides from the chemical analyses of the same rocks to cross-check if either of them can be reasonably correlated.

V-3.1 A tectonic setting discrimination diagram of the Upper Thabsila, the Chao Nen and the Tha Manao meta-siliciclastic sandstones.
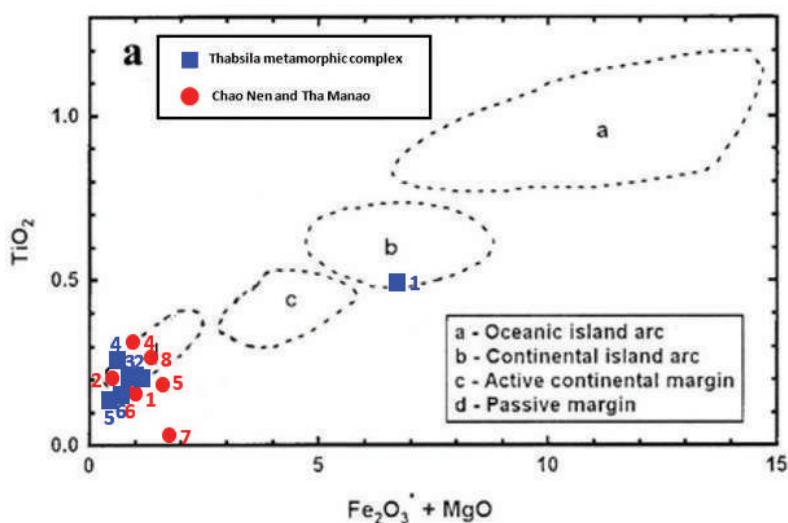
Figure 17 : A tectonic discrimination diagrams (after Bhatia, 1983) for the studied rocks.

Figure 18 shows most of the samples depicting a passive margin tectonic setting. The deviated plot of the Thabsila no1 was due to its composition is more immature, containing more mafic mudrock in the matrix now represented by an increase in the amount of biotite and muscovite among quartz and minor feldspar with additional other minor silicates and iron opaque. More collection of similar samples would fill in the Thabsila sample populations.

V-4. Degree of weathering of the Upper Thabsila, the Chao Nen and the Tha Manao source materials.

This is more or less showing the plot populations are trending in a linear line sloping from the low weathering or more immature toward the intensively weathering or the more mature end. The repeated asymmetric cyclic evolution is also can be apparent to both of the

rock units as well as illustrating in the same fashion to all of the other diagrams (comparing Figs. 15 and 19). Most of the Upper Thabsila and the Lower Paleozoic rocks are generally plotted within the moderate weathering regime. The trend of the Upper Thabsila is reached the intensive weathering zone by no.5, an indication that the no.5 was extensively affected by the intense weathering clearing the original fine-grained materials to the best maturity in the younger sequence far more maturer than the older beds. (See Fig. 18 of Thabsila no. 4, 5, and 6) for a comparison. The Thabsila no. 1 is again also far more deviated but approximately in the same trend. While the Lower Paleozoic samples appear less obvious but roughly showing a cyclic returning from the more weathering regime continuation from the Thabsila towards less weathering in the younger beds.
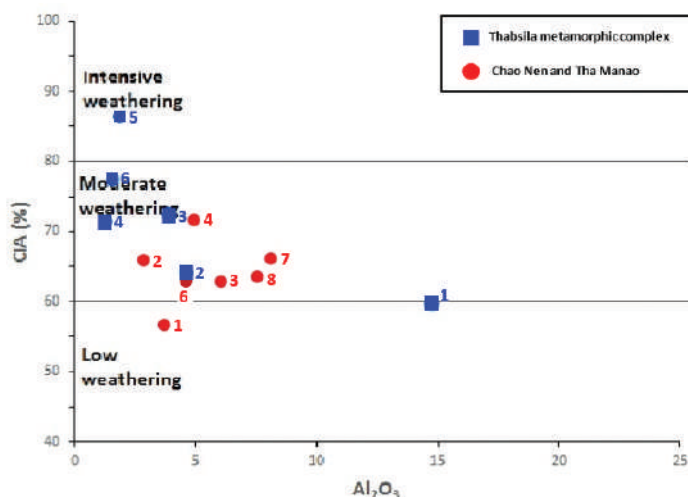
Figure 18: Chemical index of alteration (CIA) of sandstones and its correlation with Al2O3 (after Bonjour and Dabard, 1991).

**V-5. Degree of maturity of the Upper Thabsila, the Chao Nen and the Tha Manao source materials.**
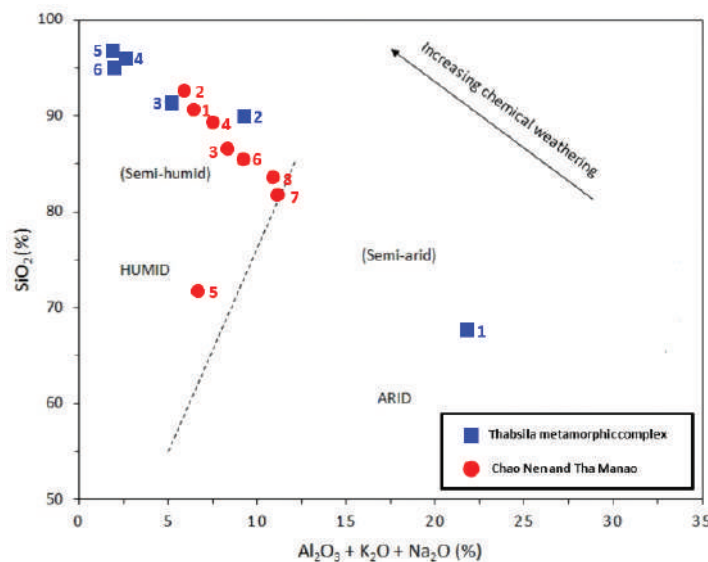
Figure 19: Chemical maturity of the sandstones expressed by the bivariate plot of SiO_2 versus $Al_2O_3 + K_2O + Na_2O$ (After Suttner and Dutta, 1986).

Chemical composition spreading of all the studied meta-siliciclastic sandstones can be seen in (Figs. 18 and 19) as they distributed in the way as to indicate the cyclic repetition suggesting rhythmic or cyclic sedimentation. They have been more or less evolving in the same trend which assuming a repeated compositional variation (silica relative to the $Al_2O_3+K_2O+Na_2O$) both in the Thabsila and the Lower Paleozoic formations. The inclining ratio ranging from SiO_2 66% towards 100% (Fig. 19) suggests all the sample populations of both lithologic groups were of the cyclic evolution starting from sub-mature or wacke composition up to super mature in the Thabsila and then continue a repetition of an asymmetric cyclic from more maturity in the lower horizon of the Lower Paleozoic to gain lesser maturity in the younger

beds as can be stratigraphically observed. (See the geologic maps, of Fig. 2 and Fig. 8).

To appreciate the degree of chemical maturity, it can be understood that, the deviated plot of the Tha Manao calcareous siliciclastic sandstone (no.5) which bears a significant amount of the non-silicate carbonate, the Ca bearing phase (Table 5) as well as their authigenetic replacement would cause the discrepancy behavior of the no5 in this diagram. Trending of the meta-siliciclastic plots reflect the cyclicity of each rock unit during their sedimentary evolution from the more immature towards the more mature and turning back reflecting the more humid weather than the arid. (Fig. 19 and Table 4, 5 and Table 6, 7) in an asymmetric (A→ B→ C→ D, A→ B→ C→ D) fashion.

V-6. Type of source rocks of the Upper Thabsila, the Chao Nen and the Tha Manao
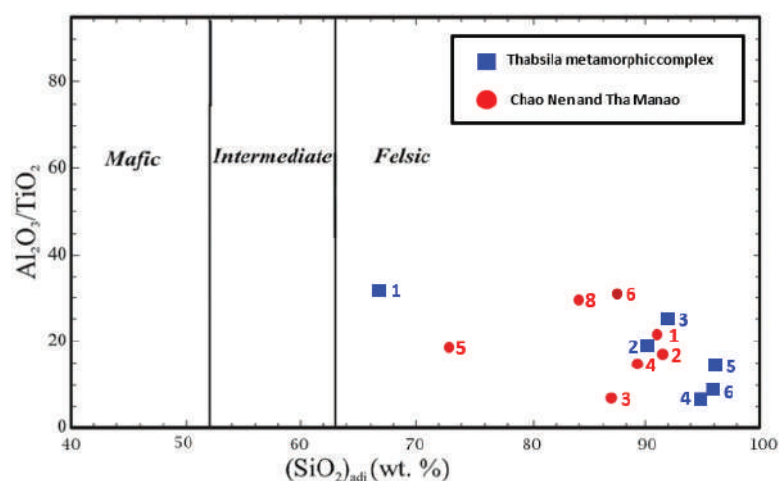
Figure 20: Geochemical classification of igneous source rocks. (Le Bas et al. 1986)

It can be further discussed in the chemical variation shown in Figure 20 relative to the modal analyses tabulated in Table 4 and 5 and geochemical analyses in Tables 6 and 7. The variation of SiO_2 which mainly extracted from the silicate mineral i.e. dominantly was from quartz with a minor variation from the content of the feldspar and micaceous minerals (see Table 4 and 5). The trend moves toward 100% SiO_2. While the content of Al_2O_3/TiO_2 also declines from about 30 % to 5% suggesting a more maturity and the elimination of feldspar and finer clay-rich material during their evolution of the Thabsila than the Lower Paleozoic formations.

Considering the felsic types of source rock material as indicated in Figure 20, it can be

interpreted from the modal and the chemical analysis as follows. Since there is no record of any lithic in all of the meta-siliciclastic sandstones studied, source rocks of them were not very likely derived from the fine to very fine-grained volcanic and other rocks, but rather from the less resistance coarser-grained plutonic or gneissic rocks. For the Thabsila meta- siliciclastic sandstones which contain Na2O only in the immature or sub-mature samples, but not in the mature ones, may reflect the source rock was less felsic and contain plagioclase which has been destroyed leaving only the finer clay material in the younger sequence during moreweathering or uplifting of the source terrane.

VI. Conclusions

Both petrographic analysis and geochemical studies suggested the Upper Thabsila and the Chao Nen Cambrian meta-siliciclastic sandstones are compositionally different due to degree of evolution. The Upper Thabsila expresses a longer evolution trend starting from the more immaturity evolving in a straight linear line of evolution towards the super mature end (as shown in the plot of Fig. 16). While the plots of the Lower Paleozoic signify a shorter and hardly defined trend classifying rock composition spanning from meta-argillaceous subarkose to arkose (Fig. 16) returning the cyclic evolution from more maturity in the older beds towards more immaturity in the younger bed complete the cyclic fashion as seen in the comparison between Figure 14 and Figure 16. The same conclusion can be read from other related figures (Figs. 18, 19 and 20) also. The lower grade regional metamorphic characteristics of the Chao Nen are signified by the preservation of diagenesis and inconsistency of their foliation development due to the variation in the amount of the original argillaceous contents, a significant variable constituent in rocks. The Chao Nen has been mildly metamorphosed developing a lessening amount of the foliated sericite (or fine-grained muscovite). Both of the rock units shared the same depositional regime on a passive margin setting and performing the repeated asymmetric cyclic evolution, a common feature of the rhythmic sedimentation of the rocks studied. The sediments might have been derived from either granite or granite gneisses (ranging in composition starting from the less felsic to the more felsic) of the unknown Precambrian basement, which presumably characterized a change in source rock composition during the Precambrian basement peeling off process or cycle of tectonic activity. The lithologic resemblance between them as well as their progressively decreasing in grades of metamorphism suggested their transitional relation and were subjected to a single episode of metamorphism. The Precambrian cratonic source terrane of this Thabsila-Cambrian-Ordovician continuous sequence is so far unknown in Thailand (Hansen et al, 2014) and possibly might have been all transformed to the common Triassic foliated S-type granite in the western Shan-Thai.

VII. Acknowledgments

References

Akinyemi, S. A., Adebayo, O. F., Ojo, A. O., Fadipe, O. A., & Gitari, W. M. (2014). Geochemistry and mineralogy of the Campanian Sandstone of Lokoja-Basange Formation, Middle Niger Basin (Lokoja sub-basin), Nigeria: Implications for provenance, weathering, tectonic setting and paleo-redox condition. *Journal of Natural Sciences Research, 4*(16), 65-89.

Akinyemi, S. A., Adebayo, O. F., Madukwe, H. Y., Aturamu, A. O., OlaOlorun, O. A., Gitari, W. M., ... Ojo, A. O. (2018). Geochemistry of Ahoko claystone-shale sequence, south eastern Bida Basin, Nigeria: implications for tectonic setting, provenance and source area weathering. *Transactions of the Royal Society of South Africa, 73*(2), 158-171.

Armstrong-Altrin, J. S., Lee, Y. I., Verma, S. P., & Ramasamy, S. (2004). Geochemistry of sandstones from the Upper Miocene Kudankulam Formation, southern India: implications for provenance, weathering, and tectonic setting. *Journal of sedimentary Research, 74*(2), 285-297.

Bas, M. J. L., Maitre, R. W. L., Streckeisen, A., & Zanettin, B. (1986). A Chemical Classification of Volcanic Rocks Based on the Total Alkali-Silica Diagram. *Journal of Petrology, 27,* 745–750.

Bhatia, M. R. (1983). Plate tectonics and geochemical composition of sandstones. *The Journal of Geology, 9*1(6), 611-627.

Bunopas, S. (1981). Pelaogeographic history of western Thailand and adjacent parts of Southeast Asia-A plate tectonics interpretation. *Geological*

Survey, Paper, 5, 810.

Dickinson, W. R., Beard, L. S., Brakenridge, G. R., Erjavec, J. L., Ferguson, R. C., Inman, K. F., ... Ryberg, P. T. (1983). Provenance of North American Phanerozoic sandstones in relation to tectonic setting. *Geological Society of America Bulletin, 94*(2), 222-235.

Folk, R. L. (1974). *Petrology of sedimentary rocks.* Texas: Hemphill Diesel Eng Schools.

Hansen, B. T., Wemmer, K., Putthapiban, P., Kleinhanns, I. C., & Wilsky, F. (2014). Do U/Pb-SHRIMP dating and Pb stepwise leaching (PbSL) analyses confirm the lack of Precambrian basement outcrops in Thailand?. *Open Journal of Geology, 4*(10), 505-517.

Hay, D. C., & Dempster, T. J. (2009). Zircon behaviour during low-temperature metamorphism. *Journal of Petrology, 50*(4), 571-589.

Herron, M. M. (1988). Geochemical classification of terrigenous sands and shales from core or log data. *Journal of Sedimentary Research, 58*(5), 820-829.

Mission, G. G. (1972). Final Report of the German Geological Mission to Thailand 1965-1971. *Bundesanstalt fur Bodenforschung, Hannover. Unpubl. Rep.*

Muangphongoen K., Winsa, T. & Salyapongse, S., (2015). LIthologic, petrographic and petrologic constraints on a continuous succession of Cambrian to Upper Precambrian? Buchan Facies Series, Thap Sila parasedimentary core. *Poster presented at 14th International conference on Gondwana.* Bangkok.

Nantasin, P., Hauzenberger, C., Liu, X., Krenn, K., Dong, Y., Thöni, M., & Wathanakul, P. (2012). Occurrence of the high grade Thabsila metamorphic complex within the low grade Three Pagodas shear zone, Kanchanaburi Province, western Thailand: Petrology and geochronology. *Journal of Asian Earth Sciences, 60*, 68-87.

Peterson, J. A. (2009). *Geochemical Provenance of Clastic Sedimentary Rocks in the Western Cordillera: Utah, Colorado, Wyoming, and Oregon* (thesis).

Roser, B. P., & Korsch, R. J. (1988). Provenance signature of sandstone-mudstone suite determined using discriminant function analysis of major element data. *Chemical Geology, 67* (1), 119-139.

Sangduen, A., Prasongasa, J., Songpracha, N., Uthairat, S., & Laotanakitphaisan T. (2016). *Geological field report along the Srinagarindra dam, Takradan, Si Sawat district to Thatungna dam, Chong Sadao, Mueang district, Kanchanaburi province* (pp. 149). Kanchanaburi: Division of Geoscience, Mahidol University Kanchanaburi Campus.

Salyapongse, S., Duangdee, P., Laising, N & Adskul, A. (2015). A note on foliated contact metamorphic rocks in Western Shan-Thai. *Proceedings Thai-Lao the 3rd Thai-Lao Technical Conference on Geology and Mineral Resources* (pp. 80-99). Bangkok.

Salyapongse, S., Hong, P., & Putthapiban, P. (2019). Thabsila gneissic complex: The Buchan / Abukuma Facies Series. *Proceedings of the conference on the 80th anniversary of Prof. Dr. Prinya Nutalai: Roles of Thai geologist for economic and social development* (pp. 91-103).

Salyapongse, S., Kongsuchko, S., Sratongyung, J., Kaewdum, N. & Putthapiban, P. (2018). The Cambrian low grade regional metamorphic rocks, meta-arkosic to meta-argillaceous subarkosic sandstones in Kanchanaburi province. *Poster presented at CCOP.* Bangkok.

Wang, Z., Wang, J., Fu, X., Feng, X., Wang, D., Song, C. & Zeng, S. (2017). Petrography and geochemistry of upper Triassic sandstones from the Tumengela Formation in the Woruo Mountain area, North Qiangtang Basin, Tibet: Implica tions for provenance, source area weathering, and tectonic setting. *Island Arc, 26*(4), e12191.

การวิเคราะห์ในเบื้องต้นและแก้ไขการทรุดตัวของถนนเนื่องจากภัยแล้ง ในพื้นที่ อ.ปากพนัง จ.นครศรีธรรมราช

Preliminary analysis and solution for collapsed road embankment due to drought in Pak Phanang, Nakhon Si Thammarat

พิสิฐ ศรีวรานันท์, ธันวา วิบูลย์ศรัณย์,
ทวีพงษ์ สุขสวัสดิ์* และกวิน สายประเสริฐกิจ
กรมทางหลวงชนบท ถ.พหลโยธิน เขตบางเขน กรุงเทพฯ 10220

**Pisit Srivaranun, Thanwa Wibunsaran
Taweephong Suksawat* and Kawin Saiprasertkij**
Department of Rural Roads, Bangkok, Thailand 10220.
*Corresponding author: Taweephong2727@gmail.com
Received 13 December 2019 ; Accepted 2 July 2020

บทคัดย่อ

กรมทางหลวงชนบทโดยสำนักงานทางหลวงชนบทที่ 11 (สุราษฎร์ธานี) และสำนักวิเคราะห์ วิจัยและพัฒนาได้เข้าพื้นที่เพื่อสำรวจ ความเสียหายของทางหลวงชนบทสายทาง นศ.4045 แยกทางหลวงหมายเลข 4103 - บ้านบางหญ้า อ.ปากพนัง จ.นครศรีธรรมราช ซึ่งเกิดจากการทรุดตัวบริเวณขอบทางเป็นแนวยาว โดยงานวิจัยฉบับนี้จะนำเสนอการวิเคราะห์สาเหตุของการทรุดตัวด้วยการวิเคราะห์ เชิงตัวเลขด้วยระเบียบวิธีไฟไนต์เอลิเมนต์โดยใช้โปรแกรม Plaxis 2D ร่วมกับการสำรวจทางธรณีฟิสิกส์โดยใช้วิธีการวัดสภาพ ต้านทานไฟฟ้า และวิธี Screw driving sounding test ผลการวิเคราะห์โดยใช้วิธีเชิงตัวเลขพบว่า ถนนจะอยู่ในสภาวะที่วิกฤติและ มีโอกาสวิบัติได้สูงในช่วงที่ระดับน้ำในคูน้ำลดลงต่ำแต่ยังคงมีน้ำคงค้างในคันทาง พบว่ามีค่าสัดส่วนความปลอดภัยเพียง 1.10 เมื่อพิจารณาจากกรณีที่ไม่มีคูน้ำขนาบข้างถนน หรือในกรณีที่มี Berm จะพบว่าค่าสัดส่วนความปลอดภัยสูงกว่า 1.30 ซึ่งปลอดภัยเพียงพอต่อการวิบัติ และสอดคล้องกับสภาพหน้างานจริงในบริเวณที่ไม่มีคูน้ำซึ่งไม่พบการวิบัติของถนน

คำสำคัญ : การสำรวจวัดค่าต้านทานไฟฟ้า, ความมั่นคงเชิงลาดคันทาง, ชั้นดินเหนียวอ่อน, ระเบียบวิธีไฟไนต์เอลิเมนต์, ทางหลวงชนบท

Abstract

The Bureau of Rural Roads 11 (Surat Thani) and the Bureau of Test, Research and Development, Department of Rural Roads, conducted the failure investigation of road embankment of Rural Highway NS4045 at Highway 4103 Ban Ban Ya, Pak Panang District, Nakhon Si Thammarat, where subsidence occurred along the edge of the road for a certain distance. This study aims to find the cause of the road failure and to give suggestion on an appropriate solution. The investigation made to use of geophysical surveys that included the Resistivity Survey and a Screw Driving Sounding test in order to evaluate the subsurface ground condition and to estimate the soil strength. The Plaxis 2D software was used to analyze the factor of safety for the slope stability of various conditions. The results achieved from the simulation demonstrated values of 1.10 for critical condition that the water level in the canal along the road is low with water pressure remains in the road embankment; and 1.30 for the condition that there is no canal presented along the road. The latter is considered stable and safe from road failure. This is also true and can also be seen in the area where there is no canal running along the road.

Key words: Department of Rural Roads, Finite Element Method, Resistivity Survey, Slope stability of Road Embankment, Soft Soil

บทนำ

    กรมทางหลวงชนบท มีภารกิจในการดูแลถนนโครงข่าย ทางหลวงชนบท ซึ่งเป็นโครงข่ายถนนสายรองที่สำคัญ เชื่อมต่อระหว่างทางหลวงท้องถิ่นกับทางหลวงสายหลัก มีถนนที่อยู่ในความดูแลเป็น จำนวนไม่น้อยที่มีความ เสียหายโดยเฉพาะคันทางวิบัติ และอีกหลายสายทางที่มี ความเสี่ยงในด้านเสถียรภาพคันทาง โดยเฉพาะอย่างยิ่ง ถนนที่ถนน ก่อสร้างบนพื้นที่ดินอ่อนเลียบคลองชลประทาน คลองสาธารณะหรือคูน้ำตามธรรมชาติ จากปัญหาดังกล่าว ก่อให้เกิดความสูญเสียงบประมาณในการซ่อมบำรุงจำนวนมาก ในช่วงเวลาที่ผ่านมา ถนนหลายสายที่อยู่ความรับผิดชอบของ กรมทางหลวง ชนบททั้งในเขตจังหวัด ปริมณฑลและหลาย จังหวัดใน ส่วนภูมิภาคเกิดการพังทลายเนื่องจากเหตุผล ดังกล่าวทั้งนี้การสำรวจและการวิเคราะห์ทางวิศวกรรมธรณี เทคนิคเป็นสิ่งที่จำเป็นเพื่อระบุสาเหตุของการพังทลาย ที่แท้จริงและเพื่อหาแนวทางแก้ไขที่ เหมาะสมมากที่สุด ดังตัวอย่างเช่นกรณีทางหลวงชนบทสาย นศ.4045 แยก ทางหลวงหมายเลข 4103 – บ้านบางหญ้า อ.ปากพนัง จ.นครศรีธรรมราช (รูป ที่ 1 (ก) และ (ข)) ได้รับความเสียหา ถนนเกิดการ ทรุดตัวเป็นระยะทาง 0.280 กม. โดยเมื่อวันที่ 6 พฤศจิกายน 2562 สำนักทางหลวงชนบทที่ 11 และ กลุ่มปฐพีวิศวกรรม สำนักวิเคราะห์ วิจัยและพัฒนา ได้ เข้าพื้นที่สำรวจโดยใช้วิธีการวัดสภาพต้านทาน ไฟฟ้า (Resistivity-Survey) และวิธี Screw driving sounding test รวมถึงวิเคราะห์สาเหตุของการทรุดตัวด้วยวิธี Finite Element Method โดยใช้โปรแกรม Plaxis2D โดย ในบทความฉบับนี้จะ อธิบายถึงวิธีการสำรวจด้วยวิธีการ ดังกล่าวและ สรุปผลการวิเคราะห์สาเหตุการวิบัติ

วิธีศึกษา

    - พื้นที่ศึกษา

จากการลงพื้นที่สำรวจสภาพสายทางพบว่าเป็นถนน 2 ช่องจราจร พบการทรุดตัวตามแนวยาวของถนนด้าน ซ้ายทาง (เมื่อพิจารณาจาก กม.ที่ 0) เป็นระยะทางประมาณ 280 ม. (ประมาณ กม.ที่ 7 - กม.ที่ 8) และบางจุดพบ รอยแตกร้าวขนาดเล็กทั้งด้านซ้ายทางและขวาทางในแนว ยาวของถนน ลักษณะทางกายภาพของพื้นที่เป็นที่ราบลุ่ม น้ำท่วมถึง ซึ่งโดยรวมจะเป็นพื้นที่เกษตรกรรม ประกอบด้วย ทุ่งนาและสวนปาล์ม บางช่วงเป็นคูน้ำขนาบข้างถนน ความลึกของคูน้ำประมาณ 3 - 5 ม. ดังแสดงในรูปที่ 1 (ค)

(ก) ที่ตั้งของพื้นที่ศึกษา อ.ปากพนัง จ.นครศรีธรรมราช
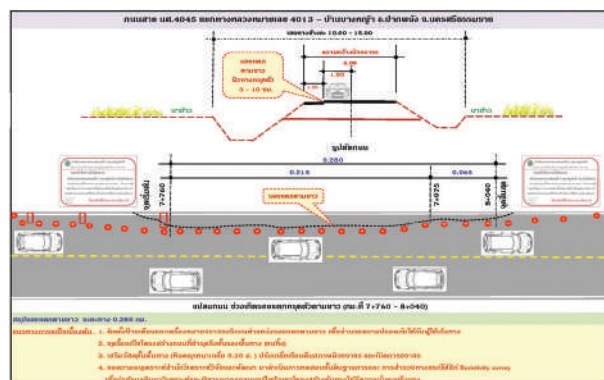
(ข) แปลนและรายละเอียดถนน ช่วงที่เกิดการทรุดตัว

(ค) ลักษณะการทรุดตัวบริเวณไหล่ทางด้านซ้าย
**รูปที่ 1:** ลักษณะของความเสียหาย และการทรุดตัวของทางหลวง ชนบทสาย นศ.4045

สมมุติฐานของการวิบัติ

คณะทำงานได้ประเมินจากสภาพพื้นที่ความเสียหาย โดยสมมุติฐานเบื้องต้นของสาเหตุที่ทำให้ถนนทรุดตัว คาดว่าเกิดจากการที่ถนนตั้งอยู่บนพื้นที่ดินอ่อนซึ่งมีความเป็นไปได้ว่าจะเกิดปัญหาเสถียรภาพของคันทาง ทำให้ถนนเกิดการแตกร้าวและทรุดตัว ซึ่งข้อมูลแผนที่ธรณีวิทยาของถนนสาย นศ.4045 แยกทล.หมายเลข 4013 - บ้านบางหญ้า อ.ปากพนัง จ.นครศรีธรรมราช พบว่าเป็นดินประเภท Qmc, ตะกอนชายฝั่งทะเลโดยอิทธิพลของน้ำขึ้น-น้ำลง ดินเหนียว ทรายแป้ง และทรายละเอียดของที่ลุ่มราบน้ำขึ้นถึง ที่ลุ่มชื้นแฉะ ที่ลุ่มน้ำขัง ป่าชายเลน และชวากทะเล ดังแสดงในรูปที่ 2

การกำหนดแนวการสำรวจ

การวางแนวสำรวจคณะทำงานได้ดำเนินการสำรวจตามแนว Profile ถนน ซึ่งได้ดำเนินการทั้งสิ้น 3 แนว โดยให้แนวสำรวจสอดคล้องกับแนวทางสำหรับวิเคราะห์สาเหตุของปัญหา จากนั้นทางคณะทำงานจึงดำเนินการในขั้นตอนการกำหนดตำแหน่งติดตั้งเครื่องมือต่อไป ดังแสดงในรูปที่ 3 และรายละเอียดของแต่ละแนวทดสอบได้แสดงในตารางที่ 1
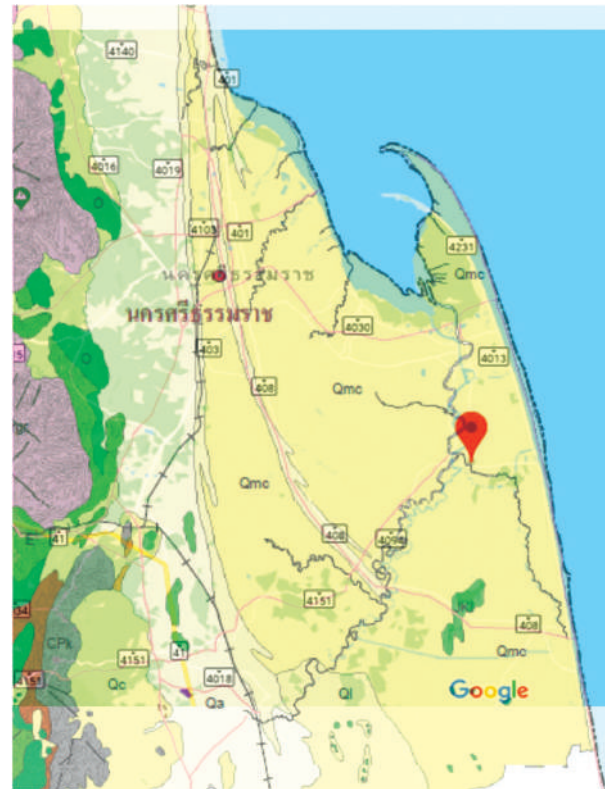
รูปที่ 2: แผนที่ธรณีวิทยาของสายทาง นศ.4045

**รูปที่ 3:** ตำแหน่งสายทาง นศ.4045 และตำแหน่งการติดตั้งเครื่องมือ Resistivity Survey

ตารางที่ 1 ตำแหน่งการติดตั้งเครื่องมือ Resistivity survey

แนวการทดสอบด้วยวิธี Resistivity Survey	ลักษณะความเสียหาย/ลักษณะทางกายภาพ
แนวที่ 1 กม.ที่ 6+900	ถนนไม่พบเสียหาย และไม่พบคูน้ำในเขตทาง แนวนี้เป็นบริเวณที่ไม่พบรอยแตกร้าว ซึ่งจะใช้เป็นเกณฑ์ในการเปรียบเทียบกับแนวการทดสอบในจุดที่เสียหาย
แนวที่ 2 กม.ที่ 7+900	บริเวณที่เป็นรอยต่อระหว่างจุดที่เริ่มมีรอยแตกร้าวและไม่มีรอยแตกร้าว เพื่อใช้ในการเปรียบเทียบจุดที่เสียหายและไม่เสียหายในแนวการทดสอบเดียวกัน
แนวที่ 3 กม.ที่ 8+100	บริเวณที่ถนนเสียหายอย่างรุนแรง มีการทรุดตัวและรอยแยกขนาดใหญ่บริเวณไหล่ทางด้านซ้าย

การวัดความต้านทาน

    หลังจากติดตั้งอุปกรณ์แล้วเสร็จจึงเริ่มดำเนินการในขั้นตอนการวัดค่าความต้านทานไฟฟ้าในดิน ซึ่งเครื่องวัดความต้านทานไฟฟ้าจะทำการอ่านค่ากระแสไฟฟ้าพร้อมทั้งจัดเก็บค่าที่อ่านได้ไว้ใน Memory card ของเครื่อง ทั้งนี้สามารถตรวจดูความสมบูรณ์ของข้อมูลจากการทดสอบ ได้จากเครื่องวัดค่าความต้านทานหลังจากที่เครื่องได้ทำการวัดแสดงในรูปที่ 4 ซึ่งคาดว่าจะเป็นชั้นดินเหนียวอ่อนค่อนข้างหนา (ค่าความต้านทานไฟฟ้าต่ำ) รองรับใต้ชั้นโครงสร้างทาง สำหรับข้อมูลแบบละเอียดที่ใช้ในการวิเคราะห์นั้นจะต้องใช้ซอฟท์แวร์ภายนอกมาช่วยเสริมเพื่อความสะดวกและถูกต้อง
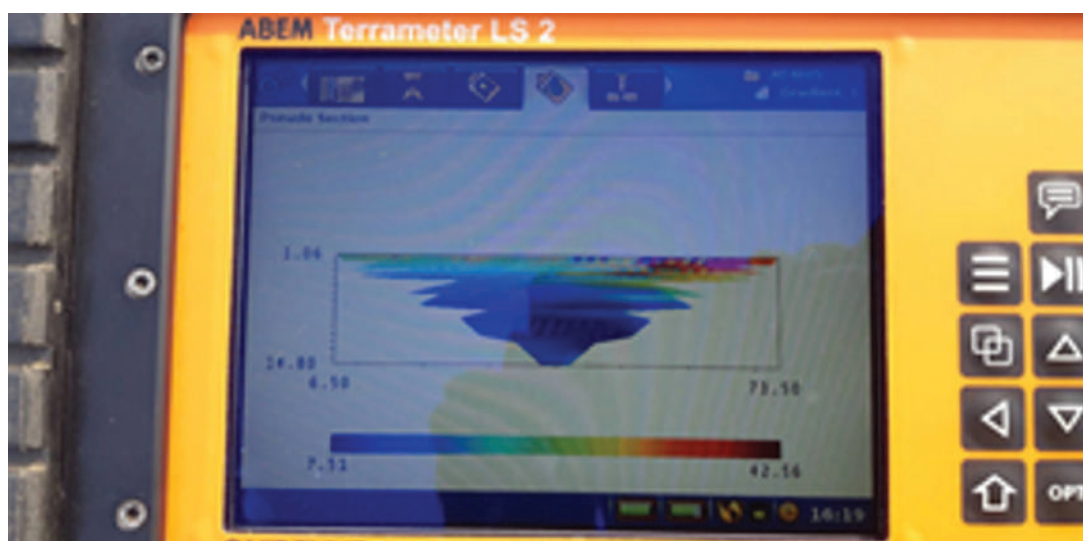
รูปที่ 4: ผลการวัดค่าความต้านทานไฟฟ้าเบื้องต้น

การวิเคราะห์ผลการทดสอบ

    ผลการวิเคราะห์การสำรวจด้วยวิธีวัดสภาพต้านทานไฟฟ้า (Resistivity survey) ของถนนดังกล่าวสามารถประมวลผลออกมาเป็น Model Resistivity Section ดังนี้

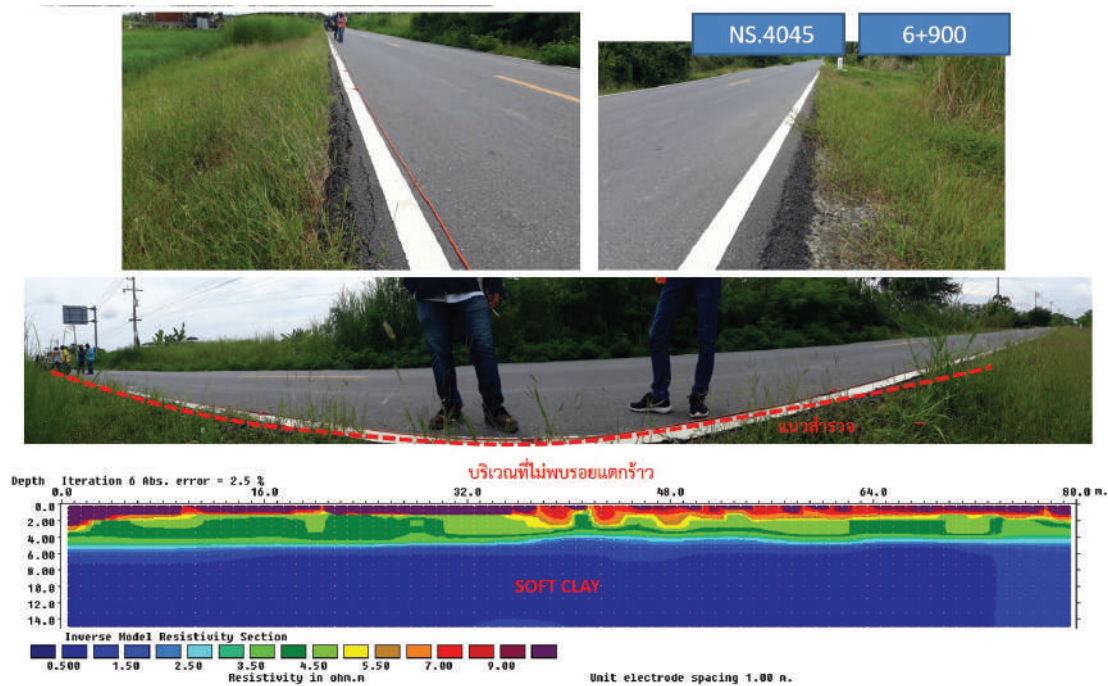   ตำแหน่ง กม.ที่ 6+900 บริเวณนี้เป็นจุดที่ถนนไม่มีรอยแตกร้าว และไม่มีคูน้ำขนาบข้างถนน จาก Model Resistivity Section พบว่าชั้นโครงสร้างทางเดิม (ความลึกจากผิวดินถึงระดับความลึก 1 ม.) บริเวณนี้ค่อนข้างแข็งแรง (ค่าความต้านทานไฟฟ้ามากกว่า 9 ohm.m) จากนั้นจนถึงระดับความลึก 4 - 5 ม. เป็นชั้นดินเหนียวแข็งปานกลาง (ค่าความต้านทานไฟฟ้า 3.5 - 5.5 ohm.m) และจากนั้นเป็นชั้นดินเหนียวอ่อนค่อนข้างลึก (มากกว่า 14 ม.)

รองรับใต้ชั้นโครงสร้างทาง (ค่าความต้านทานไฟฟ้า 0.5 - 1.5 ohm.m) ดังแสดงในรูปที่ 5

ตำแหน่ง กม.ที่ 7+900 บริเวณนี้เป็นจุดที่เป็นรอยต่อระหว่างถนนที่ทรุดตัวและไม่ทรุดตัว จาก Model Resistivity Section พบว่าชั้นโครงสร้างทางเดิม (ความลึกจากผิวดินถึงระดับความลึก 1 ม.) บริเวณนี้ค่าความต้านทานไฟฟ้ามีต่ำในบริเวณที่ถนนทรุดตัวค่อนข้างชัดเจน โดยมีค่าความ

ต้านทานไฟฟ้าเพียง 4.5 - 7.0 ohm.m เท่านั้น และจากนั้นจนถึงระดับความลึก 3.5 - 4.0 ม. เป็นชั้นดินเหนียวอ่อนถึง ดินเหนียวแข็งปานกลาง (ค่าความต้านทานไฟฟ้า 2.5 - 3.5 ohm.m) และจากนั้นเป็นชั้นดินเหนียวอ่อนค่อนข้างลึก (มากกว่า 14 ม.) รองรับใต้ชั้นโครงสร้างทาง (ค่าความต้านทานไฟฟ้า 0.5 - 1.5 ohm.m) ดังแสดงในรูปที่ 6

ตำแหน่ง กม.ที่ 8+100 บริเวณนี้เป็นจุดที่ถนนทรุดตัว

รูปที่ 5: ผลการวิเคราะห์ถนนสาย นศ.4045 กม.ที่ 6+900

รูปที่ 6: ผลการวิเคราะห์ถนนสาย นศ.4045 กม.ที่ 7+900

มากที่สุด และมีคูน้ำลึก 3 - 5 ม. ขนาบข้างตลอดแนว ถนนจาก Model Resistivity Section พบว่าชั้นโครงสร้าง ทางเดิม (ความลึกจากผิวดินถึงระดับความลึก 1 ม.) บริเวณนี้ค่าความต้านทานไฟฟ้ามีต่ำกว่าแนวทดสอบที่ 1

และ 2 ค่อนข้างชัดเจน โดยมีค่าความต้านทานไฟฟ้าเพียง 4.5 – 7.0 ohm.m เท่านั้น ซึ่งเป็นค่าที่ค่อนข้างต่ำเมื่อ เปรียบเทียบกับบริเวณที่ถนนที่ไม่พบความเสียหายดังแสดง ในรูปที่ 7


รูปที่ 7: ผลการวิเคราะห์ถนนสาย นศ.4045 กม.ที่ 8+100

ช่วงเดือนมีนาคม 2562 ก่อนเกิดเหตุประมาณ 6-7 เดือน สำนักทางหลวงชนบทที่ 11 (สุราษฎร์ธานี) ตระหนัก ถึงปัญหาถนนทรุดตัวในพื้นที่อำเภอปากพนังอยู่ก่อนแล้ว จึงได้ทำหนังสือขอความอนุเคราะห์มายังสำนักวิเคราะห์ วิจัยและพัฒนา เพื่อดำเนินการตรวจสอบ ในครั้งนั้นได้ ดำเนินการสำรวจทางธรณีเทคนิคและธรณีฟิสิกส์ในพื้นที่ ข้างเคียง (5 จุดใน 3 สายทาง) ด้วยวิธี Screw driving sounding test และ วิธี Resistivity survey พบว่า ลักษณะทางธรณีวิทยาคล้ายคลึงกันในทุกจุดที่ทดสอบ กล่าวคือ เป็นชั้นดินเหนียวกำลังต่ำ ค่อนข้างหนาประมาณ 10-12 ม และจากนั้นพบว่ากำลังของดินเพิ่มขึ้นตาม ความลึก และสอดคล้องกับแผนที่ธรณีวิทยาตำแหน่งของ การทดสอบในช่วงเดือน มีนาคม 2562 และจุดที่วิบัติ ในครั้งนี้ดังแสดงในรูปที่ 8 และผลการทดสอบด้วยวิธี Screw driving sounding test ได้แสดงไว้ในรูปที่ 9

ผลการสำรวจ

จากความเสียหายที่เกิดขึ้น คณะทำงานได้สำรวจทาง ธรณีฟิสิกส์ด้วยวิธี Resistivity survey เพื่อตรวจสอบความ เสียหายของถนนสาย นศ.4045 แยกทางหลวงหมายเลข 4103 - บ้านบางหญ้า อ.ปากพนัง จ.นครศรีธรรมราช โดย สามารถสรุปได้ดังนี้
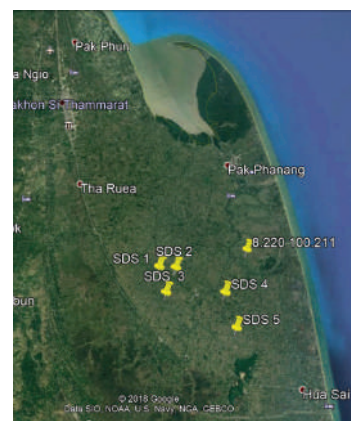
รูปที่ 8: ตำแหน่งถนนสาย นศ.4045 (บริเวณที่เสียหาย) และตำแหน่งที่ทดสอบด้วยวิธี SDS (มีนาคม 2562)
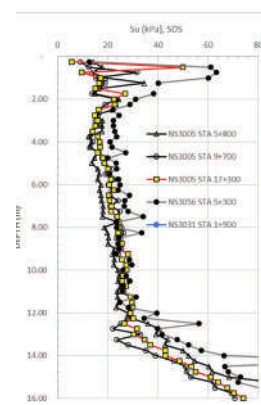

รูปที่ 9: ผลการทดสอบการวัดกำลังของดินในสนามด้วยวิธี Screw driving sounding test (มีนาคม 2562)

คณะทำงานได้สำรวจทางธรณีฟิสิกส์ในสายทาง นศ.4045 จำนวน 3 แนวซึ่งครอบคลุมบริเวณที่ถนนอยู่ใน สภาพดี และถนนที่เสียหายด้วยวิธี Resistivity survey พบว่า ลักษณะทางธรณีวิทยาคล้ายคลึงกันในทุกจุดที่ ทดสอบและสอดคล้องกับแผนที่ธรณีวิทยา กล่าวคือ เป็น ชั้น ดินเหนียวกำลังต่ำค่อนข้างหนา และมีความลึกมากกว่า 14 ม.

เมื่อพิจารณาเฉพาะชั้นโครงสร้างทาง ที่ความลึกไม่เกิน 1 ม. จากระดับผิวจราจร ได้มีการดำเนินการซ่อมสร้าง โดยสำนักทางหลวงชนบทที่ 11 (สุราษฎร์ธานี) โดยวิธี Pavement in-place recycling ซึ่งการซ่อมสร้างวิธีนี้ มีจะกระทบต่อชั้นดินเหนียว Soft Clay น้อยมาก และ ผลการสำรวจยังพบว่า ในบริเวณที่เสียหาย ช่วง กม.ที่ 8+100 จะมีค่าความต้านทานไฟฟ้าต่ำกว่าบริเวณที่ถนน มีสภาพดี คือ ช่วง กม.ที่ 6+900 ที่มีค่าความต้านทานไฟฟ้า

สูงกว่า แต่จุดสำรวจช่วงรอยต่อ กม.ที่ 7+900 จะเป็น จุดแบ่งระหว่างถนนที่มีความเสียหายและไม่พบความ เสียหายซึ่งค่าความต้านทานไฟฟ้าก็แสดงออกมาอย่าง ชัดเจนเช่นกันซึ่งเป็นไปได้ว่าโครงสร้างทางเดิมในจุดที่เกิด ความเสียหายอาจมีกำลังต่ำตั้งแต่ก่อนมีการดำเนินการ ซ่อมสร้าง ดังแสดงในรูปที่ 10 เมื่อพิจารณาจากลักษณะ ทางกายภาพของคันทาง บริเวณที่ถนนเกิดความเสียหายช่วง กม.ที่ 7+900 ถึง กม.ที่ 8+100 พบว่าทั้งสองข้างทางจะมี ร่องหรือคูน้ำค่อนข้างลึกขนาดยาวไปตามแนวของถนน ความลึกประมาณ 3-5 ม แต่ในบริเวณที่ไม่เกิดความเสียหาย จะไม่มีคูน้ำขนาบข้างสองข้างทาง และเมื่อพิจารณาจากรูปที่ 11 พบว่าช่วง กม.ที่ 8+000 พบจุดที่ไม่พบความเสียหาย ยาวประมาณ 8-10 ม เนื่องจากมีการถมดินเพื่อใช้เป็นทาง เข้า-ออก ทำให้เกิดชานพัก Berm ช่วยให้คันทางเกิดเสถียรภาพ ขึ้น จึงไม่เกิดรอยแตกร้าว/ความเสียหายเช่นจุดอื่นๆ
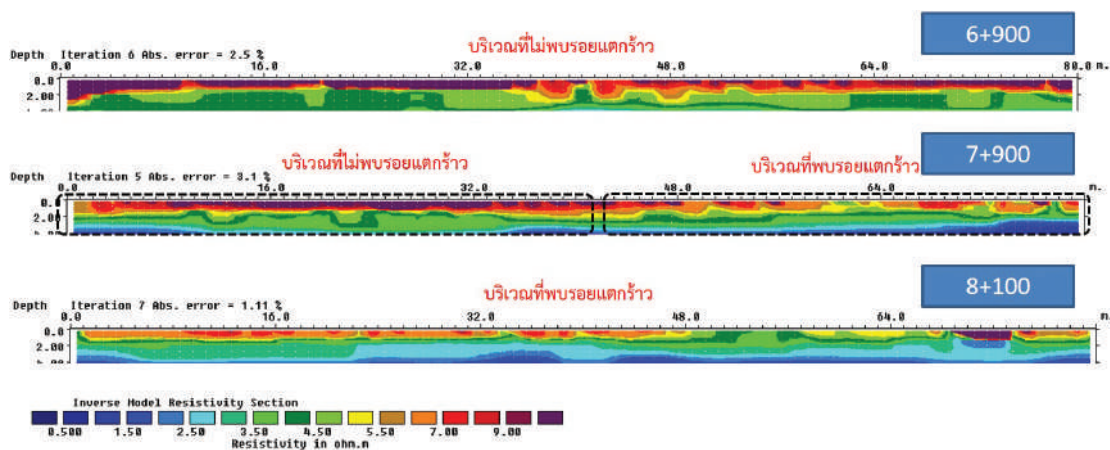
**รูปที่ 10:** เปรียบเทียบผลการทดสอบด้วยวิธี Resistivity Survey ในชั้นโครงสร้างทาง

**รูปที่ 11:** ลักษณะทางกายภาพของพื้นที่ ในบริเวณที่พบรอยแตกและไม่พบรอยแตก

สรุป

จากข้อมูลดินในเชิงวิศวกรรมธรณีเทคนิคที่ได้การ
ทดสอบทั้ง 2 วิธี ได้นำมาวิเคราะห์ด้วยวิธี Finite Element
Method โดยใช้โปรแกรม Plaxis 2D ซึ่งพัฒนาโดย
Brinkgreve and Broere (2006) โดยการจำลองนี้พิจารณา
ความลึกของคูน้ำ (หรือความสูงของคันทาง) เพียง 3 ม. พบว่า
ถนนอยู่ในสภาวะที่วิกฤติ และมีโอกาสวิบัติได้สูง โดยเฉพาะ
ช่วงที่ระดับน้ำในคูน้ำลดลงต่ำแต่ยังคงมีน้ำคงค้างในคันทาง

พบว่ามีค่าสัดส่วนความปลอดภัยเพียง 1.10 เท่านั้น (รูปที่
12) รวมทั้งแนวการวิบัติจากผลการวิเคราะห์ค่อนข้าง
สอดคล้องกับลักษณะความเสียหายที่เกิดขึ้นจริง
อย่างไรก็ตาม เมื่อพิจารณาจากกรณีที่มี Berm ขนาบข้าง
จะพบว่าค่าสัดส่วนความปลอดภัยสูงกว่า 1.30 ในกรณีที่
แย่ที่สุด (รูปที่ 13) ซึ่งปลอดภัยเพียงพอต่อการวิบัติ และ
สอดคล้องกับสภาพหน้างานจริงในพื้นที่ลักษณะดังกล่าว
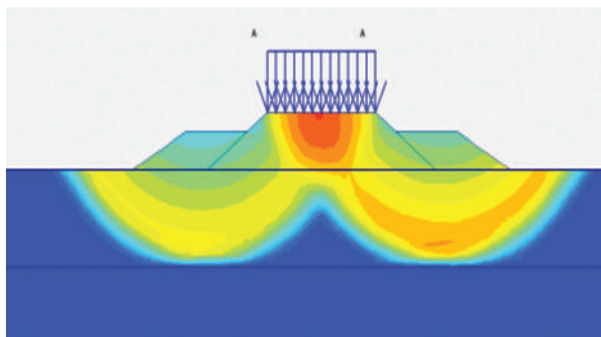ถนนก็ไม่วิบัติเช่นกัน
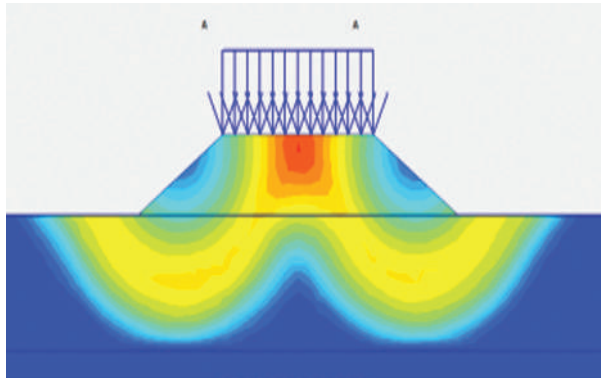
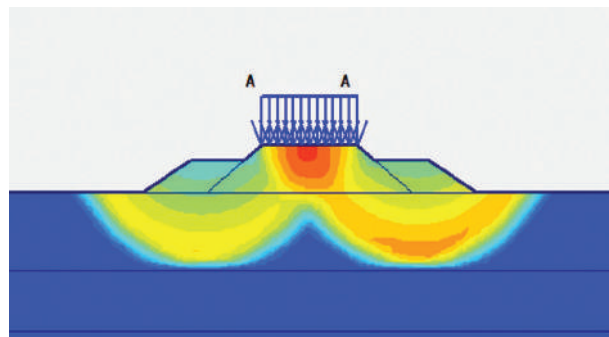(ก) Factor of Safety (Normal Condition) = 1.23
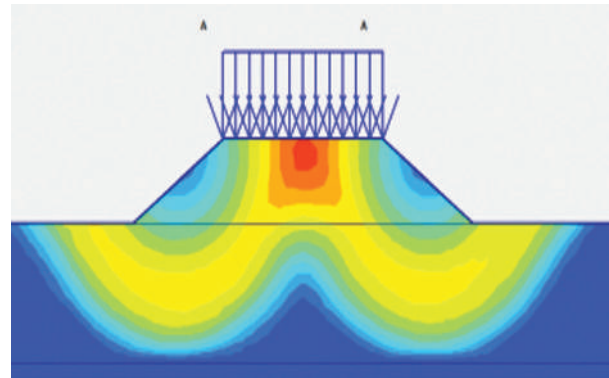
(ข) Factor of Safety (Worst Condition) =　1.10

รูปที่ 12: ผลการวิเคราะห์ด้วยวิธี Finite Element Method ของกรณีมีคูน้ำลึก (หรือคันทางสูง) 3 ม.

(ก) Factor of Safety (Normal Condition) = 1.50

((ข) Factor of Safety (Worst Condition) = 1.32

**รูปที่ 13:** ผลการวิเคราะห์ด้วยวิธี Finite Element Method

จากข้อมูลปริมาณน้ำฝนรายเดือนของจังหวัด
นครศรีธรรมราช (ที่มา : สรุปสถานการณ์น้ำในจังหวัด
นครศรีธรรมราช วันที่ 8 พฤศจิกายน 2562, โครงการ
ชลประทานนครศรีธรรมราช) พบว่าปริมาณน้ำฝนรายเดือน
ของปี 2562 (กราฟแท่งสีแดงในรูปที่ 14) มีปริมาณต่ำกว่า
ค่าเฉลี่ย (เส้นสีเขียว) เกือบตลอดปี โดยช่วงต้นปี 2562
เกิดพายุปาบึก ทำให้ฝนตกหนักในพื้นที่และหลักจากพายุ
ปาบึกผ่านไป (ก.พ. 2562) ปริมาณน้ำฝนลดลงต่ำกว่า
ค่าเฉลี่ยอย่างมีนัยสำคัญ รวมทั้งพบว่าหลังจากการซ่อม
สร้างแล้วเสร็จ (ประมาณเดือน ก.ค. 2562) ฝนทิ้งช่วงหรือ

มีปริมาณน้ำฝนค่อนข้างต่ำกว่าค่าเฉลี่ย ส่งผลให้ระดับน้ำ
ในคูที่ขนาบข้างถนนมีระดับลดลงต่ำเช่นกันทำให้แรงดัน
จากน้ำลดลง ถนนเริ่มแตกร้าวและทรุดตัวเนื่องจากขาด
เสถียรภาพ ในช่วงเวลานี้ สำนักทางหลวงชนบทที่ 11
(สุราษฎร์ธานี) ได้ดำเนินการแก้ไขในเบื้องต้นตามหลักวิชาการ
และหลักปฏิบัติอย่างเหมาะสมคือ การอุดรอยแยกด้วย
น้ำยางมะตอยเพื่อป้องกันมิให้น้ำไหลลงสู่ชั้นโครงสร้างทาง
โดยสรุปจากลักษณะทางธรณีวิทยาที่เป็นดินเหนียวอ่อน
ค่อนข้างหนา ประกอบกับช่วงที่เกิดเหตุคือสิงหาคม - กันยายน
2562 ซึ่งเป็นช่วงที่ฝนทิ้งช่วงและปริมาณน้ำฝนต่ำกว่า

ที่ควรจะเป็น ดังนั้น ระดับน้ำในท้องนาหรือคูน้ำข้างทาง ลดลงต่ำ ทำให้แรงดันจากระดับน้ำลดลงเช่นกัน อีกทั้งบริเวณ ดังกล่าวมีคันทางที่ค่อนข้างสูง (มีคูน้ำค่อนข้างลึกขนาบข้าง ถนนตลอดแนวที่เสียหาย) ทำให้เสถียรภาพของคันทาง ลดลงต่ำในช่วงเวลานี้ และเกิดรอยแตกร้าวที่ผิวทาง

อีกทั้งช่วงเดือนตุลาคม 2562 ปริมาณน้ำฝนสูงกว่าค่าเฉลี่ย อย่างผิดปกติ ทำให้น้ำฝนไหลลงสู่รอยแตกที่ผิวทาง และ ส่งผลให้เกิดแรงฉุดเนื่องจากดินเหนียวในคันทางเดิม ไม่สามารถระบายน้ำได้เร็ว จึงเป็นสาเหตุที่ถนนบริเวณ ดังกล่าวขาดเสถียรภาพเชิงลาดและทรุดตัวในที่สุด
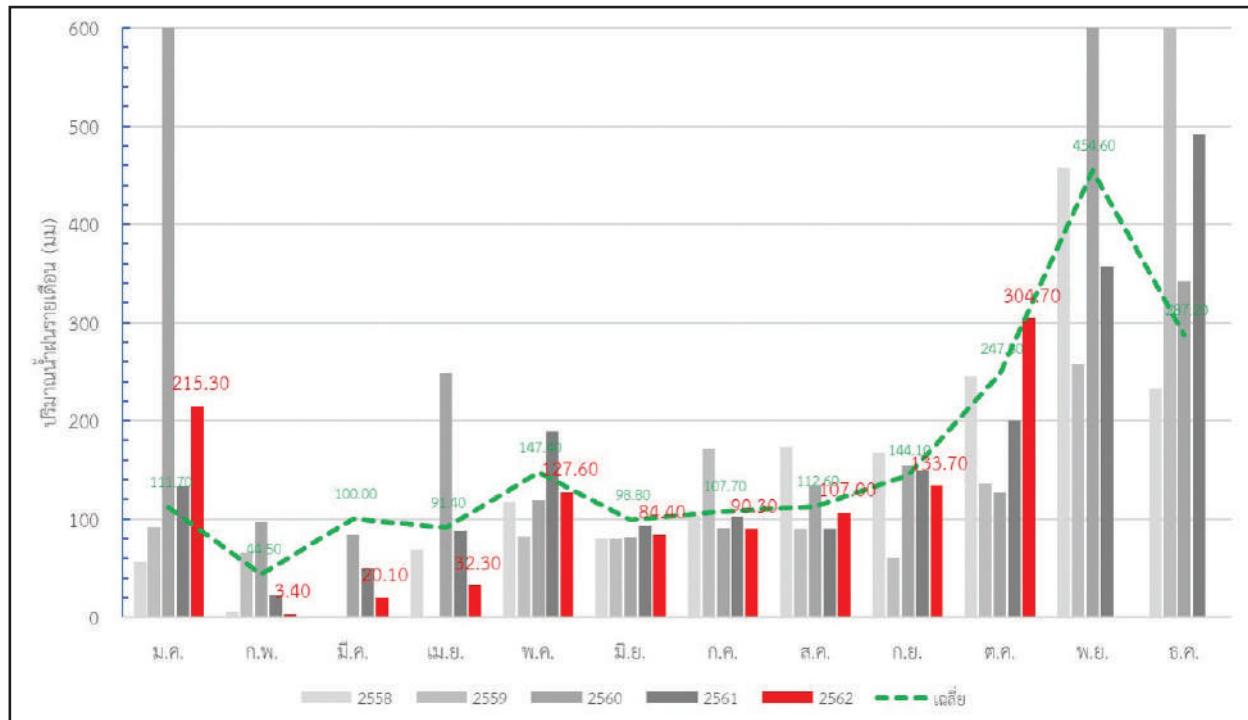
	ปริมาณน้ำฝนรายเดือน (มม)											
	ม.ค.	ก.พ.	มี.ค.	เม.ย.	พ.ค.	มิ.ย.	ก.ค.	ส.ค.	ก.ย.	ต.ค.	พ.ย.	ธ.ค.
เฉลี่ย	111.70	44.50	100.00	91.40	147.40	98.80	107.70	112.60	144.10	247.80	454.60	287.20
2558	56.70	6.00	1.40	69.50	117.30	80.00	103.50	173.50	167.60	245.10	457.50	233.00
2559	92.10	65.80	0.10	-	81.60	80.00	171.40	89.60	60.30	136.50	257.40	694.30
2560	834.35	97.20	84.10	248.23	119.80	80.50	90.50	133.82	155.31	127.09	603.10	342.10
2561	113.10	22.90	50.00	88.30	189.46	92.64	102.60	90.30	148.50	200.60	356.40	491.90
2562	215.30	3.40	20.10	32.30	127.60	84.40	90.30	107.00	133.70	304.70		

รูปที่ 14: ปริมาณน้ำฝนรายเดือนย้อนหลังจากปี 2558 – ปัจจุบัน
(ที่มา : สรุปสถานการณ์น้ำในจังหวัดนครศรีธรรมราชวันที่ 8 พฤศจิกายน 2562, โครงการชลประทานนครศรีธรรมราช)

อ้างอิง

กลุ่มปฐพีวิศวกรรม สำนักวิเคราะห์ วิจัยและพัฒนา กรมทางหลวง
    ชนบท. (2562). *รายงานการสำรวจธรณีฟิสิกส์ สายทาง
    นศ.4045 แยกทางหลวงหมายเลข 4103 - บ้านบางหญ้า
    อ.ปากพนัง จ.นครศรีธรรมราช. กรุงเทพ :* สำนักวิเคราะห์ วิจัย
    และพัฒนา, กรมทางหลวงชนบท.

ส่วนบริหารจัดการน้ำและบำรุงรักษา สำนักงานชลประทานที่ 15
    กรมชลประทาน. (2562). *สรุปสถานการณ์น้ำในจังหวัด
    นครศรีธรรมราช,* สืบค้น 8 พ.ย. 2562, *http://rio15.rid.
    go.th/water/index.php/2016-11-28-01-57-52*

Brinkgreve, R.B., & Vermeer, P.A. (2006). *PLAXIS
    2D Manual*. Rotterdam: Brookfield

Department of rural road. (2016) *Standard for rural
    road construction*. Bangkok: Bureau of test,
    research and development, Department of rural
    road.

Farshidfar, N. & Nayeri, A. (2015). Slope Stability
    Analysis by Shear Strength Reduction Method.
    *Journal of Civil Engineering and Urbanism,
    5*(1), 35-37.

Reinforced embankment constructed along irrigation canal

**Kritsada Teerachavalvong, Surasak Kaipinit,
Taweephong Suksawat* and Kawin Saiprasertkij**
Department of Rural Roads, Ministry of Transport, Thailand.
*Corresponding author: Taweephong2727@gmail.com
Received 16 December 2019 ; Accepted 2 July 2020

Abstract

The Department of Rural Roads has reconstructed the asphalt concrete road during April to May 2016, KS.4064 that is along the Right Main Canal (RMC) of the Lam Pao Dam in Yang Talat district, Kalasin province, the northeast region of Thailand. The distance of road is 1.60km, approximately. During construction, the road embankment collapsed about 300 meters after the asphaltic concrete was paved. This paper focuses on the stability of reinforced road embankment on the KS.4064 by using geogrids and soil replacement methods in order to reinforce the embankment. The PLAXIS 2D software is used to analyze the Factor of Safety of the reinforced road embankment. The required minimum Factor of Safety of 1.30 for the rapid drawdown condition is considered as the criteria for this project. The results from simulations demonstrated 1.563 and 1.640 for geogrid reinforcement and soil replacement methods which indicates that the stability of slope is adequate even though the worst-case condition is considered.

Introduction

Infrastructure systems are the basic physical and organizational structures needed for the services and facilities necessary for an economy to function. Generally, it refers to the technical structures that support a society, for instance, highway, bridge, dam, tunnel, water supply, etc. (Suksawat, 2014).

Rural roads were numerous developed in rural areas of Thailand for the last fifteen years for the facility to societies, supplied as the connection linkage between cities from urban to sub-urban areas (Department of Rural Road, 2016). Therefore, the rural roads were dramatically expanded and enlarged until a present caused automobile gained popularity; consequently (Suksawat, 2008), numerous roads were constructed along the irrigation canals. However, the rural road in Kalasin province, KS.4064 locates on the northeast region of Thailand that failed during construction. This area called the Khorat plateau, which is composed of sand and silty sand-sized soil and covered with hilly landscapes presented higher soil strength than the central region.

The Department of rural roads has operated to reconstruct the asphalt concrete road, KS.4064 that is along the Right Main Canal (RMC) of the Lam Pao Dam in Yang Talat district, Kalasin. The KS.4064 constructed during April to May 2016 which is summer season in Thailand. It was constructed in 2016 and planned to continue until 22.00 km. The road collapsed one day after the asphaltic concrete was paved as shown in Figure 2. The 2-D Finite Element software, Plaxis 2D, was conducted to determinate the cause of failure. In general, the Plaxis 2D can used to perform deformation, stability and flow analysis for various types of geotechnical application by modelled either by a plane strain or an axisymmetric model. In this study, the Plaxis 2D was performed to determinate the Factor of Safety, FS, in order to evaluate the stability of road.

Figure 1: Asphalt concrete surface construction

Figure 2: The road collapsed one day after the construction

Approach/Methodology

The Bureau of Test, Research and Development sent a team to look into the site. The type of damage was observed and the causes identified. The team would study two possible causes: a drop in the underground water level after the negative impacts of agricultural drainage water into irrigation areas, or natural conditions such as soil quality.

Both site and laboratory geotechnical testing were carried out to analyze the causes of the failure. Disturbed and undisturbed soil sample were taken from the selected site

Site Investigation

Three boreholes were conducted soon after failure occurred as shown in Figure 3. The BH-1 and BH-3 are tested on the opposite side of the first failure spot while BH-2 is tested on the stable slope out of the construction area (Sta 21+100). In addition, a test pit of 4.0 m depth was performed nearby BH-3 in order to collect undisturbed samples for direct shear and pinhole tests.

Section 1-1 and Section 2-2 (BH-1 to BH-3 and BH-3 to BH-2, respectively) show the soil profiles as illustrated in Figure 4. The first layer is soil-cement base and fill material having a thickness of 0.5 m to 1.0 m and underlain by loose to medium dense silty sand which extends down to about 3.0 m depth approximately. The shear strength parameters obtained from the direct shear test are cohesion vary from 7.0 to 12.0 kPa and internal friction angle around 25° to 28°. The very stiff to hard clay layer was found to underlie the loose to medium dense silty sand at 3.0 m onward having Standard Penetration test (SPT) more than 30 blows/foot.
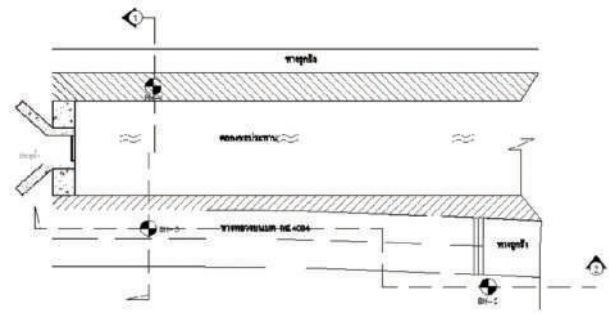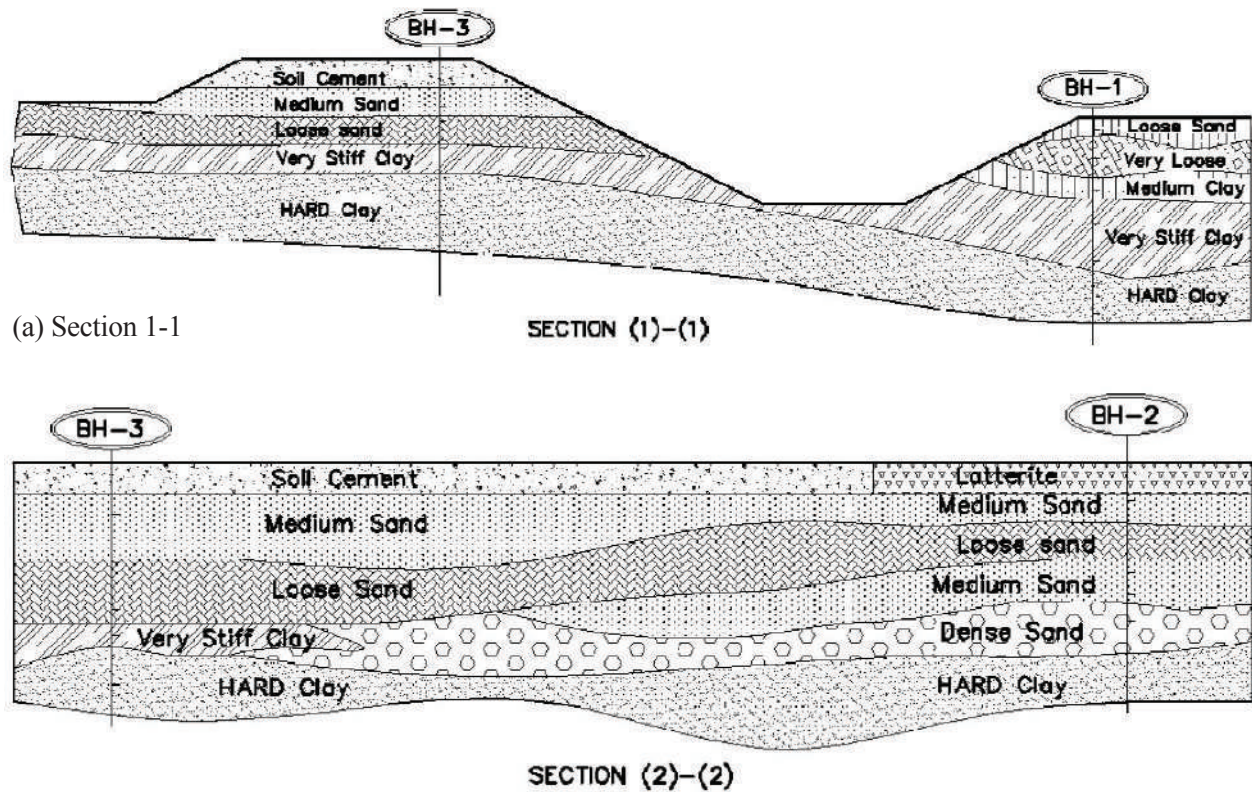

(a) Location of boreholes

(b) BH-1 and BH-3

(c) Sampling with standard penetration test (SPT)

(d) Test pit sampling
Figure 3: Locations of soil boring and test pit

(a) Section 1-1

(b) Section 2-2

Fig. 4 Soil profile of Se ction 1-1 and Section 2-2

Figure 5 demonstrates the SPT with depth of the three boreholes. The SPT with Depth indicated the weak zone locates from 1.0 to 3.0 m then the SPT gradually increases with depth. After 6 meters depth, the SPT is greater than 30 Blow/foot. It implies that the failure surface should not be lower than 3.0 to 4.0 m from the surface. Finally, the BH-1 (located on the opposite site of the failure spot) is used as the representative Geotechnical parameters because it is the lowest SPT values. In addition, the pinhole testing results indicate ND1 class which indicates that Non- dispersive soil.

Finite Element Discretization

Finite element simulations are performed using the PLAXIS 2D software developed by Brinkgreve and Broere (2006) that allows for a realistic simulation of construction sequences. The basic soil elements are represented by the 2D, 15-node elements. The Mohr Coulomb Model (MCM) is selected to model the behavior of all soils.
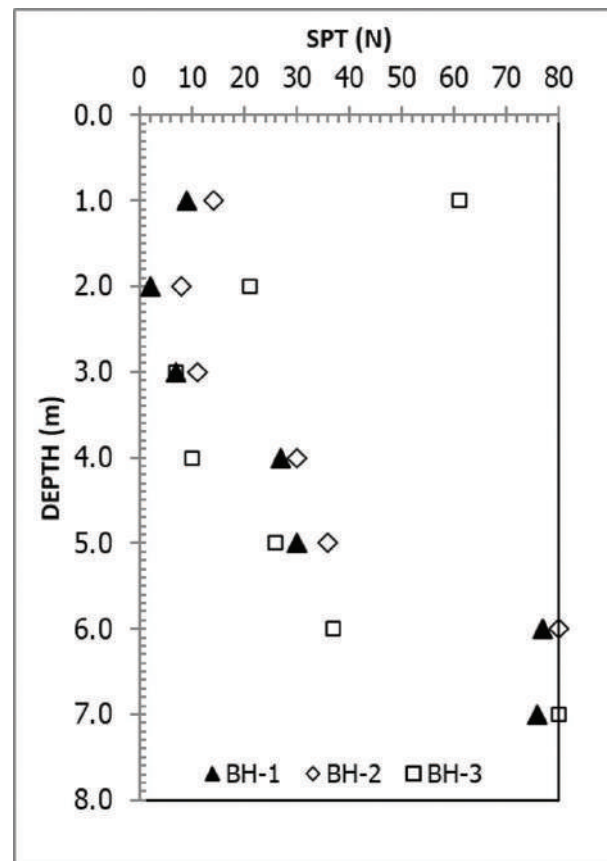

Figure 5: SPT with Depth

The strength reduction method is applied to evaluate the Factor of Safety (Farshidfar and Nayeri, 2015). Generally, the determination of the Factor of Safety for slopes is defined as the proportion of soil shear strength to the minimum shear stress required for creating preliminary failure following:

$$\text{Factor of Safety} = \frac{\text{Allowable strength}}{\text{Strength at Failure}} \quad (1)$$

In the Factor of Safety approach, the shear strength parameters like cohesion (c) and internal friction angle (ϕ) as well as tensile strength are successively until failure of the structure occurs.

Several solutions are proposed, for example, bearing unit, gabion wall, geosynthetic reinforcement, concrete pile wall and so on (Gu, 2011). However, two solutions are adopted which are geogrid reinforcement and soil replacement methods for 100 m and 300 m, respectively because budget is limited. The excavation depth of 3.0 m and 2.0 m for geogrid reinforcement method and soil replacement method, respectively, are requested to remove the existing soil and replace with the suitable materials. The advantages of Geogrid reinforcement method are lower excavation depth, faster construction time and less effect to agriculturists since it is not necessary to reduce the water level in the canals. However, Geogrid reinforcement is very expensive and it is not widely used in rural areas. On the other hand, the soil replacement method requires a greater volume of fill material as well as longer construction time but cheaper and easier for quality control during construction. The pros and cons of both methods are tabulated as shown in Table 1. The selected material type A (following DRR.204-2002) is applied as the filled material for the soil replacement method while the sub-base material (following DRR.202-2014) is used as the embankment material for the geogrid reinforcement method.

Table 1 comparison between pros and cons of soil replacement and geogrid

| Method	Pros	Cons
Soil replacement method	- Cheap - Easy to control the quality of construction - Use filled material nearby construction site	- 3 m or more excavation is needed - May faced the flooding problem - Slow construction
Geogrid Reinforcement	- Faster than Soil replacement method - 2m excavation only - less effect to agriculturists since it is not necessary to reduce the water level	- Expensive - Required expert to control during construction - Not widely used in rural areas

Results

The appropriate material parameters obtained from back analysis as well as laboratory testing are tabulated in Table 2. The Factor of Safety is 1.036 which is compatible to the fail slope at Sta 21+500 for instability slope as shown in Figure 6.

Table 2 Soil Parameters from back analysis

Soil	Y_{unsat}	Y_{sat}	E (kPa)	c (kPa)	φ (°)
Embankment	18.0	20.0	10000	20	0
Layer_1	19.8	22.3	9000	1.5	25
Layer_2	19.9	22.2	9000	1.5	25
Layer_3	18.7	21.2	15000	15	35
Layer_4	18.7	21.7	67500	135	0
Layer_5	18.0	20.0	750000	150	0
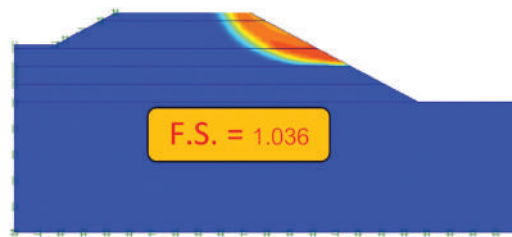
Figure 6: The slip surface of the back analysis model of Sta 21+500.

The minimum requirement of the Factor of Safety of 1.30 for the rapid drawdown condition is considered as the criteria for this project. Fill material of geogrid reinforcement and soil replacement methods is tabulated in Table 3 and geogrid properties for simulation is shown in Table 4, respectively.

The results from simulations demonstrated 1.563 and 1.640 for geogrid reinforcement and soil replacement methods, respectively as shown in Figure 7. Even though, the first method illustrated lower Factor of Safety, however, the displacement is lesser since higher stiffness than the soil replacement method.

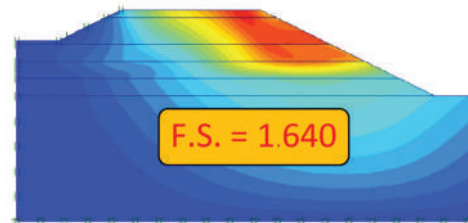**Table 3** Parameters for fill material

Soil	Y_{unsat}	Y_{sat}	E (kPa)	c (kPa)	φ (°)
Embankment	18.0	20.0	10000	20	0

Table 4 Parameters for geogrid material

Geogrid	TYEP	EA (kN/m)
HDPE Geogrid	ELASTIC	2000
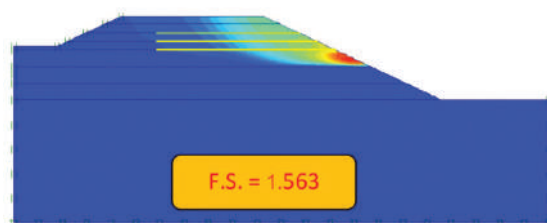
(a) Geogrid reinforcement method

(b) Soil replacement method

Figure 7: The Factor of Safety results

Conclusions

Rural road No.KS.4064 was constructed along the irrigation canal of Lam Pao Dam, Kalasin province during the dry season of 2016 and collapsed soon after paving phase. The cause of failure was investigated by the Bureau of Test, Research and Development together with the local officers a few days after.

Based on the remaining evidences as well as Geotechnical properties obtained from the several laboratory testings, the reasons are weak soil strength underneath together with rapid drawdown during construction. Furthermore, the failure occurrence not only on a roadside, but also on the existing ground opposite site as well. Therefore, the major reason of this road failure is the loose silty sand below the road construction.

In order to remedy this problem, two solutions are proposed, which are geogrid reinforcement method and soil replacement method. The advantages of the first method are faster construction, lower excavation and lesser effect to the farmer. However, the second method seems to be easier for construction and cheaper but cannot construct during rainy season because the high-water level. The Factor of Safety of both methods are greater than 1.3 which indicates that the stability of slope is adequate even though the worst-case condition is considered.

References

Brinkgreve, R.B., & Vermeer, P. A. (2006). *PLAXIS 2D Manual.* Rotterdam: Brookfield.

Department of Rural Road. (2016). Standard for rural road construction. Bangkok: Bureau of Test, Research and Development, Department of Rural Road.

Farshidfar, N., & Nayeri, A. (2015). Slope Stability Analysis by Shear Strength Reduction Method. *Journal of Civil Engineering and Urbanism, 5* (1), 35-37.

Gu, J. (2011). *Computational modeling of geogrid reinforced soil foundation and geogrid rein forced base in flexible pavement.* (Doctoral dissertation). Louisiana: Louisiana State University and Agricultural and Mechanical College.

Suksawat, T.Z. (2008). *Numerical simulation of SDCM and DCM piles under axial and lateral loads and under embankment load: A parametric study No. GE-08-09* (M. Eng. Thesis). Bangkok: Asian Institute of Technology.

Suksawat, T. Z. (2014). *Geotechnical infrastructure asset management focusing on performance deterioration process of ground anchors* (Doctoral dissertation). Kyoto: Kyoto University.

The Furongian (late Cambrian) trilobite *Thailandium*'s endemicity reassessed along with a new species of *Prosaukia* from Ko Tarutao, Thailand

Shelly J. Wernette[1*], Nigel C. Hughes[1,2], Paul M. Myrow[3], Apsorn Sardsud[4]

[1] *Department of Earth and Planetary Sciences, University of California, Riverside, CA 92521, USA.*
[2] *Geological Studies Unit, Indian Statistical Institute, 208 B.T. Road, Kolkata, 700018, India.*
[3]*Department of Geology, Colorado College, Colorado Springs, CO 80903, USA*
[4]*Department of Mineral Resources, 75/10 Rama VI Road,*
Ratchatewi, Bangkok 10400, Thailand.
Corresponding author: swern001@ucr.edu
Received 30 March 2020 ; Accepted 2 July 2020

Abstract

The trilobite *Thailandium solum,* the type species of *Thailandium,* is a large "saukiid" species known only from the Ao Mo Lae Formation of the Tarutao Group, Thailand. In addition to the type species occurrence in Thailand, *Thailandium* is also reported from northern Henan, China as *Thailandium truncatum* Zhou and from Australia's Pacoota Sandstone as an undeterminate species. Type material of *Prosaukia misa,* the type species of *Prosaukia,* as well as recent collections of *Thailandium solum, Prosaukia tarutaoensis* (Kobayashi, 1957), and a new species of *Prosaukia, P. oculata,* from Ko Tarutao, Thailand are used to reevaluate the generic identity of the Australian and north Chinese material using landmark-based morphometric analysis. The new material of *Prosaukia* and *Thailandium*, all from the Ao Mo Lae Formation, reveal that the Australian material is better characterized as *Prosaukia.* The cranidium of north China's *Thailandium truncatum* is geometrically comparable to *Thailandium solum,* but differs notably in overall relief and in the anterior border structure and proportions. Here we assign it tentatively to another "saukiid" genus. These morphometric and qualitative comparisons facilitate a refined generic diagnosis for *Thailandium,* resulting in its restriction to a monospecific genus.

Key words: landmark morphometric, Tarutao, "saukiid", *Thailandium, Prosaukia*

Introduction

The trilobite genera commonly referred to as "saukiid" are among the most diverse, abundant, and spatio-temporally important late Cambrian trilobite groups, but their taxonomy is not well-resolved. At a broad taxonomic level, there is little agreement on whether "saukiid" trilobites collectively are a clade, part of a clade, or are a polyphyletic assemblage within Dikelocephalidae (Adrain, 2011; Lee and Choi, 2011; Park and Kihm, 2015). At the genus level, some differential diagnoses are ambiguous among genera, resulting in some "saukiid" species being reassigned to several different genera after their initial description (e.g. *Eosaukia micropora* Qian, 1985; Lee and Choi, 2011). Refining "saukiid" relationships at both the genus and family levels is important, because "Saukiidae" encompasses numerous genera that are of great importance to late Cambrian (Furongian) biostratigraphy and paleogeography. As of 2002, Jell and Adrain recognized 30 distinct genera referred to as Saukiidae Ulrich and Resser (1930). Of these *Mictosaukia* Shergold (1975), *Sinosaukia* Sun (1935), *Eosaukia* Lu (1954), *Lophosaukia* Shergold (1972), *Saukia* Walcott (1914), and *Saukiella* Ulrich and Resser (1933) have all been used to characterize Cambrian Stage 10 trilobite biostratigraphic zones and subzones in Laurentia, Australia, Kazakhstan, South China, North China, and South Korea (Shergold and Geyer, 2003; Lee and Choi, 2011). *Caznaia* Shergold (1975) characterizes two middle Jiangshanian zones in Australia while *Saukia* and *Saukiella* define the uppermost Jiangshanian zones and subzones in Laurentia (Peng et al., 2012; Ogg et al., 2016). In addition to their biostratigraphic application, "saukiid" genera are also important for paleogeographic reconstruction: Gondwana contains a suite of "saukiid" genera unique to its terranes, including but not limited to *Lophosaukia, Mictosaukia,* and *Eosaukia.*

The taxonomic challenges associated with "saukiids" limit their current application to broader geologic questions. The characters differentiating many of the "saukiid" genera are not the discrete presence or absence of particular traits but rather the exaggeration or reduction of traits common to many or all "saukiids". Some are differentiated by the presence, length, or inflation of the preglabellar field (Ulrich and Resser, 1933; Ludvigsen and Westrop, 1983). Shergold (1991) recognized three morphological groupings of "saukiid" cranidia, the first of which comprises *Prosaukia*-like genera, including *Thailandium, Caznaia, Lichengia,* and *Saukiella,* which have a distinct preglabellar field fully distinguishable from the anterior border.

Within this group of "saukiids" with a distinct preglabellar field, *Thailandium* Kobayashi, 1957 has an exceptionally long preglabellar field and a strongly differentiated anterior border. This genus has been reported from three regions: Thailand's Ko Tarutao (also called Tarutao Island) in Satun Global Geopark (Kobayashi, 1957), northern Henan, China (Zhou et al., 1977), and Australia's Amadeus Basin (Shergold,

1991). The type species, *Thailandium solum* Kobayashi, 1957, was described from the Ao Mo Lae Formation of the Tarutao Group, then known as the Tarutao Formation, in the initial description of the fauna of Ko Tarutao. Zhou et al. (1977) erected a second species, *Thailandium truncatum,* on a single specimen and reassigned the genus to Elviniidae Kobayashi, 1935 with no reasons given for this change in family assignment. This species was characterized as coming from the North China block by Zhu (2008). In their more extensive description of the Tarutao Group's trilobite fauna, Shergold et al. (1988) did not illustrate or discuss *Thailandium* with the exception of reassigning certain librigena and pygidia form Kobayashi's (1957) figured material to other species such as *Quadraticephalus planulatus* (Kobayashi, 1957) and *Lichengia tarutaoensis* (Kobayashi, 1957; *sensu* Shergold et al., 1988). Shergold (1991) assigned specimens from the Pacoota Sandstone of the Amadeus Basin (Fig. 1) to an undetermined species of *Thailandium* based on a similarly long frontal area and defined anterior border as *Thailandium solum* with the caveat that they likely belong to *Prosaukia.* Shergold (1991) suggested that the
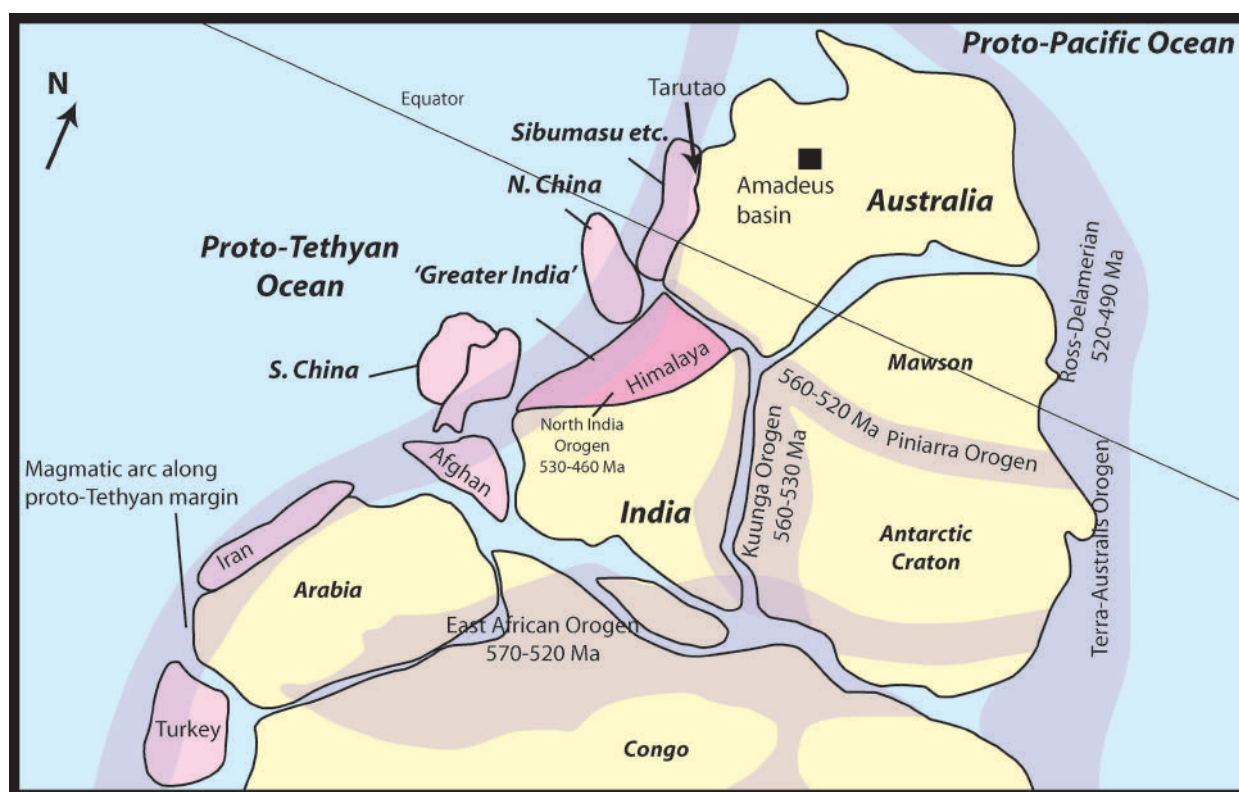
Figure 1: Cambro-Ordovician paleogeographic reconstruction of northern Gondwana. Locations of the Amadeus Basin and Tarutao are only approximations to indicate their relative locations and proximity. Modified from Hughes, 2016; orogenies from Cawood et al., 2007; equator from Cocks and Torsvik, 2013.
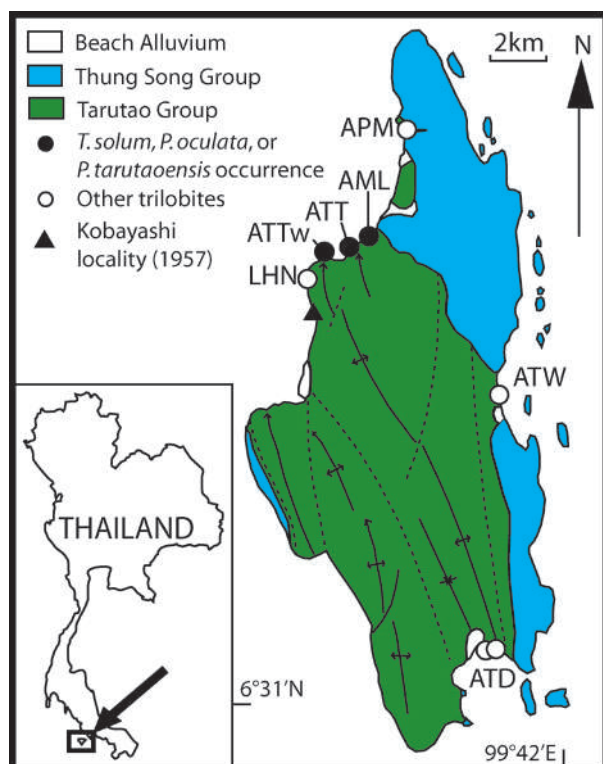
Figure 2: Trilobite Occurrences on Ko Tarutao: AML = Ao Mo Lae; ATT = Ao Talo Topo; ATTw = Ao Talo Topo west; LHN = Laem Hin Ngam; ATD = Ao Talo Udang; APM = Ao Phante Malacca; ATW = Ao Talo Wao. Modified from Bunopas et al., 1983 and Wernette et al., 2020.

status of his Australian material could be meaningfully evaluated only after reevaluation of the *T. solum* type material with greater consideration of possible morphologic variation within it and did not comment on *T. truncatum*. A series of excursions from 2008 to 2018 have greatly expanded trilobite collections from Ko Tarutao (Fig. 2). This new material permits reevaluation of the cranidial morphology of *T. solum,* prompting reassessment of Shergold's (1991) question of whether the specimens from the Pacoota Sandstone are truly *Thailandium* and reconsideration of the relationship of *Thailandium truncatum* from North China. Species of *Prosaukia* found during the same excursions, *Prosaukia tarutaoensis* (Kobayashi, 1957; *non Lichengia tarutaoensis* in Shergold et al., 1988) and *P. oculata* n. sp. facilitate comparison of species assigned to *Thailandium* with those of the related genus, *Prosaukia.*

Landmark-based morphometric analysis is a useful tool for objectively considering morphological variation within and between groups. This tool was herein applied to *Thailandium solum, Prosaukia tarutaoensis,* and *Prosaukia oculata*

from Ko Tarutao, the figured type material of *P. misa* (Hall, 1863), the *Prosaukia* type species, the figured material of *Thailandium* sp. undet. from Australia, and the figured holotype of *Thailandium truncatum* from China in order to determine whether a consistently diagnosable difference exists between *Thailandium* and *Prosaukia* and, if so, to which genus *Thailandium* sp. undet. is best assigned. As demonstrated herein, the continued recovery of new species from poorly explored terranes like Sibumasu offers material with which to refine definitions of existing genera such as *Prosaukia* and *Thailandium.*

Tarutao Localities

The Tarutao Group is the stratigraphically lowest Paleozoic unit in western Thailand. While the Tarutao Group cops out on both the mainland of southern Thailand and Ko Tarutao, only outcrops on Ko Tarutao are documented to contain identifiable fossils (Wangwanich et al., 2002). Ko Tarutao is sufficiently removed from the Bentaung Raub Suture Zone between Sibumasu and the East Malaysian Terrane to the east and from the Sumatran Fault Zone to the west that it represents a reasonably tectonically stable area, and the fossils show no evidence of tectonic deformation (Burrett et al., 2014). The Tarutao Group is a clastic succession of mostly very fine to fine-grained sandstones with interbedded siltstones, mudstones and rhyolitic tuffs. It is distinct from the overlying carbonate-rich Thung Song Group, the only other lithologic unit to occur on the island. Of the four formations that comprise the Tarutao Group (Ao Makham, Ao Tami, Ao Mo Lae, and Talo Wao), only the upper two, Ao Mo Lae and Talo Wao, have yielded trilobite fossils.

Of the five fossiliferous localities and six stratigraphic sections on which our teamworked during visits made between 2008–2018 (. 2) the materials of relevance to this paper are only found at Ao Talo Topo (ATT) (06°40'08"N, 099°37'46"E), Ao Talo Topo west (ATTw) (06°39'49"N, 099°37'08"E), and Ao Mo Lae (AML) (06°40'13"N, 099°38'02"E). ATTw is separated from ATT by a prominent bay. Both localities were originally given the same name by the authors, but they are here differentiated. All stratigraphic measurements were completed at ATT, and only a single bed was sampled with little stratigraphic context at ATTw as part of the 2008 exploratory excursion; this is also
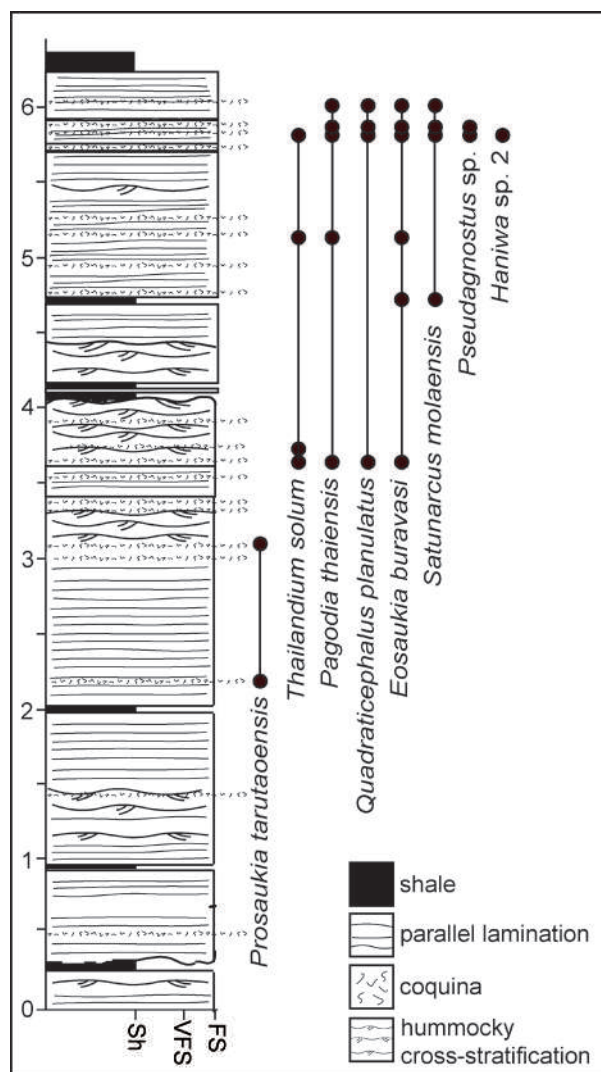
Figure 3: Measured lithostratigraphic section and faunal ranges for Ao Mo Lae (AML). Sh = shale; vfs = very fine sand; fs = fine sand; coq = coquina. Measurements are in meters.

the bed in which *Satunarcus molaensis* Wernette and Hughes, 2020 was collected, so any references to ATT in Wernette et al. (2020) refer to what is here called ATTw.

All three localities with material considered in this paper consist exclusively of the Ao Mo Lae Formation, the second highest of the four formations included within the Tarutao Group (Imsamut and Yathakam, 2011). The entire formation, only a small portion of which is exposed at Ao Mo Lae, is estimated to be ~600m thick, but this estimate is speculative due to the prevalence of faults around the island and discontinuity of exposures (Imsamut and Yathakam, 2011). It primarily consists of purplish red and gray fine-grained quartzarenites. Rhyolitic tuff deposits occur mostly in the upper portions of this formation (Imsamut and Yathakam, 2011). Disarticulated, mildly

fragmented fossils are concentrated into dense coquinas on some bedding surfaces. Fossil preservation is as molds which may appear white where silica has become concentrated as a thin staining on the surface of the mold but not enough to form a silicic cast.

The similarity of faunal content indicates that the Ao Mo Lae Formation is from Cambrian Stage 10, and the ATTw and AML fauna appear to be of nearly the same depositional age (see Fig. 3 and following paragraph for faunal content); ATT (Fig. 4) may have a slightly different age than the other two. Based on the shallow northeastward dip evident at both ATT and AML, the latter may be slightly younger if these sections are in stratigraphic continuity, but they are separated by a small, sandy inlet which may conceal one of Ko Tarutao's many faults. The lithology of all three localities is similar except that ATT and ATTw contain several prominent horizons of rhyolitic tuffs. ATT has a slightly different faunal assemblage than the other two localities (Figs. 3 and 4) with much of their shared fauna occurring only in material from ATT or AML that was not located to a specific horizon.

Collections of fossils made from single beds at specified localities, but whose particular horizon was not located within a measured section are included here, because these collections are informative regarding the diversity of the Ao Mo Lae Formation and regarding taxon cooccurrences. The single horizon at ATTw contains *Thailandium solum* Kobayashi (1957), *Prosaukia tarutaoensis* (Kobayashi, 1957), *Haniwa* sp. 1, *Pagodia thaiensis* Kobayashi (1957), *Quadraticephalus planulatus* (Kobayashi, 1957), *Satunarcus molaensis* (Wernette et al., *2020),* and *Eosaukia buravasi* Kobayashi (1957). One poorly localized horizon at Ao Talo Topo, henceforth referred to as ATT h1 contains *Koldinioidia* sp. and *Prosaukia oculata*. Five not-localized-within-section collections were assembled from AML, henceforth referred to as Ao Mo Lae horizons 1–5 (AML h1–AML h5). AML h1 and AML h2 correspond to horizons 1 and 2 from Wernette et al. (2020). AML h2 contains *Thailandium solum, Quadraticephalus planulatus, Satunarcus molaensis, and Eosaukia buravasi;* AML h3 contains *T. solum, P. tarutaoensis, P. thaiensis,* and *E. buravasi;* AML h4 contains *T. solum, Q. planulatus,* and
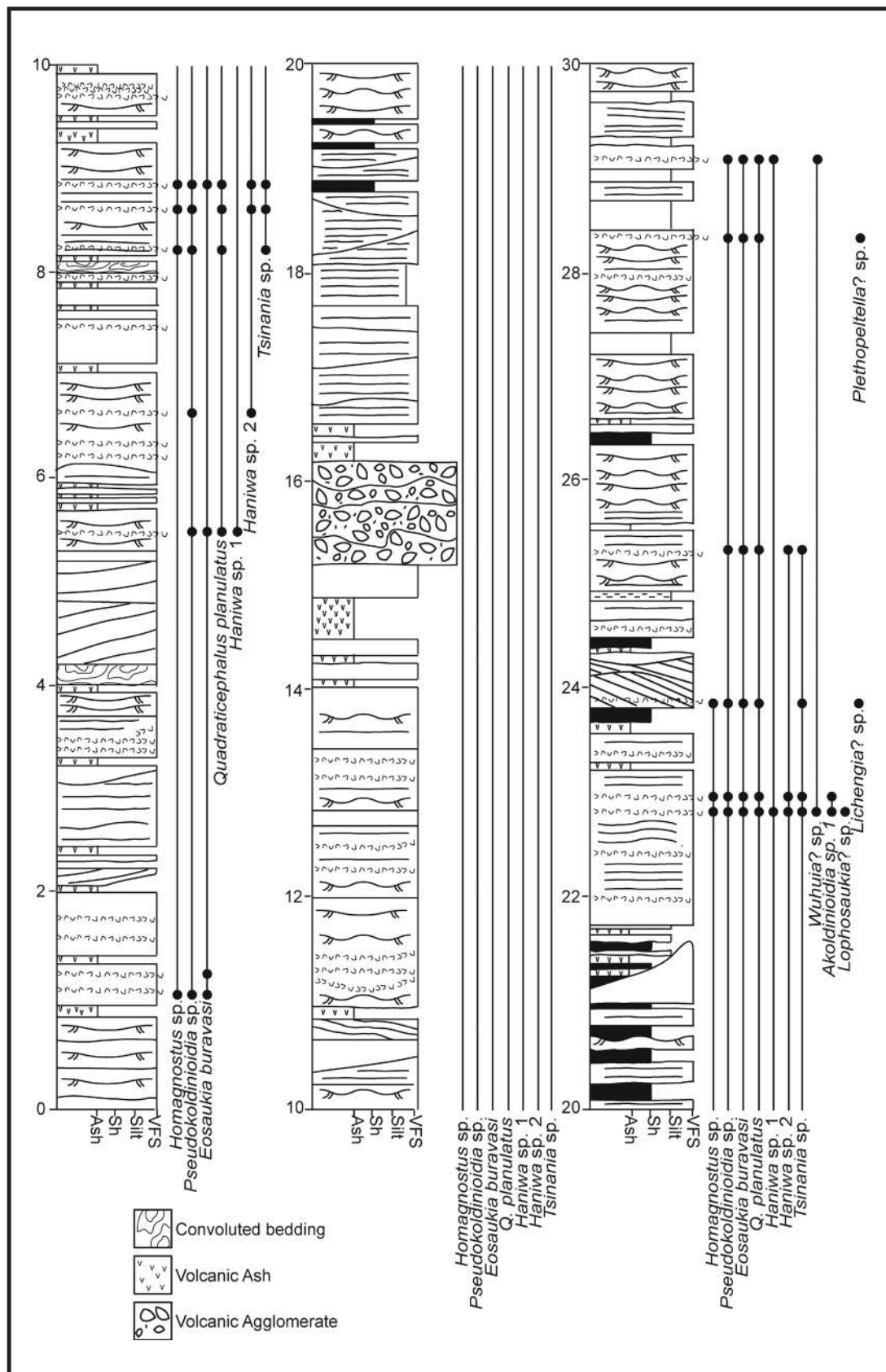
Figure 4: Measured lithostratigraphic section and faunal ranges for Ao Talo Topo (ATT). Measurements are in meters. See Fig. 3 for abbreviations and additional legend symbols.

E. buravasi; AML h5 contains *T. solum, E. buravasi,* and *Pacootasaukia?* sp. The fauna listed herein, excluding *P. tarutaoensis* and *P. oculata,* uses the names originally given by Kobayashi (1957), Shergold et al. (1988), or Wernette et al. (2020); previously undescribed species collected on the recent excursions (excluding those described herein) are listed by genus only. This paper is part of ongoing work revising the Kobayashi (1957) and Shergold et al. (1988) material as well as describing newly collected material (e.g. Wernette et al., 2020).

Materials and Methods

The morphometric analysis that follows is based on 22 discrete landmarks (Fig. 5) and 30 cranidia. Only specimens with sufficient preservation to distinguish all axial landmarks and at least one of each paired landmark were eligible for use in the analysis. 15 cranidia are of *Thailandium solum,* all from Ko Tarutao (DGSC F0419, F0435, F0543, F0544, F0568, F06569, F0570, F0574, F0583, F0595, F0601, F0606, F0607, F0609, and CMC IP87617). The holotype *of Thailandium,* though figured from a vinyl polysiloxane cast herein, was excluded from the analysis as the original figure (Kobayashi, 1957, pl. 4, fig. 9) lacks a clear posterior occipital margin Four cranidia assigned to *Thailandium* sp. undet. from the Pacoota Sandstone in the Amadeus Basin of Australia are considered (Shergold, 1991 pl. 4, figs 16–18, 21; CPC26805A, CPC26806, CPC26807, CPC26825). One cranidium assigned to *Thailandium truncatum* from northern Henan, China is included (Zhou et al., 1977 pl. 55, fig. 23; Hubei Institute of Geoscience IV70109). Two syntype cranidia are included of *Prosaukia misa* (Hall, 1863), the type species of *Prosaukia* Ulrich and Resser, 1933 (pl. 24 figs 3 and 7; USNM 84538, MPM 5968). Four cranidia belong to *Prosaukia oculata* n. sp. (DGSC F0461, F0503, F0511, and F0512), and four cranidia are of *Prosaukia tarutaoensis* (Kobayashi, 1957, pl. 5 fig. 12, and three recently collected specimens; UMUT PA02298c, DGSC F0566, F0546, and F0545 respectively). The published figures of *P. misa* (in Ulrich and Resser, 1933), *Prosaukia tarutaoensis* (Kobayashi, 1957), *Thailandium truncatum* Zhou, 1977, and *Thailandium* undet. (Shergold, 1991) are of sufficient quality that landmarks could be mapped directly onto
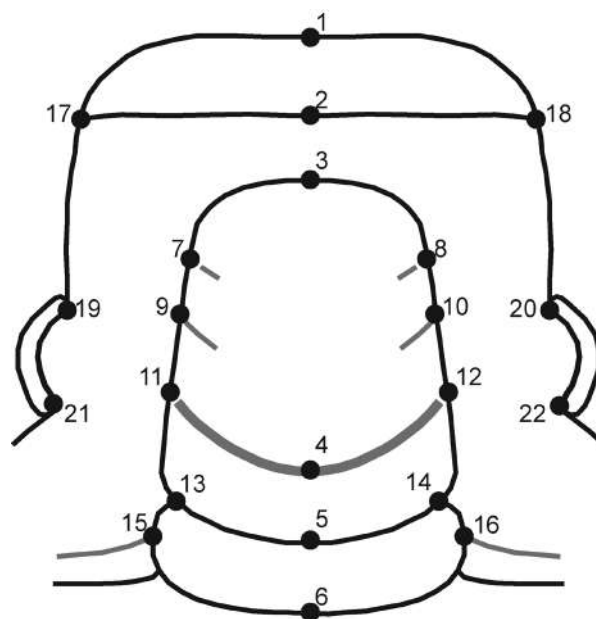

Figure 5: Landmark scheme showing the 22 landmarks used in the morphometric analysis of *Prosaukia* and *Thailandium.*

digitized copies of the original published illustrations. The size range for each taxon, measured by the length of the preoccipital glabella, is as follows: 2.47–16.53 mm for *Thailandium solum,* 4.57–8.37 mm for *Thailandium* sp. undet., 11.03–15.96 mm for *P. misa,* 2.31–6.34 mm for *P. oculata,* and 2.50–7.71 mm for *P. tarutaoensis.*

Thai specimens from the 2008, 2016, and 2018 excursions were prepared manually using a Dremel vibrotool, then blackened with India ink, whitened with ammonium chloride, and photographed with a Leica stereoscopic camera model MZ16 or M205C. All figures and plates were created using Adobe Illustrator CS2 and Adobe Photoshop CC2017. External molds were figured in positive relief by using the color inversion feature available in Photoshop CC2017. Molds of Kobayashi's (1957) type material were made using vinyl polysiloxane in the form of light bodied President Plus by Coltene.

Geometric morphometric analysis was conducted using the free software ImageJ and the Integrated Morphometrics Package (Coord-Gen8, BigFix8, Regress8, and PCAGen8), a set of compiled software tools for displaying and analyzing 2-D landmark-based geometric morphometric data (Webster and Sheets, 2010; http://www.filogenetica.org/cursos/Morfometria/IMP_installers/index.php). Landmarks were reflected and averaged across the sagittal axis.
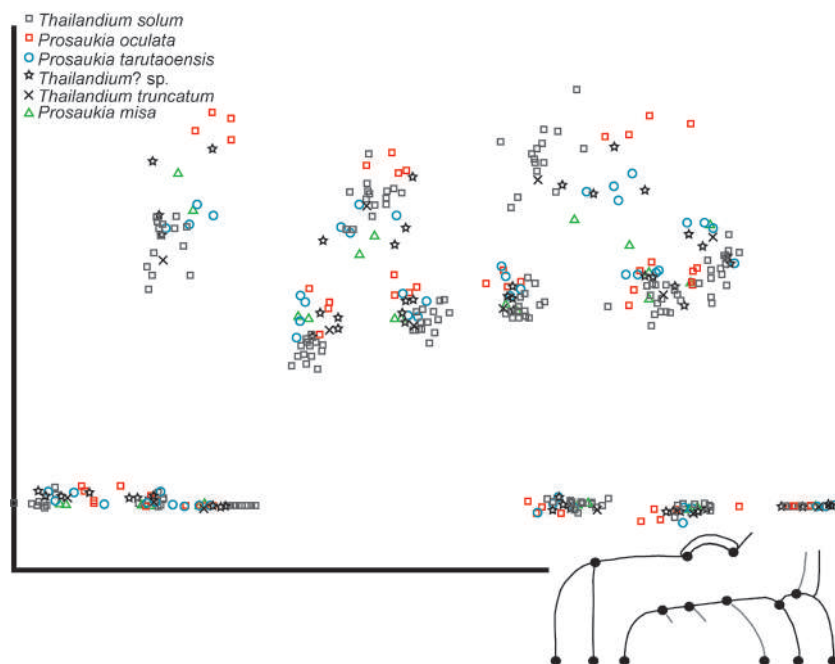
Figure 6: Sliding baseline registration of 22 landmarks across 30 cranidia of "saukiid" dikelocephalids. The x-axis anchored baseline landmarks are landmarks 3 and 6. See Fig. 5 for landmark scheme. *Thailandium?* sp. is the taxon from Australia (Shergold, 1991) herein reassigned to *Prosaukia* sp.

All figured specimens and select unfigured specimens from the 2008-2018 excursions are reposited at Thailand's Department of Mineral Resources' Geological Referenced Sample Collection (DGSC). Additional unfigured specimens are curated at the Cincinnati Museum Center (CMC). Type material from Kobayashi (1957) is reposited at the University of Tokyo University Museum (UMUT); one or more polysiloxane molds of each specimen in the Kobayashi (1957) collection at UMUT is also reposited in the plastotype collection at CMC. Additional specimens used in the morphometric analysis are curated in the Commonwealth Palaeontological Collection, Bureau of Mineral Resources, Canberra (CPC) and the Smithsonian National Museum of Natural History (USNM), Hubei Institute of Geoscience, and the Milwaukee Public Museum (MPM).

Results and Discussion

Sliding baseline registration (SBR) best displays the variation within the dataset and so is used consistently throughout the following discussion of morphometrics except where Procrustes superimposition is required for statistical calculations of group mean differences (Webster and Sheets, 2010). The SBR distribution of landmarks (Fig. 6) indicates that *Thailandium solum* and *Thailandium* sp. undet. (*sensu* Shergold, 1991) have similarly long frontal areas relative to glabellar length and similar division of the frontal area into preglabellar field and anterior border. The relative length of the frontal area of *Thailandium truncatum* is, however, somewhat shorter than that of *Prosaukia misa*. With regard to the palpebral lobe position (Fig. 5, landmarks 19–22), *T. solum*'s positions align more with *Prosaukia oculata;* the eyes for these species are more abaxially placed than in the other species; the palpebral lobes of *P. oculata* are, however, longer with the posterior end extending further backwards. *Prosaukia misa, Prosaukia tarutaoensis,* and *Thailandium* sp. undet. have similarly long palpebral lobes that are more posteriorly centered than in *T. solum.* The palpebral lobes of *T. truncatum* are relatively short and anteriorly placed, as in *T. solum.* All six species have a similar longitudinal placement of the anterior end of the palpebral lobe, so it is the position of the posterior end that reveals differences in overall palpebral length. The lateral corner of the anterior border (Fig. 5, landmarks 17, 18) is similarly placed in *P. misa, P. tarutaoensis, T. solum, T. truncatum,* and *Thailandium* sp. undet., but in *P. oculata* it is more posterolaterally positioned,
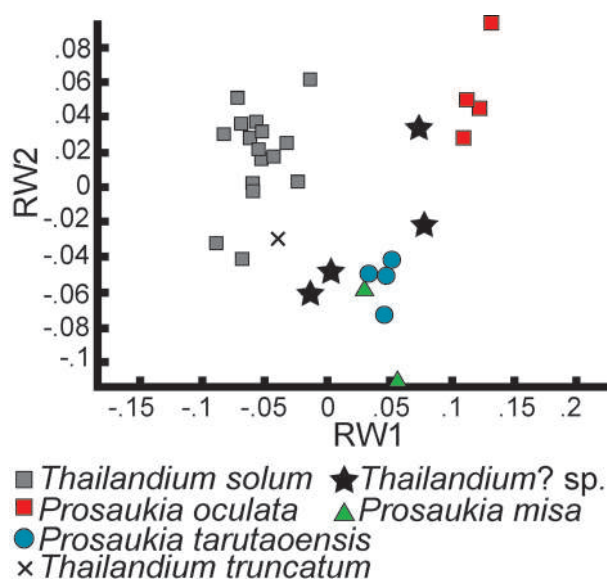
Figure 7: First two relative warps (RW1 and RW2), accounting for 42.90% and 20.19% of the variance respectively. *Thailandium?* sp. is the taxon from Australia (Shergold, 1991) herein reassigned to *Prosaukia* sp.

attributable to the very short preglabellar field and wide-set fixigena in that form. If isolated clusters of landmarks were to be required for generic distinction, no evident differences separate *Thailandium* from *Prosaukia*. However, the collective alignment of the six lateral most landmarks (Fig. 5, landmarks 17–22) is different in *T. solum* and *T. truncatum* than in the other four species. In *T. solum* the landmarks aligned along an anteromedial trendline. In the other four species the anterior palpebral landmarks (Fig. 5, landmarks 19, 20) are more medial than the posterior palpebral landmarks or lateral corners of the anterior border (Fig. 5, landmarks 21, 22, 17, 18). In this way *T. solum* and *T. truncatum* form a distinctly separate group, and *Thailandium* sp. undet. follows the same trend as the species of *Prosaukia*.

The first two relative warps of a thin plate spline decomposition (Bookstein, 1991) of the shape variation in the sample (RW1 and RW2; Fig. 7) account for 42.90% and 20.19% of the variance respectively; other relative warps account for less than 10% of variance each. The distribution of specimens along the first two relative warps, particularly RW1, further support the differentiation of *Thailandium solum* and *Thailandium truncatum* from the other four species discussed with a distinct group of the former two and overlap among *P. misa, P. tarutaoensis, P. oculata,* and *Thailandium* sp.

undet. This view is supported by the significant shape difference between *Thailandium* sp. undet. and *T. solum* (using a Procrustes superimposition to compare shape differences Goodalls's F, p >0.00001; F test p = 0.0004 with 2500 bootstraps). Between *Thailandium* sp. undet. and the pooled *Prosaukia* sample the difference is not significant (using a Procrustes superimposition to compare shape differences Goodalls's F, p =0.28578; resampling F test with 2500 bootstraps p = 0.3188). Thus the similarity of specimens of *Thailandium* sp. undet. to those of the three species of *Prosaukia* (Fig. 7) and its evident separation from the specimens of *T. solum* and *T. truncatum* indicate that *Thailandium* sp. undet. should be reclassified as a species of *Prosaukia*.

Relative warp 1 largely captures differences in the lateral placement of the anterior border's lateral corner, the length of the frontal area, and the longitudinal placement of the palpebral lobe's posterior point (Fig. 8). Relative warp 2 primarily captures the width of the fixigena and lateral position of the palpebral lobes. The differentiation of *Prosaukia* and *Thailandium* along RW1 (Fig. 7) is consistent with the SBR landmark distribution (Fig. 6) in differentiating *Thailandium solum* and *Thailandium truncatum* from *Prosaukia,* including *Thailandium* sp. undet., by the anterior convergence of the anterior facial suture branches, shorter palpebral lobes, and a particularly long frontal area. *Thailandium solum* also has wider fixigena than is typical for *Prosaukia* as indicated by distribution along RW2, but this is not a reliably diagnostic character since P. oculata has fixigena of comparable width to *T. solum*. A reliable diagnosis for the difference in length and longitudinal position of the palpebral lobe of *Thailandium* versus *Prosaukia* is that the posterior end of the palpebral lobe is opposite S1 in *T. solum* but in all other species included herein it is opposite L1.

The separate clustering of *P. oculata* on RW1 and RW2 reflects its wide fixigena and short preglabellar field. The short preglabellar field is consistent with some other species of *Prosaukia* (e.g. *P. subaequalis* Ulrich and Resser, 1933). Broad fixigena are also known in other species of *Prosaukia* (e.g. *P. delecostata* Ulrich and Resser, 1933). Therefore, these characters do not suggest the need to establish a separate genus.
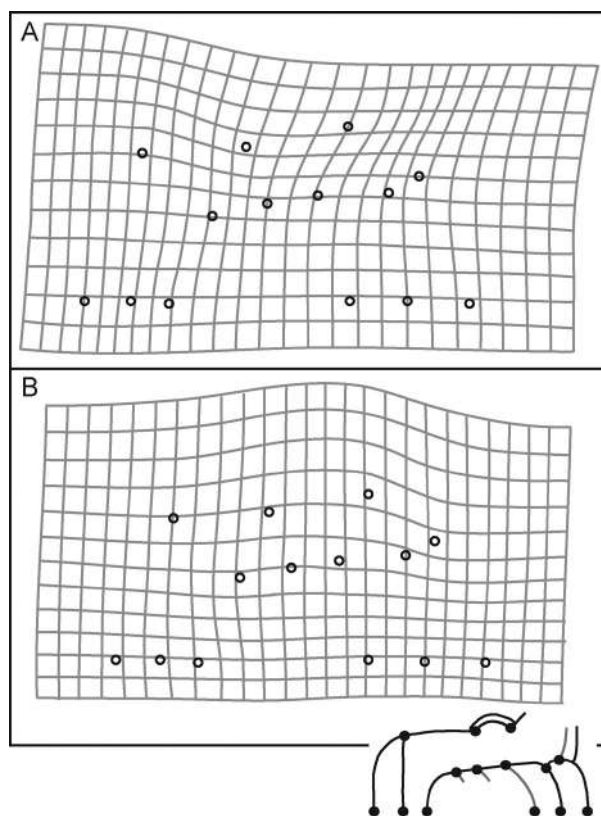
Figure 8: Relative warp grids using SBR superimposition for RW1 and RW2 for the 22 cranidial landmarks of all specimens of *Thailandium solum, Prosaukia misa, Prosaukia oculata, Prosaukia tarutaoensis,* and *Thailandium* sp. undet. (1) shape variation related to Relative Warp (RW) 1, 42.90% of total variance; (2) shape variation related to RW2, 20.19% of total variance.

Based on the landmark morphometric analysis alone, *T. solum* and *T. truncatum* differ only in the length of the frontal area and width of the occipital lobe. However, they are readily distinguished by characters not captured in our geometric analysis, including overall convexity and the manner of incision of the anterior border furrow, to the extent that *T. truncatum* is unlikely to be a species of *Thailandium*. For additional comments regarding the affinity of *T. truncatum* see the generic remarks for *Thailandium*.

Systematic Paleontology

The systematic paleontology section is by Shelly Wernette and Nigel Hughes. Measurements and species descriptions are based on internal molds unless otherwise specified. The abbreviations SO and S1–S3 refer to the occipital furrow and lateral glabellar furrows respectively; LO and L1-L3 refer to the occipital and glabellar lobes.

Superfamily DIKELOCEPHALOIDEA Miller, 1889

Family DIKELOCEPHALIDAE Miller, 1889

Remarks.—The dikelocephalid trilobites discussed herein are those historically assigned to Saukiidae Ulrich and Resser (1930) and still commonly referred to as "saukiid" trilobites. The taxonomic ranking or validity of the "saukiid" grouping has long been controversial. Saukiinae was initially established as a subfamily within Dikelocephalidae (Ulrich and Resser, 1930). Raasch (1951) elevated Saukiinae to the level of family, arguing for a closer link to Ptychaspidiidae Raymond (1924) than to other dikelocephalids. This view quickly became widely accepted (e.g. Hupé, 1955; Lochman, 1956). However its taxonomic position has not been stable with Kobayashi (1960), Longacre (1970), Stitt (1971, 1977), and Taylor and Halley (1974) relegating it to a subfamily of Ptychaspididae and Ludvigsen and Westrop (1983) retaining the family designation but reassigning it to Dikelocephaloidea. Due to the inability to establish synapomorphic characters for all of Saukiidae, Ludvigsen et al. (1989) abandoned this grouping, claiming that it is a paraphyletic group and thus a junior synonym of a larger, monophyletic Dikelocephalidae. This scheme has been widely accepted by Laurentian and Gondwanan trilobite workers (e.g. Adrain, 2011 and Lee and Choi, 2011), although some authors continue to use Saukiidae as a family- level designation within Dikelo-cephaloidea (e.g. Park and Kihm, 2015; Shergold et al., 2007). Herein we follow the scheme assigning the "saukiid" trilobites to Dikelo-cephalidae but without strong opinion as to whether the existence of Saukiidae is supported by synapomorphies either as a paraphyletic or monophyletic group.

Genus *Thailandium* Kobayashi, 1957
Type species.—*Thailandium solum* Kobayashi, 1957 from the Ao Mo Lae Formation, Tarutao Group, Ko Tarutao (by original designation)

*Emended diagnosis.*—As for *Thailandium solum.*

Remarks.—The results of the above landmark morphometric analysis indicate that *Thailandium*

possesses anteriorly convergent facial sutures and that *Thailandium* sp. undet. (sensu Shergold, 1991) is a species of *Prosaukia* rather than of *Thailandium*. The shorter frontal area of *T. truncatum* is evident from the morphometrics, but other notable differences between *T. solum* and *T. truncatum* are not. In *Thailandium truncatum* Zhou et al., 1977 the anterior border furrow shallows notably medially, while other furrows are deeply incised, and the fixigena and preglabellar field are inflated, strongly convex rather than relatively flat as in *T. solum*. Furthermore the occipital lobe is much broader than L1.

The single cranidium known for *T. truncatum* does not fit with the concept of *Thailandium* as a flat, broad taxon with a long frontal area. The inflated preglabellar field with a medially shallowing anterior border furrow is well-developed in two "saukiid" genera, *Hoytaspis* Ludvigsen and Westrop, 1983 and *Caznaia* Shergold, 1975. The short (tr.) S2 and S3, nearly straight (tr.) anterior border furrow, strongly anteriorly tapering glabella, and lack of coarse granulation preclude assignment to *Hoytaspis* (Ludvigsen and Westrop, 1983; Shergold, 1975). *Caznaia* Shergold, 1975 is a better match. Though the generic diagnosis for *Caznaia* includes anteriorly divergent facial sutures, *Caznaia sectarix* Shergold, 1975, one of the two species originally included in the genus, has anteriorly convergent sutures. The medially deep S1 of *T. truncatum* and relatively straight-sided preoccipital glabella are more problematic for assignment to *Caznaia,* but variation among *C. sectarix* and *Caznaia squamosa* is sufficient to suggest that these character states may not preclude assignment. The pygidia and librigena of *Thailandium* and *Caznaia* are sufficiently distinct that recovery of these would help significantly in determining to which, if either, of these genera *T. truncatum* belongs, but until such material is recovered, we reassign *T. truncatum* to *Caznaia? truncata*. While its genus is uncertain, *Caznaia? truncata* more likely belongs to Dikelocephalidae than to Elviniidae Kobayashi, 1935 as it lacks the notable eye ridges evident in species that have been assigned to Elviniidae (e.g. Palmer 1965, pl. 3, figs. 9, 11, 12, 14, 16).

With the exclusion of *Caznaia? truncata* and *Thailandium* sp. undet. *Thailandium* is left as a monospecific genus known only from Ko Tarutao, Thailand.
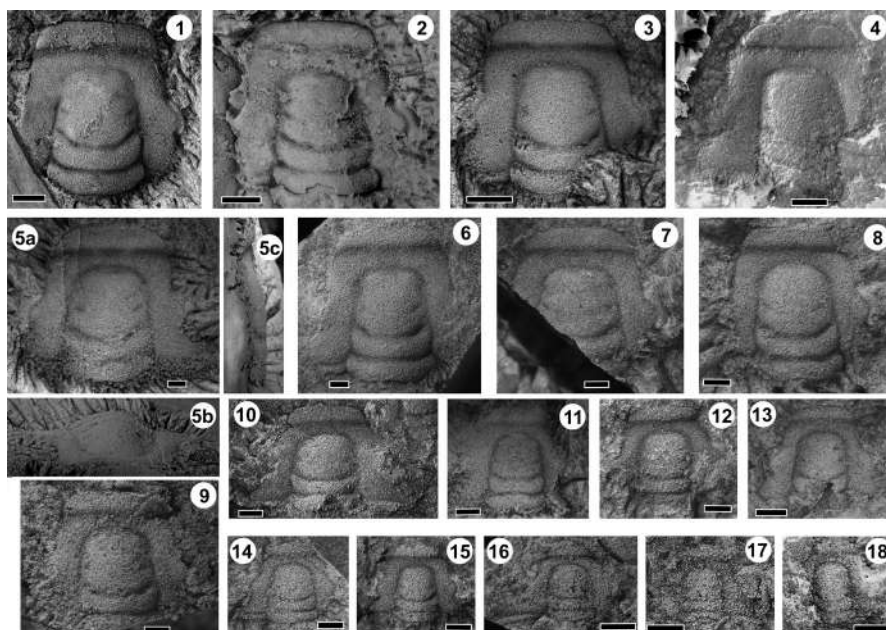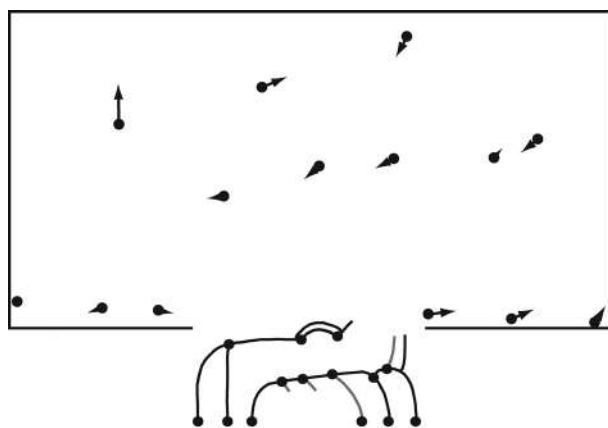

Figure 9: *Thailandium solum* Kobayashi, 1957 cranidia from Ko Tarutao. (1) DGSC F0570, Ao Mo Lae (AML) 3.72 m; (2) DGSC F0419, Ao Talo Topo west (ATTw); (3) DGSC F0609, AML 581 m; (4) CMC IP87037, vinyl polysiloxane cast, original of UMUT PA02299b-1, Kobayashi (1957) pl. 4 fig. 9, holotype; (5a–c) dorsal, anterior, and left lateral views respectively, DGSC F0607, AML 5.81 m; (6) DGSC F0568, AML 3.62 m; (7) DGSC F0602, AML 5.81 m; (8) DGSC F0601, AML 5.81 m; (9) DGSC F0596, AML 5.81 m; (10) DGSC F0435, ATTw; (11) DGSC F0583, AML 5.81 m; (12) DGSC F0576, AML 5.81 m; (13) DGSC F0598, AML 5.81 m; (14) DGSC F0595, AML 5.81 m; (15) DGSC F0544, AML h3; (16) DGSC F0569, AML 3.62 m; (17) DGSC F0574, AML 5.17 m; (18) DGSC F0591, AML 5.81 m. All internal molds except 18, external mold. Scale bars = 5 mm for 10.1–10.4 and 2 mm for 10.5–10.18.
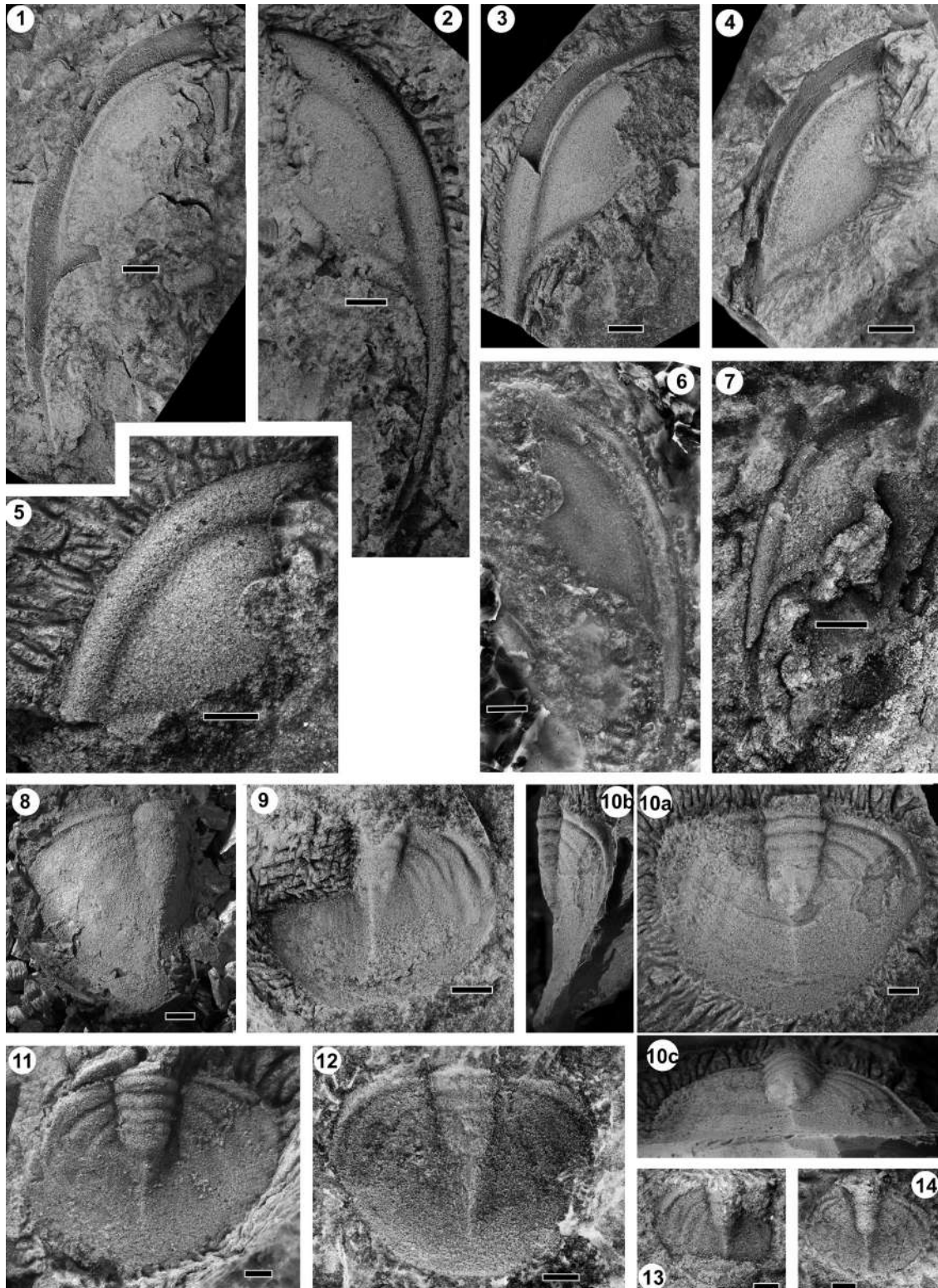
Figure 10: *Thailandium solum* Kobayashi, 1957 librigena (1–7) and pygidia (8–14) from Ko Tarutao. (1) DGSC F0621 Ao Mo Lae (AML) h2; (2) DGSC F0554, AML h3; (3) DGSC F0612, AML 5.81 m; (4) DGSC F0616, AML 5.81 m; (5) DGSC F0631, AML 5.81 m; (6) CMC IP87039, vinyl polysiloxane cast, original of UMUT PA02299b-2, Kobayashi, 1957 pl. 4, fig. 10; (7) DGSC F0418, Ao Talo Topo west (ATTw); (8) CMC IP87046, vinyl polysiloxane cast, original of UMUT PA02299d-1, Kobayashi (1957) pl. 4, fig. 16; (9) DGSC F0610, AML 5.81 m; (10a–c) dorsal, right lateral, and posterior views respectively, DGSC F0611, AML 5.81 m; (11) DGSC F0565 AML 2.2 m; (12) DGSC F0509, AML 5.81 m, external mold; (13) DGSC F0604, AML 5.81 m; (14) DGSC F0560, AML h4. All internal molds except 5. Scale bars = 5 mm for 1–3, 8–13 and 2 mm for 4–7, 14.

Figure 11: Shape change with growth for *Thailandium solum* Kobayashi, 1957, produced from the regression of Procrustes distance vs. log of centroid size (LCS) using the three smallest specimens as reference. P=0.007 for 1600 bootstraps.

Thailandium solum Kobayashi, 1957
Figs 9, 10

1957 *Thailandium solum* Kobayashi p. 373, pl. 4 fig. 9,10; not figs 11,12 *(Quadraticephalus planulatus)*.
1957 *Coreanocephalus planulatus* Kobayashi pl. 4 figs 16,17 only, not figs 13–15 *(Quadraticephalus planulatus)*.

Diagnosis.—Trapezoidal cranidium with long frontal area long (sag.) equally to subequally divided into the anterior border and preglabellar field, anteriorly convergent facial suture branches, low convexity, shallow furrows, strongly bowed, medially continuous S1; palpebral lobes short (exsag.) with posterior point opposite S1. Pygidium subcircular to subtriangular, axis short with four axial rings and long post-axial ridge occupying about half the pygidial length (sag.), pleural field broad, effaced.

Occurrence.—Ao Mo Lae (AML) 3.62–5.81m, AML horizons 3–5, and Ao Talo Topo west; Ao Mo Lae Formation of the Tarutao Group, Thailand; lower to middle Cambrian Stage 10.

Emended Description.—Cranidium as described by Kobayashi (1957, p. 374) except that the entire surface is very faintly granulose, not smooth. Occipital glabellar length (sag.) up to 1.6 cm.

Librigena moderately broad with smooth, gently sloping pleural area and firmly-incised posterior and lateral border furrows defining wide, inflated borders; posterior border furrow confluent with lateral border furrow, extending to posterior margin so as to fully separate lateral and posterior borders. Genal spine long with broad base and slow posterior tapering; uninterrupted extension of lateral border. Doublure same width (exsag. and tr.) as lateral border. Eye semi-circular with distinct eye socle.

Pygidium subtriangular, spatulate, with widest (tr.) point varying but typically with terminal piece; pygidial width (tr.) 125–130% of pygidial length (sag.); margin most strongly curved at widest point and medioposterior point. Axial width (tr.) at first ring ~25% pygidial width at widest (tr.) point; axial length 40–50% pygidial length (sag.); 4 axial rings; transverse axial furrows straight to slightly wavy; axial furrows sharp, straight, and slightly posteriorly convergent; terminal piece short; post axial ridge distinct anteriorly but obsolete at ~2/3 distance from terminal piece and posterior margin. Pleural furrows proximally well-defined but distally effaced; interpleural furrows shallow and short (tr.), abaxially or completely effaced; anterior pleural band short (exsag.) and crescent-shaped, pinching out on pleural slope; posterior pleural band distally broadens. Broad, poorly defined border flat to concave with posterior curving upwards. *Materials.*—The new collections of *Thailandium solum* include 27 cranidia: 21 from Ao Mo Lae (AML) 3.62 m (DGSC F0568, F0569), 3.72 m (DGSC F0571, F0570), 5.17 m (DGSC F0574), 5.81 m (DGSC F0576, F0583, F0595, F0596, F0598, F0601, F0602, F0606, F0607, F0609, and CMC IP87617, IP87618), AML h3 (DGSC F0543, F0544), and AML h5 (DGSC F0591, F0618); six from Ao Talo Topo west (ATTw) (DGSC F0398, F0388, F0421, F0419, F0434, F0435). Nine librigenae: eight from AML 5.81 m (DGSC F0612, F0616, F0631 and CMC IP87612, IP87622, IP87623), AML h1 (DGSC F0554), and AML h4 (CMC IP87607); one from ATTw (DGSC F0418). 10 pygidia: eight from AML 2.2 m (DGSC F0565), 5.81 m (DGSC F0509, F0584, F0604, F0610, F0611 and CMC IP87610), and AML h4 (DGSC F0560); 2 from ATTw (DGSC F0395, F0420). *Remarks.*—The larger sample size available in this study allows for new understanding of the ontogeny of *Thailandium solum*. The regression of partial Procrustes distances compared to the mean of the smallest specimens determines the extent to which shape change is related to size (Webster and Sheets, 2010). The same landmark configurations of 15 specimens of *T. solum* used in the shape

analysis were regressed against the mean shape of the smallest 3 specimens in the sample (e.g. DGSC F0544, Fig. 9.15) and the partial Procrustes distance from the mean calculated. While there is considerable scatter of this partial Procrustes distance plotted against log of the centroid size, ontogenetic change accounts for 16.63% of morphological variance (Fig. 11; $p = 0.0075$ bootstrapped by 1600 repetitions) The most prominent ontogenetic change is the widening (tr.) of the frontal area. Additionally, the palpebral lobe shortens (exsag.) by both anterior and posterior migration of the posterior and anterior ends respectively. Another change with increasing size is that the relative glabellar length anterior to S1 increases, and the S1 furrow becomes more strongly posteriorly bowed. In terms of partial Procrustes distance from the mean form, shape variance for all 15 specimens of *T. solum* was 0.0048 (bootstrapped by 1600 repetitions with a 95% confidence interval of 0.0031–0.0060). For comparison, a single specimen (Fig. 9.3, DGSC F0609) was remounted, photographed, and marked for landmarks ten times; the variance for these ten images of a single specimen was 0.0008 over 1600 bootstraps.

Accordingly, morphological variation among cranidia of *T. solum* greatly exceeds measurement error. The shape variance value for the sample is broadly comparable to that seen among cranidial meraspid instars in the Silurian aulacopleurid *Aulacopleura koninckii* (see Hong et al., 2014, supplemental data 4), although the set of cranidial landmarks assessed in the two studies were different in both landmark number and location. At present studies of comparative morphological variance among trilobite taxa in landmark selection are too few to allow assessment of the effects of landmark scheme selection and taphonomic factors such as flattening in shales on variance, but the consistent distinction between sample variance and measurement error seen in these studies does suggest that future comparative studies of this kind may be worthwhile.

When defining *Thailandium solum* Kobayashi (1957) tentatively assigned a relatively short and broad pygidium to the species. That pygidium instead belongs to *Quadraticephalus planulatus* (Kobayashi, 1957). Shergold et al. (1988)

reassigned this pygidium to *Lichengia? tarutaoensis* (Kobayashi, 1957), recognizing it as "saukiid" in form and with a somewhat similar shape to the *Lichengia? tarutaoensis* pygidium (Shergold et al., 1988, fig. 5W). However, the pygidium herein assigned to *T. solum* has a notably broader pleural and postaxial region and is not easily confused with that of *L.? tarutaoensis.* Shergold et al.'s (1988) assumption that their collections came from the same stratigraphic horizons as those of Kobayashi (1957) was the basis for some of their taxonomic decisions (e.g. *Pagodia thaiensis* as *Parakoldinioidia thaiensis* and *Saukiella tarutaoensis* as *Lichengia? tarutaoensis; S. tarutaoensis* instead is herein recognized as a species of *Prosaukia*). It is now clear that Kobayashi's (1957) collection represents an interval distinct from Shergold et al.'s (1988) and the only cooccurring taxa are those that are relatively long-lived in the Ao Mo Lae Formation, including *Eosaukia buravasi* Kobayashi (1957) and *Quadraticephalus planulatus* (Kobayashi, 1957). The pygidium initially assigned to *C. planulatus* Kobayashi (1957) and incorrectly assigned to *Lichengia? tarutaoensis* by Shergold et al. (1988), belongs to in fact to *Thailandium,* which itself was absent from all the collections that Shergold et al. (1988) observed. The large pygidium is inconsistent with even the largest cranidia of any other species in either Kobayashi's (1957) collection or the collection presented herein excepting perhaps *Quadraticephalus planulatus* and *Eosaukia buravasi;* the shape and pleural divisions are notably "saukiid"-like, ruling out assignation to *Quadraticephalus,* and the broad pleural field is inconsistent with the lenticular shape of an *Eosaukia* pygidium which is otherwise well-documented in the Tarutao collections.

The cranidium of *Thailandium* is similar to that of *Prosaukia* Ulrich and Resser (1933) save for the angle of the anterior suture branches and length of the palpebral lobe (Fig. 9). Likewise, the pygidium of *Thailandium* differs from that of *Prosaukia,* at least the type species, mainly by degree of axial length, post-axial length, and effacement of the pleural field (Fig. 10). *Thailandium's* cranidium also approaches the condition seem in some dikelocephalinids, such as *Osceolia* and some *Briscoia* in form of the preglabellar field (Ulrich and Resser, 1930), but

the form of the glabella, anterior position of the eyes, and the convergent anterior sutures are distinctive in *Thailandium.*

The librigena of *Thailandium solum* is distinct from the librigena of similar genera, including *Prosaukia* and *Tellerina* Ulrich and Resser (1933), in that the posterior and lateral border furrows are firmly-incised and truly confluent (e.g. DGSC F0418, Fig. 10.7). In both *Tellerina* and *Prosaukia* the joining of the furrows is marked by a continuous curve for the posterior border furrow and a bend, often sharply dog-legged, in the lateral border furrow. In *Prosaukia* the lateral furrow may become effaced with an inflated extension of the pleural field separating it from the posterior border furrow; this state is particularly well-developed on *Prosaukia misa* (Hall, 1863) and to a lesser extent on *Prosaukia oculata* n. sp.

Though cephalically distinct, particularly in the frontal area, *Thailandium* has a similar overall pygidial structure to that of *Tellerina* Ulrich and Resser (1933) and *Calvinella* Walcott, 1914. Similarities include a short axis, long postaxis, broad and poorly-defined flat to concave border without a border furrow. Some species of *Calvinella* (e.g. the type species,

C. spiniger) have well-defined postaxial ridges; these are rare in *Tellerina.* In *C. spiniger* the pygidium is more circular or subellipsoidal than in *Thailandium,* but *Tellerina,* at least for the type species *Tellerina crassimargniata* (Whitfield, 1882), has a subtriangular to spatulate pygidium, like that of *Thailandium.* Of the three genera, *Thailandium* has the most effaced interpleural furrows and shortest (tr.) pleural furrows (Fig. 10). All three genera grow to sizes larger than is typical for "saukiids" though not as large as some species of *Dikelocephalus* (e.g. *Dikelocephalus minnesotensis* Owen, 1852; see Hughes, 1994). *Dikelocephalus minnesotensis* has a similarly broad, poorly defined and flat border with a long postaxial area. The broad, flat, effaced border may reflect a convergence of all dikelocephalid trilobites that grow to be more than a few centimeters in total length.

Genus *Prosaukia* Ulrich and Resser, 1933
Type species.—Dikelocephalus misa Hall (1863)
*Remarks.—*The generic diagnosis of *Prosaukia* has been discussed thoroughly in previous work (Ulrich and Resser, 1933, Ludvigsen and Westrop, 1983), but the divergent anterior suture
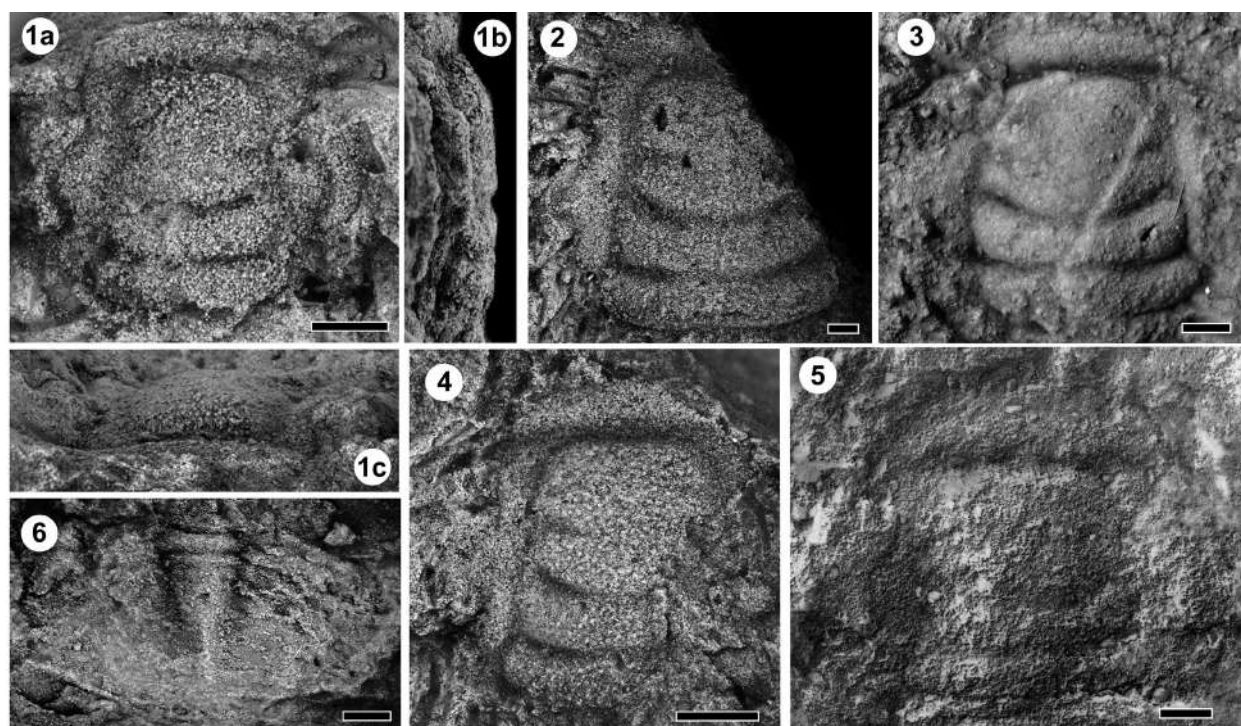
Figure 12: *Prosaukia tarutaoensis* n. sp. cranidia (1–5) and pygidium (6). (1a–c) dorsal, left lateral, and anterior views respectively, DGSC F0566, AML 2.2 m; (2) DGSC F0567, Ao Mo Lae (AML) 3.1 m; (3) DGSC F0413, Ao Talo Topo west (ATTw); (4) DGSC F0546, AML h3; (5) CMC IP87029, vinyl polysiloxane cast, holotype, original of UMUT PA02298c, Kobayashi, 1957, pl. 5, fig. 12; (6) DGSC F0453, ATTw. All internal molds. Scale bars = 2 mm.

branches has not been noted previously as a diagnostic feature. This character is helpful in differentiating *Prosaukia* from *Thailandium* Kobayashi (1957) and also from *Hoytaspis* Ludvigsen and Westrop (1983).

Prosaukia tarutaoensis (Kobayashi, 1957)
Fig. 12
1957 *Saukiella tarutaoensis* Kobayashi, p. 378, pl. 5, fig. 12.
non 1988 *Lichengia? tarutaoensis* (Kobayashi) Shergold et al., p. 309, figs 5S–W.

Emended diagnosis.—Species of *Prosaukia* with short (sag.) preglabellar field, long (sag.) and weakly bowed anterior border, strongly ante-riorly tapering glabella, fine granulation, wide (tr.) LO, and narrow (tr.) pygidial axis.

Occurrence.—Ao Mo Lae (AML) 2.2–3.1 m, AML h3, and Ao Talo Topo west; Ao Mo Lae Formation of the Tarutao Group, Thailand; Furongian.

Emended description.—Cranidium subtrapezoidal; width across palpebral areas 90% of cranidial length in smallest holaspids to 105% of cranidial length in largest holaspids. Occipital glabellar length (sag.) up to 1.1cm; glabellar width across L1 60% width across palpebral areas in smaller holaspids and 70% in larger; length of glabella and LO 82–85% of cranidial length; glabella trunco-conical with low dosoventral relief; axial furrows straight or slightly pinched at S2, weakly incised; anterior glabellar margin transverse to gently curved; LO 15–20% wider than L1; SO gently posteromedially bowed, shallowing medially; S1 moderately to strongly posteromedially bowed, shallowing medially; S2 short (tr.) and well-defined, less posteromedially angled than S1; anteromedially angled S3 poorly-defined to effaced. Palpebral lobe moderately arched with greatest curvature in posterior part; widest palpebral point slightly anterior to S1 in smaller holaspids and slightly posterior in larger; palpebral lobe length (exsag.) 30% cranidial length (sag.) in smaller holaspids to 40% in larger; width (tr.) across anterior palpebral corners 80–90% width across posterior corners. Fixigena narrow (tr.) with moderately wide preocular areas; anterior suture branches anteriorly divergent from anterior palpebral corners, curving gently adaxially for rounded lateral margins of frontal area; frontal area widest (tr.) point slightly posterior to anterior border. Preglabellar field short, depressed; anterior border furrow gently anteromedially bowed; anterior border 15% cranidial length, weakly inflated, horizontally oriented. All surfaces densely granulated.

Pygidium subellipsoid to lenticular; width (tr.) twice length (sag.); axial width (tr.) at anterior-most ring 20% pygidial width at widest point; axial length (sag.) 65% pygidial length (sag.); four axial rings, only first three clearly defined; axial furrows converging at 15° from sagittal axis; terminal piece narrow and long; postaxial ridge short, not extending to pygidial margin. Pleural furrows poorly-defined and pleural field effaced.

Material.—Five cranidia from Ao Mo Lae (AML) 2.20 m (DGSC F0566), AML 3.1 m (DGSC F0567), AML h3 (DGSC F0545, F0546), and Ao Talo Topo west (ATTw) (DGSC F0413); one pygidium from ATTw (DGSC F0453); all internal molds.

Remarks.—*Prosaukia tarutaoensis* represents a typical species of *Prosaukia* in many ways; in the dimensions and shape of the glabella, length of the palpebral lobes, width of the fixigena, length of the anterior border, surface texture, and expression of furrows it clearly resembles the type species, *Prosaukia misa* (Hall, 1863). *Prosaukia tarutaoensis* differs cranidially from many other known species of *Prosaukia* primarily in the notably short (sag.) preglabellar field and wide (tr.) occipital lobe (e.g. DGSC F0566, Fig. 12.1a). In *Prosaukia misa* (Hall, 1863) and most other species of *Prosaukia* the occipital lobe is either slightly narrower than L1 as in *Prosaukia oculata* n. sp. or else the axial furrows flank the occipital lobe along the same path as the preoccipital glabella. In *P. tarutaoensis* the axial furrows curve sharply around the occipital lobe (Fig. 12). The pygidium of *P. tarutaoensis* is distinct as it is the only known species of *Prosaukia* with a lenticular pygidium.

Shergold et al. (1988) considered the single specimen of *Prosaukia tarutaoensis* known at that time (Kobayashi, 1957; pl. 5 fig. 12; Fig. 12.5) to be synonymous with new material that

they called *Lichengia? tarutaoensis* on account of the frontal area and palpebral lengths and positions. It is clear from the strong anteriorly narrowing glabella and medial discontinuity of the lateral glabellar furrows in the latter material that these specimens are not synonymous with *Prosaukia tarutaoensis*. Therefore *Lichengia? tarutaoensis* is excluded from Kobayshi (1957) concept of the species. Additional specimens of *Lichengia tarutaoensis* (*sensu* Shergold et al., 1988) have been recovered from the Ao Mo Lae Formation, and revision of this species will appear in future work.
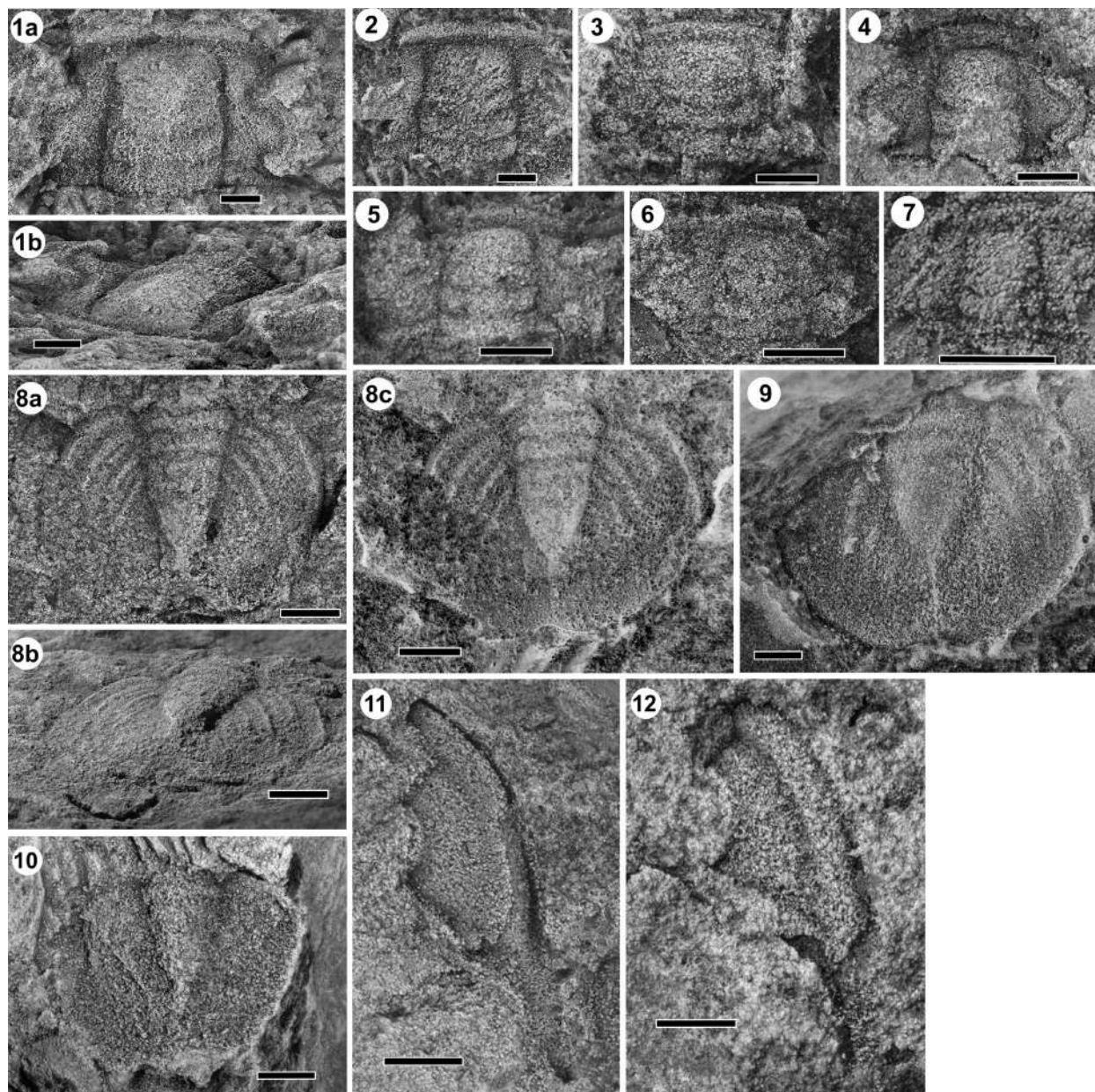
Figure 13: *Prosaukia oculata* n. sp. cranidia (1–7), pygidia (8–10), and librigena (11,12). (1a–b) dorsal and left anterolateral views respectively, DGSC F0512; (2) DGSC F0503; (3) DGSC F0498; (4) DGSC F0532; (5) DGSC F0511; (6) DGSC F0461; (7) DGSC F0534, Ao Talo Topo (ATT) 22.88 m; (8a–c) internal dorsal, internal right posterolateral oblique, and external dorsal views respectively, DGSC F0510; (9) DGSC F0470, external mold; (10) DGSC F0497; (11) DGSC F0488; (12) DGSC F0513. All from ATT 22.78 m except 7; all internal molds unless otherwise indicated. Scale bars = 2 mm.

Prosaukia oculata n. sp.

Fig. 13

?1988 *Lichengia? tarutaoensis* (Kobayashi) Shergold et al., p. 309–310, fig. 5W only, *not* figs 5S–V = *Lichengia simplex* Shergold, 1991)

Type material.—Holotype, DGSC F0512 (Fig. 13.1a–b) from Ao Talo Topo 22.78 m; paratypes DGSC F0461, F0489, F0498, F0503, F0511, F0532, F0534; Ao Mo Lae Formation, Tarutao Group, Ko Tarutao, Thailand; Furongian.

Occurrence.—Ao Talo Topo 22.78–22.88 m and horizon 1 (Figs 2, 5), Ao Mo Lae Formation of the Tarutao Group, Thailand; Furongian.

Diagnosis.—Species of *Prosaukia* with wide, flat fixigena, including palpebral areas, short (sag.) preglabellar field, and subcircular pygidium with strongly inflated posterior pleural bands and reduced but well-defined anterior pleural bands.

Description.—Cranidium subrectangular; width across palpebral areas 120%–135% cranidial length (sag.). Occipital glabellar length (sag.) up to 0.9cm; glabellar width (tr.) across L1 50% width across palpebral areas; length of glabella and LO 85% cranidial length (sag.); glabella bullet-shaped with moderate dorso-ventral relief; axial furrows smoothly curved around glabella or slightly bowed at L1, well-defined; anterior glabellar margin transverse to gently curved; L1 slightly wider than LO; SO transverse or gently posteromedially bowed, shallowing medially; S1 slightly more strongly posteromedially bowed than SO, shallowing medially; S2 medially discontinuous and weakly to moderately well defined, less posteromedially angled than S1; S3 poorly-defined to effaced, oriented slightly postermedially to transverse. Palpebral lobe strongly curved, nearly symmetric about the midpoint; palpebral midpoint opposite S1; palpebral lobe length (exsag.) 35%–40% cranidial length (sag.); width (tr.) across anterior palpebral corners equal or slightly less than width across posterior corners. Fixigena broad (tr.) with wide preocular areas only slightly narrower than palpebral areas; anterior suture branches anteriorly divergent 35-40° from sagittal, curving strongly adaxially at anterior border furrow. Preglabellar field very short to furrow-like, depressed; anterior border furrow gently anteromedially bowed; anterior border 15% cranidial length, strongly inflated, horizontally oriented. Weakly granulated surface sometimes effaced.

Librigena with narrow, gently convex genal field; lateral and posterior border furrows well-defined; lateral border furrow shallowing near junction with posterior border furrow; lateral border broad, nearly 75% genal field width measured orthogonally from cephalic margin to ocular suture.

Pygidium subcircular with slight posterior marginal embayment; length (sag.) 80% Shelly J. Wernette et al. / Thai Geoscience Journal 1 (2020), p. 65-87 width (exsag.); widest (tr.) point of pygidium near pygidial mid-length (exsag.); axial width (tr.) at anterior-most ring 30%–35% pygidial width at widest point; axial length (sag.) 60%–70% pygidial length (sag.); 4 axial rings, only first 2 clearly defined; axial furrows converging at 10°–15° from sagittal axis; terminal piece posteriorly angular; postaxial ridge distinct and extending to pygidial margin. Pleural furrows and interpleural furrows well-defined; anterior pleural bands narrow; posterior pleural bands strongly inflated; pleural furrows broader than interpleural furrows; all pleurae well-aligned with axial rings; all pleurae maintain width to edge of pleural field and become effaced where pleural field slopes into border; border flat without defined furrow; doublure short, not reaching terminal axia piece.

Etymology.—A fusion of ocula- and -lata, Latin for eye and wide respectively.

Material.—Seven cranidia (DGSC F0461, F0489, F0498, F0512, F0511, F0532 – internal molds, DGSC F0503 – external mold), 2 librigena (DGSC F0488, F0513 – internal molds), and 4 pygidia (DGSC F0510 – internal and external mold, F0430 – external mold, F0470 – external mold, F0497 – internal mold) all from Ao Talo Topo 22.78 m, one cranidium internal mold from Ao Talo Topo 24.1 m (DGSC F0534), and one cranidium from ATT h1 (DGSC F0459).

Remarks.—*Prosaukia oculata,* as its name suggests, has more widely set apart palpebral lobes than is typical for the genus (e.g. DGSC

F0532, Fig. 13.4). The greater distance between the eyes results from broader fixigena rather than a wider glabella. *Prosaukia delcostata* Ulrich and Resser (1933) also has relatively broad fixigena, but it differs from *P. oculata* by the former's longer preglabellar field, broader lateral cephalic border, more rectangular anterior glabellar margin, and less circular pygidium.

The preglabellar field of *P. oculata* is very short, nearly absent compared with most *Prosaukia,* but it is still clearly recognizabl on some specimens (e.g. DGS F0532, Fig. 13.4), and this intraspecific variation proves the presence of the preglabellar field within the taxon.

References

Adrain, J.M. (2011). Class Trilobita Walch 1771. *Zootaxa, 3148,* 104–109.

Bookstein, F. L. (1991). *Morphometric tools for landmark data* (p.435). New York: Cambridge University Press.

Bunopas, S., Muenlek, S., & Tansuwan, V. (1983). Geology of Tarutao Island. *Journal of the Geological Society of Thailand, 6,* 121–138.

Burrett, C., Zaw, K., Meffre, S., Lai, C. K., Khositanot, S., Chaodumrong, P., … Halpin, J. (2014). The configuration of Greater Gondwana—Evidence from LA ICPMS, U–Pb geochronology of detrital zircons from the Palaeozoic and Mesozoic of Southeast Asia and China. *Gondwana Research, 26,* 31–51.

Cawood, P.A., Johnson, M.R.W., & Nemchin, A.A. (2007). Early Palaeozoic orogenesis along the Indian margin of Gondwana: Tectonic response to Gondwana assembly. *Earth and Planetary Science Letters, 255*, 70–84.

Cocks, L.R.M., & Torsvik, T.H. (2013). The dynamic evolution of the Palaeozoic geography of eastern Asia. *Earth-Science Reviews, 117,* 40–79.

Hall, J. (1863). Preliminary notice of the fauna of the Potsdam sandstone, with remarks upon the previously known species of fossils, and description of some new ones from the sandstones of the Upper Mississippi Valley. *Report of the New York State Cabinet of Natural History, 16,* 119–222.

Hong, P.S., Hughes, N.C., & Sheets, H.D.S. (2014). Size, shape and systematics of the Silurian trilobite *Aulacopleura koninckii. Journal of Paleontology, 88*(6), 1120–1138.

Hughes, N.C. (1994). Ontogeny, intraspecific variation, and systematics of the Late Cambrian trilobite *Dikelocephalus. Smithsonian Contributions to Paleobiology, 79,* 1-89.

Hughes, N.C. (2016). The Cambrian palaeontological record of the Indian subcontinent. *Earth-Science Reviews, 159,* 428–461.

Hupé, P. (1955). Classification des trilobites. *Annales de Paleontologie, 41,* 91–325.

Imsamut, S., & Yathakam, W. (2011). Stratigraphic correlation of the Tarutao-Langkawi, area,

(Thai side): *Report Bureau of Geological Survey* (pp. 1–64). Bangkok: DMR.

Jell, P.A., & Adrain, J.M. (2002). Available generic names for trilobites. *Memoirs of the Queensland Museum, 48*(2), 331–552.

Kobayashi, T. (1957). Upper Cambrian fossils from peninsular Thailand. *Journal of the Faculty of Sciences of the University of Tokyo, 2,* 367–382.

Kobayashi, T. (1960). Cambro-Ordovician formations and faunas of South Korea, Pt. 7, Paleontology 6. *Journal of the Faculty of Science, University of Tokyo, Section 2 , 2,* 329–420.

Lee, S.-B., & Choi, D.K. (2011). Dikelocephalid trilobites from the *Eosaukia* fauna (Upper Furongian) of the Taebaek Group, Korea. *Journal of Paleontology, 85*(2), 279–297.

Lochman, C. (1956). The evolution of some Upper Cambrian and Lower Ordovician trilobite families. *Journal of Paleontology, 30*(3), 445–462.

Longacre, S.A. (1970). Trilobites of the Upper Cambrian Ptychaspid Biomere Wilberns Formation, Central Texas. *Paleontological Society Memoir, 44,* 1-61.

Lu, Y.-H. (1954). Upper Cambrian trilobites from Santu, southeastern Kueichou. *Acta Palaeontologica Sinica, 2*(2), 117–152.

Ludvigsen, R., & Westrop, S.R. (1983). Franconian Trilobites of New York State. *New York State Museum Memoir, 23,* 45.

Ludvigsen, R., Westrop, S.R., & Kindle, C.H. (1989). Sunwaptan (Upper Cambrian) trilobites of the Cow Head Group, western Newfoundland, Canada. *Palaeontographica Canadiana 6,* pp.175.

Miller, S. A. (1889). North American Geology and Paleontology for the use of amateurs, students and scientists. *Western Methodist Book Concern* (pp. 718). Ohio: Cincinnati.

Ogg, J. G., Ogg, G. M., & Gradstein, F. M. (2016). 5 - Cambrian. In J. G. Ogg, G. M. Ogg, & F. M. Gradstein (Eds.), *A Concise Geologic Time Scale* (pp. 41-55). Elsevier.

Owen, D.D. (1852). *Report of a geological survey of Wisconsin, Iowa, and Minnesota, and, incidentally, a portion of Nebraska Territory. (Philadelphia)* (pp. 638).

Park, T.-Y.S., & Kihm, J.-H. (2015). Furongian (late Cambrian) trilobites from the *Asioptychaspis subglobosa* Zone of the *Hwajeol Formation, Korea. Alcheringa: An Australasian Journal of Palaeontology, 39,* 181–199.

Peng, S.C., Babcock, L.E., & Cooper, R.A. (2012). The Cambrian Period, in: *The Geologic Time Scale,* 437–488.

Qian, Y.Y., (1985). a Trilobites. In J.-Y., Chen, Y.-Y., Qian, Y.-K., Lin, J.-M., Zhang, Z.-H., Wang, L.-M., Yin, & B. D., Erdtmann (eds.), *Study on Cambrian-Ordovician Boundary Strata and its Biota in Dayangcha, Hunjiang, Jilin, China* (p. 65-83). Beijing: China Prospect Publishing House.

Raasch, G. O. (1951). Revision of Croixan dikelo cephalids. *Illinois Academy of Science Transactions, 44,* 137–151.

Raymond, P.E. (1924). New Upper Cambrian and Lower Ordovician trilobites from Vermont. *Proceedings of the Boston Society of Natural History 37* (pp. 389–466).

Shergold, J.H. (1972). Late Upper Cambrian Trilobites from the Gola Beds, Western Queensland. *Bulletin of the Bureau of Mineral Resources, Geology and Geophysics 112* (pp. 126).

Shergold, J.H. (1975). Late Cambrian and Early Ordovician Trilobites from the Burke River Structural Belt, Western Queensland, Australia. *Bulletin of the Bureau of Mineral Resources, Geology and Geophysics 153* (pp. 251).

Shergold, J.H. (1991). The Pacoota sandstone, Amadeus Basin, Northern Territory: stratigraphy and palaeontology. *Bulletin of the Bureau of Mineral Resources, Geology and Geophysics 237* (pp. 93).

Shergold, J.H., Burrett, C., Akerman, T., & Stait, B. (1988). Late Cambrian trilobites from Tarutao Island, Thailand. *New Mexico Bureau of Mines and Mineral Resources Memoir, 44,* 303–320.

Shergold, J.H., & Geyer, G. (2003). The Subcom mission on Cambrian Stratigraphy: the status quo. *Geologica Acta, 1*(1), 5–9.

Shergold, J.H., Laurie, J.R., & Shergold, J.E. (2007). Cambrian and Early Ordovician trilobite taxonomy and biostratigraphy, Bonaparte Basin, Western Australia. *Australasian Palaeontological Memoirs, 34,* 17–86.

Stitt, J. H. (1971). Late Cambrian and earliest Ordovician trilobites, Timbered Hills and lower Arbuckle groups, Western Arbuckle Mountains, Murray County, Oklahoma. *Oklahoma Geological Survey Bulletin 110* (pp. 83).

Stitt, J. H. (1977). Late Cambrian and earliest Ordovician trilobites, Wichita Mountains area, Oklahoma. *Oklahoma Geological Survey Bulletin 124* (pp. 79).

Sun, Y.-C. (1935). The Upper Cambrian trilobite faunas of North China. *Palaeontologica Sinica, series B, 7* (pp. 69).

Taylor, M.E., & Halley, R.B. (1974). Systematics, environment, and biogeography of some Late Cambrian and Early Ordovician trilobites from eastern New York State. *U.S. Geological Survey Professional Paper 834* (pp. 38).

Ulrich, E.O., & Resser, C.E. (1930). The Cambrian of the Upper Mississippi Valley, Part 1: Trilobita, Dikelocephalinae and Osceolinae. *Bulletin of the Public Museum of the City of Milwaukee, 12*(1), 1–122.

Ulrich, E.O., & Resser, C.E. (1933). The Cambrian of the Upper Mississippi Valley, Part 2, Trilobita; Saukiinae. *Bulletin of the Public Museum of the City of Milwaukee, 12*(2), 123–306.

Walcott, C.D. (1914). Cambrian geology and paleontology, No. 1. The Cambrian faunas of eastern Asia. *Smithsonian Miscellaneous Collection,s 64* (pp. 75).

Walcott, C.D. (1924). Geological formations of Beaverfoot-Brisco-Stanford Range, British Columbia, Canada. *Smithsonian Miscellaneous Collections, 75,* 1–51.

Webster, M., & Sheets, H.D. (2010). A practical introduction to landmark-based geometric morphometrics. *The Paleontological Society Papers, 16,* 163–188.

Wernette, S.J., Hughes, N.C., Myrow, P.M., & Sardsud, A. (2020). *Satunarcus,* a new late Cambrian trilobite genus from southernmost Thailand and a reevaluation of the subfamilyMansuyiinae Hupé, 1955. *Journal of Paleontology,* 1–14.

Whitfield, R.P., (1882). *Palaeontology: Geology of Wisconsin, 4*(3), 163–363.

Wongwanich, T., Tansathien, W., Leevongcharoen, S., Paengkaew, W., Thiamwong, P., Chaeroenmit, J., & Saengsrichan, W. (2002). The Lower Paleozoic Rocks of Thailand. *The Symposium on Geology of Thailand, 26-31 August 2002* (pp. 16–21). Bangkok.

Regolith-landform mapping of the Gnaweeda Greenstone Belt, western Australia

Siriporn Soongpankhao

The Royal Thai Department of Mineral Resources, 75/10 Rama VI Road,
Rathchathewi district, Bangkok, 10400, Thailand.
Corresponding author: s.soongpan@gmail.com
Received 2 June 2020 ; Accepted 2 July 2020

Abstract

Regolith-landform mapping of the Gnaweeda Greenstone Belt located at Meekatharra, Western Australia. It was conducted at a scale of 1: 100,000, covering the Turnberry Au prospect and the Mistletoe Au deposit, in order to assist mineral exploration in this area. Understanding the regolith is a fundamental tool in developing and establishing effective mineral exploration techniques in regolith-dominated terrain. Apart from mineral exploration, knowledge of regolith also applies to natural resource management as it links many facets of the natural environment. The process of map production begins with creating a preliminary regolith-landform map using aerial photographs and ASTER data. Unit identification and digitization on screen were performed. Field verification was conducted along the tracks where access was possible. A preliminary map, field observation and all available data were brought together in order to compile a final map. The regolith-landform in this area consists of fourteen units. Five types of landforms are recognized: depositional plain, erosional plain, alluvial plain, sandplain and erosional rise. The landform is dominated by depositional plains.

Key words: ASTER data, Geochemical exploration, Mineral exploration, Regolith, Regolith-landform, Regolith-landform map

Introduction

The definition of regolith is the entire altered, unconsolidated or secondarily re-cemented cover that overlies more coherent bedrock which has been formed by the weathering, erosion, transport and/or deposition of older materials. It, thus, includes fractured and weathered basement rocks, saprolites, soils, organic accumulations, glacial deposits, colluvium, alluvium, evaporitic sediments, loess and aeolian deposits and groundwater (Butt and Zeegers, 1992; Robertson and Butt, 1997; Eggleton, 2001). In other words, regolith is 'everything from fresh rock to fresh air' (Eggleton, 2001).

Regolith-landform mapping is defined as an area delineated on a map as a specific association of regolith materials, landform and may correlate bedrock geology (Butt et al., 1997). Regolith-landform units allow a quick visual assessment of landscapes. For example, in these study areas, the landscape is dominantly flat (depositional and alluvial plains) with some slightly angled slopes (erosional plains) and low rises (erosional rises).

Regolith-landform mapping is a useful complement to geochemical exploration in the Yilgarn Block of Western Australia (Craig, 2001). As rock outcrop in Australia is less than 15% of the land area, this makes regolith mapping important. The regolith is a barrier to mineral exploration and understanding its distribution and origin is important for exploration planning. The methods used for the regolith-landform mapping of the study areas for this project are based on the techniques of Pain (2008) and Craig (2001). The purpose of the map is to give an overview of the distribution of regolith materials and their landform expressions on a regional scale and to produce a tool for mineral exploration. Apart from this, regolith-landform mapping could be applied to landscape research and land management (Hill, 2002).

The study areas are approximately 35 km northeast of Meekatharra (Fig.1), the historical Au mining town and the largest centre in the Murchison Province, Western Australia. Meekatharra is approximately 765 km north east of Perth. The Gnaweeda Greenstone Belt lies at the east of Meekatharra-Wydgee Greenstone Belt which is highly-auriferous.
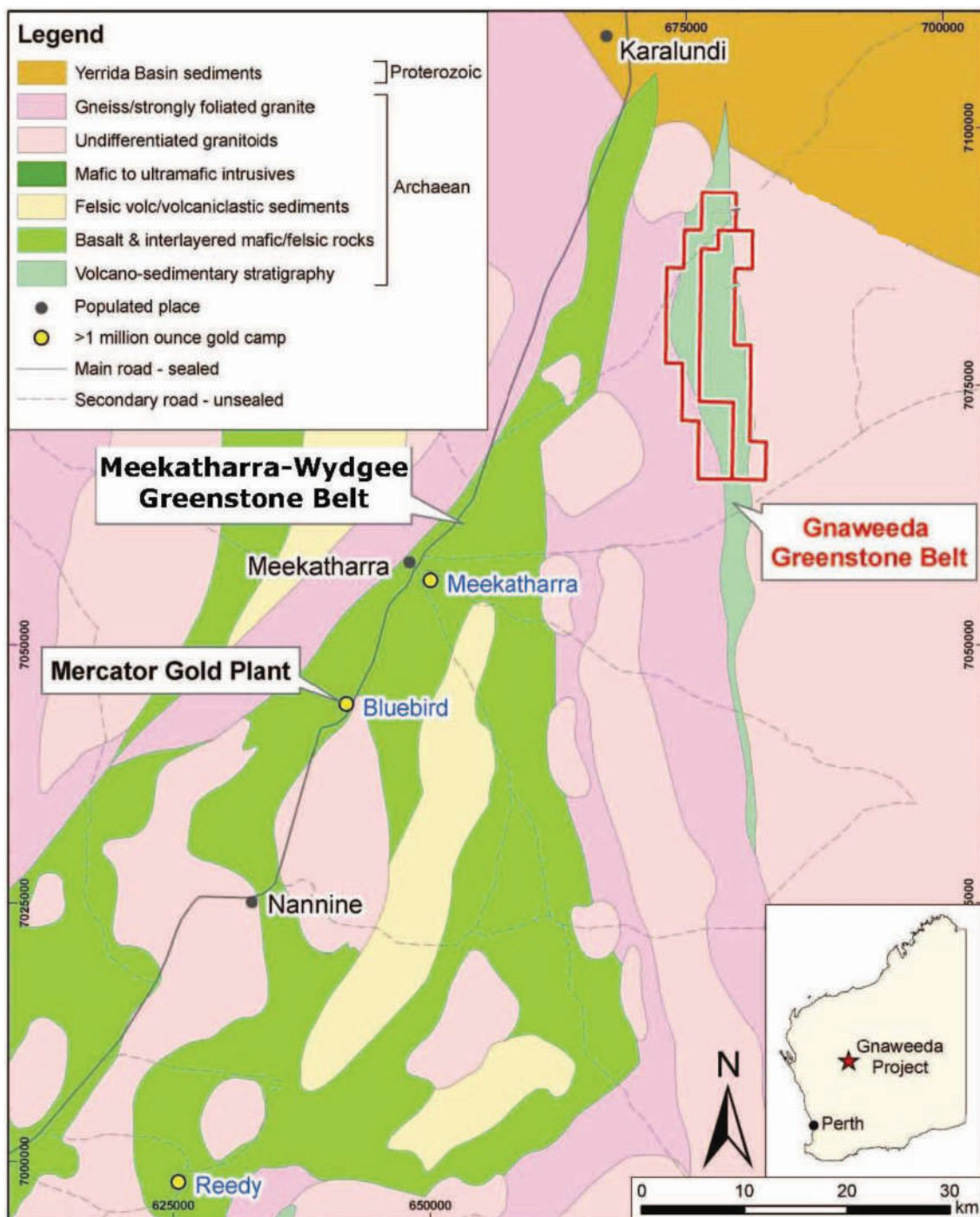
Figure 1: Location of the study areas, the Turnberry Au prospect and the Mistletoe Au deposit within the Gnaweeda Greenstone Belt, Western Australia (modified from Ray and Reardon, 2010) (Map projection is GDA94, MGA Zone 50UTM).

Geology of the greenstone belt Gnaweeda

The Gnaweeda Greenstone Belt consists of three litho-tectonic subdomains (Western, Central and Eastern Sub-domains) (Fig.2) based on aeromagnetic interpretation, drill hole data and geological information (Bunting and McIntyre, 2003). The Western Sub-domain includes a broadly conformable package of non-magnetic mafic

volcanics and intrusive rocks, with extensive, continuous interlayered strongly magnetic units of mafic to ultramafic rocks. These magnetic units identify large-scale isoclinal folding (Bunting and McIntyre, 2003).

The Central Sub-domain consists of a package of gabbro or dolerite, with weakly magnetic ultramafic units and discrete lenses of

felsic volcanics, sediments and felsic intrusives. The strikes of these rock units are broadly parallel to the overall strike of the Gnaweeda Greenstone Belt. The foliated magnetic package (AM2 - Fig.2) is patchy. It appears to represent a high strain and shear within the greenstone and it associated with Turnberry mineralisation (Bunting and McIntyre, 2003).

The Eastern Sub-domain comprises a sequence of complexly folded, mainly mafic and ultramafic volcanic rocks with variably magnetic properties. These include strongly magnetic fragments of olivine orthocumulate that probably represent fragmented remnants of a larger layered mafic-ultramafic intrusion. Cumulate layering in the ultramafic rock is often at a high angle to the overall strike of the greenstone belt and it appears to have been intruded or truncated by the eastern granitoid

rocks (Bunting and McIntyre, 2003).

The boundary between the Central and Eastern Sub-domains appears to be a major structure that is associated with Au mineralisation in the foliated magnetic package (Bunting and McIntyre, 2003).

There are many mafic dykes throughout the area and the dominant swarms are oriented northeast and east-west (J. Bunting, pers. comm. to David Tellick, Teck Cominco Australia).

In the Gnaweeda Greenstone Belt, mineralisation is developed both in mafic and felsic rocks. In mafic rocks, Au is extensive but low grade. In felsic rocks with quartz veining, Au is higher grade. Anomalous Au and As were identified in the foliated magnetic package. Host rocks for Au in this magnetic package include mainly mafic volcanics, mafic intrusive (i.e. gabbro or dolerite) and felsic porphyries (McIntyre, 2005).
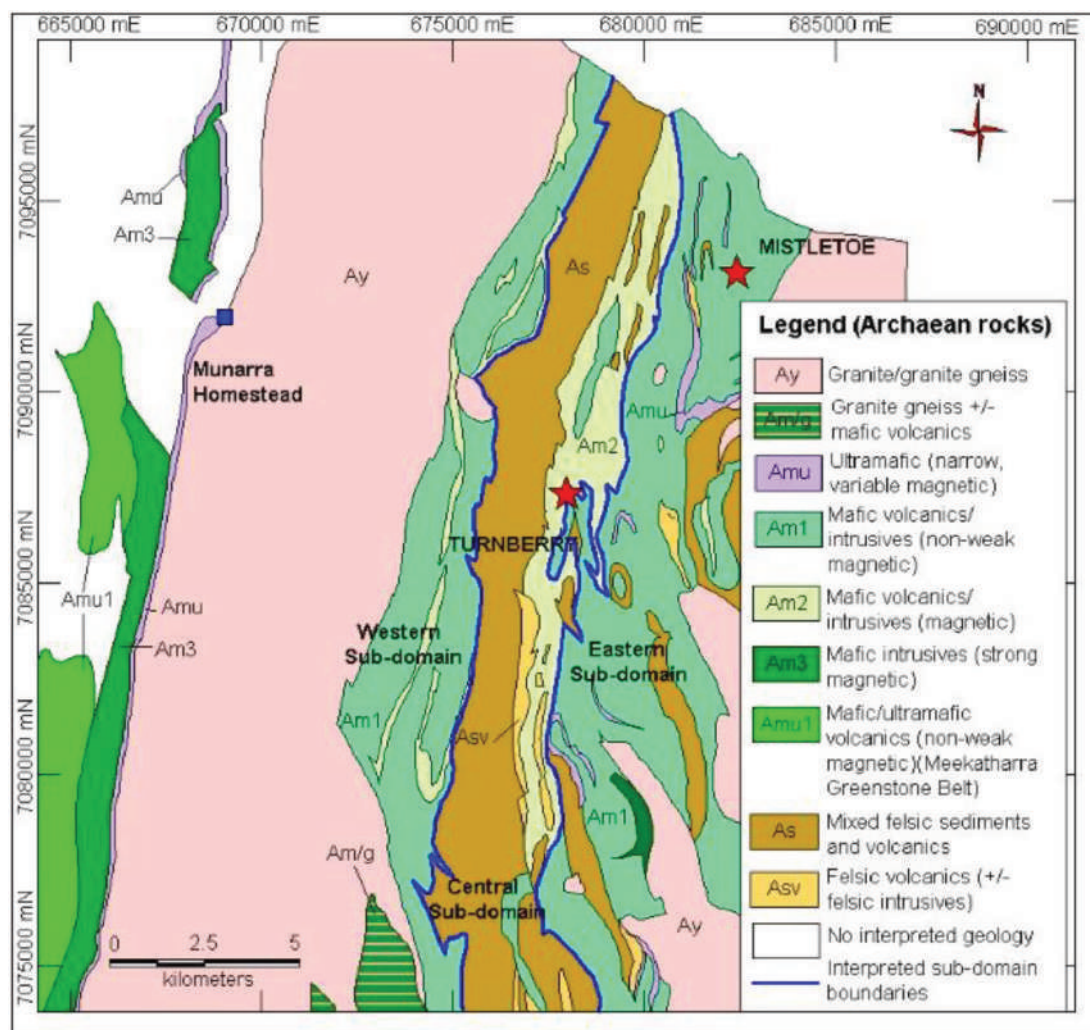
Figure 2: Geology of the Gnaweeda Greenstone Belt and location of the Turnberry prospect and the Mistletoe Au deposit (star symbols), Western Australia (modified from interpreted geology from Teck Cominco Australia).

Map production

A preliminary map was produced using aerial photographs and ASTER data (Figs. 3 and 4). ASTER provides satellite images. It can be used for land surface studies. ASTER is also expected to apply in many areas of global change-related such as vegetation and ecosystem dynamics, hazard monitoring, geology and soils, and the generation of digital elevation models (DEMs). The ASTER data bands were combined using the ER Mapper program. For this work, the ASTER data band 321 through RGB creating a natural color composite image was used. After unit identification, digitization on screen was done using the MapInfo program. The completed preliminary regolith-landform units digitized over aerial photography and ASTER data are shown in Figure 5. Field verification point was conducted along the tracks where access was possible. Field notes, regolith materials and photographs were

taken from each regolith-landform unit. The location of each regolith-landform unit was recorded by GPS. The field verification points are displayed in Figure 6.

After field verification, all available data were brought together to enable extrapolation and interpolation to the areas that were not accessible. Apart from aerial photographs, ASTER data and field observations, other data that were used to produce this map as reliably as possible are geological maps (Pirajno et al., 1998), interpreted geology (Teck Cominco Australia Pty Ltd), and the geochemical and regolith map 1:250,000 of Glengary sheet (Crawford et al., 1996). Some boundaries of the preliminary regolith-landform units were modified or changed in the light of information from field observations. The compiled regolith-landform map and units are presented in Figure 7. The final regolith-landform map with a full detailed legend is included as an Appendix.
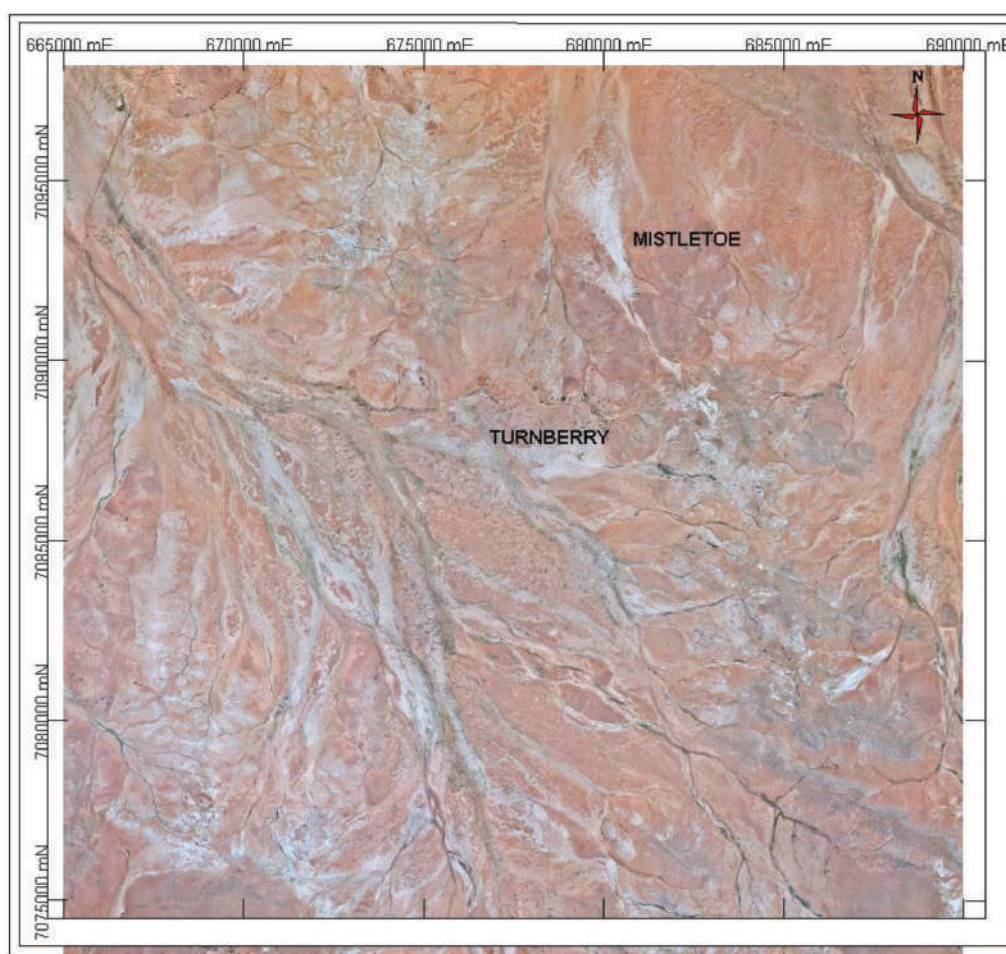
Figure 3: Aerial photography at the study area used for making a preliminary regolith-landform map, the Gnaweeda Greenstone Belt, Meekatharra, Western Australia.
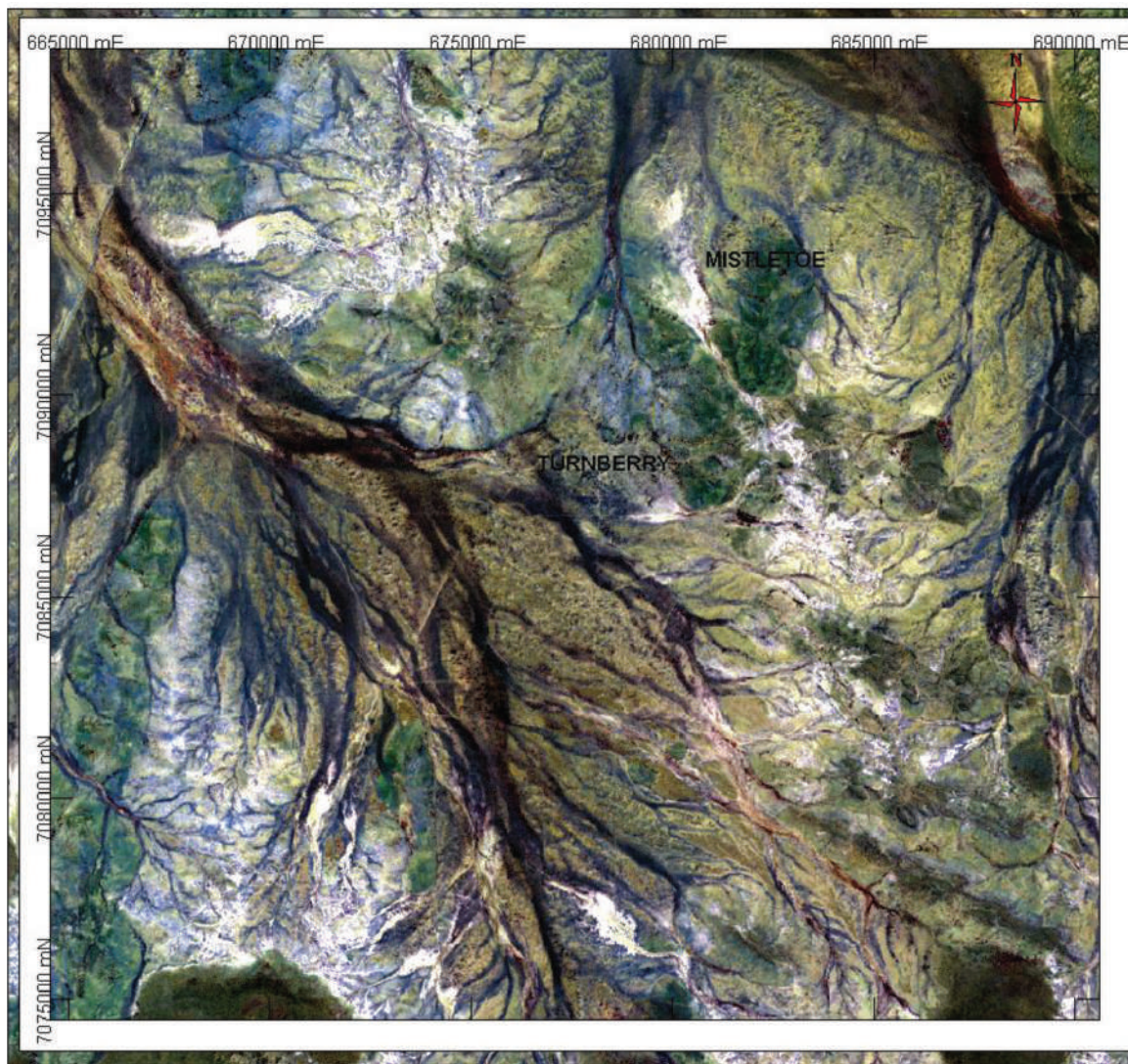
Figure 4: ASTER data band 321 used for making a preliminary regolith-landform map, the Gnaweeda Greenstone Belt, Meekatharra, Western Australia.

Regolith-landform map

The regolith-landform in this area consists of fourteen units (Fig.7). Five types of landforms are recognized: depositional plain, erosional plain, alluvial plain, sandplain and erosional rise. The landform is dominated by depositional plains.

The Gnaweeda Greenstone Belt comprises transported and *insitu* regolith. Transported regolith contains colluvial sediment, alluvial sediments and evaporite. *Insitu* regolith consists of residual material and saprolite. Regolith materials comprise mainly colluvial sediments, with alluvial sediments developed along the channel, some residual material, and saprolite found beside the channel systems. Transported regolith of the Gnaweeda Greenstone Belt occupies the largest surface area of the map. Colluvial sediments in this area are

sheetwash. Colluvial sheetwash is found both on the erosional and depositional plain. Transported regolith on the depositional landform has been divided into four regolithlandform units, and all the materials fall into the broad category of colluvial sheetwash. Each type of sheetwash is associated with a characteristic vegetation type. On unit CHpd1, the regolith is dominated by orange sand with some angular quartz gravel and angular-subrounded ferruginous lag. *Acacia aneura, Eremophila fraseri* and *Eremophila forrestii* are dominant (Fig. 8). On unit CHpd2, which comprises pebble to cobble size siliceous fragments, sparse and smaller vegetation, *Acacia aneura* and *Eremophila fraseri* are found. At the northeast of the map, colluvial sheetwash consists of ferruginous loose sand (CHpd3). This regolith

material is associated with a medium density of *Acacia aneura* (2-5 m high), *Eremophila fraseri* and *Eremophila forrestii* (Fig. 9). The merging of the depositional landform with alluvial plain is the main characteristic of CHpd4.

This unit contains ferruginous loose sand, mud and quartz gravel with a common distribution of *Acacia aneura* and *Eremophila fraseri, Eremophila forrestii* and *Triodia* (spinifex) (Fig. 10).
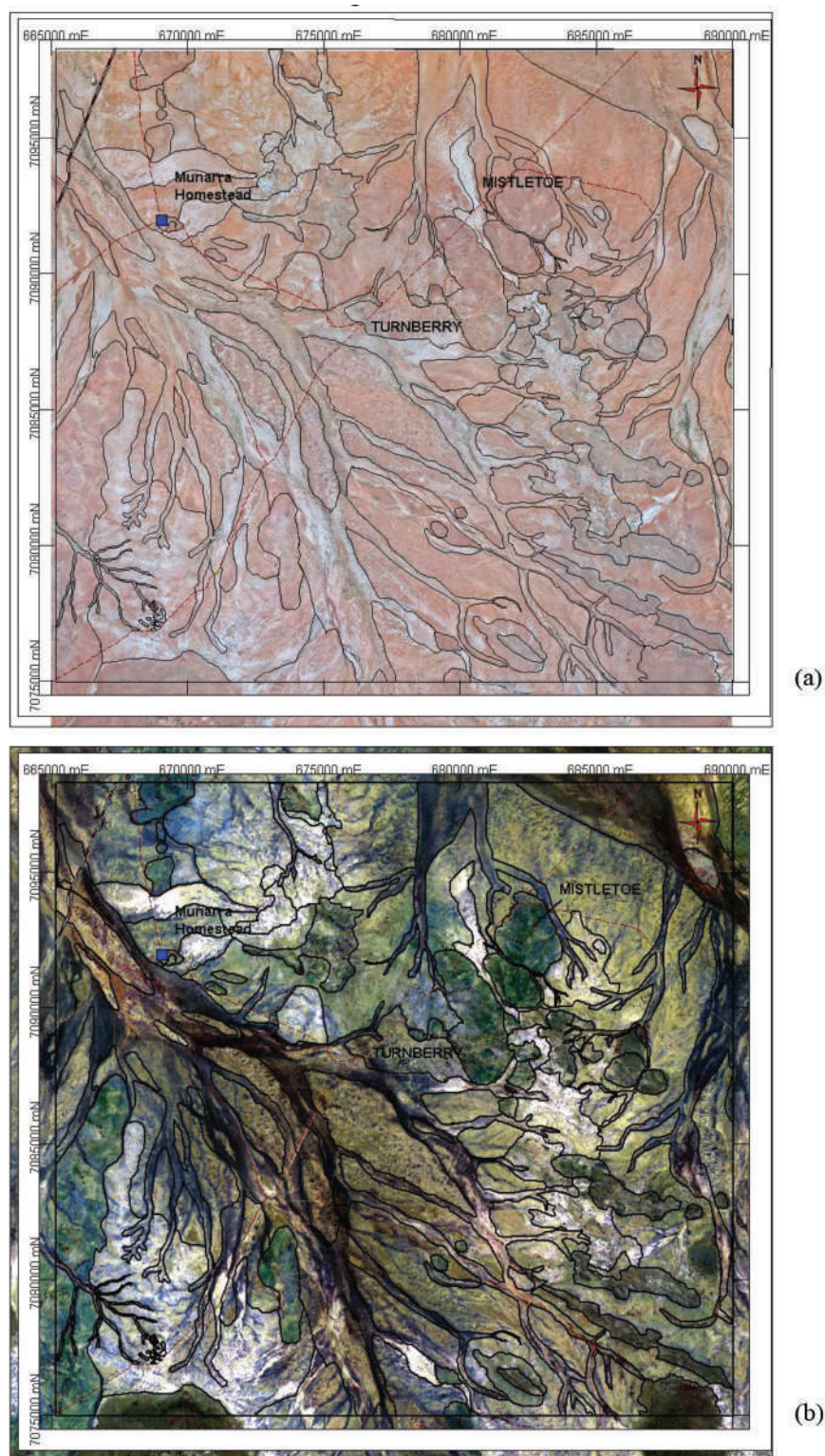
Figure 5: A completed digitization on the screen of the preliminary map overlying (a) aerial photography and (b) ASTER regolith-landform map of the Gnaweeda Greenstone Belt, Western Australia.
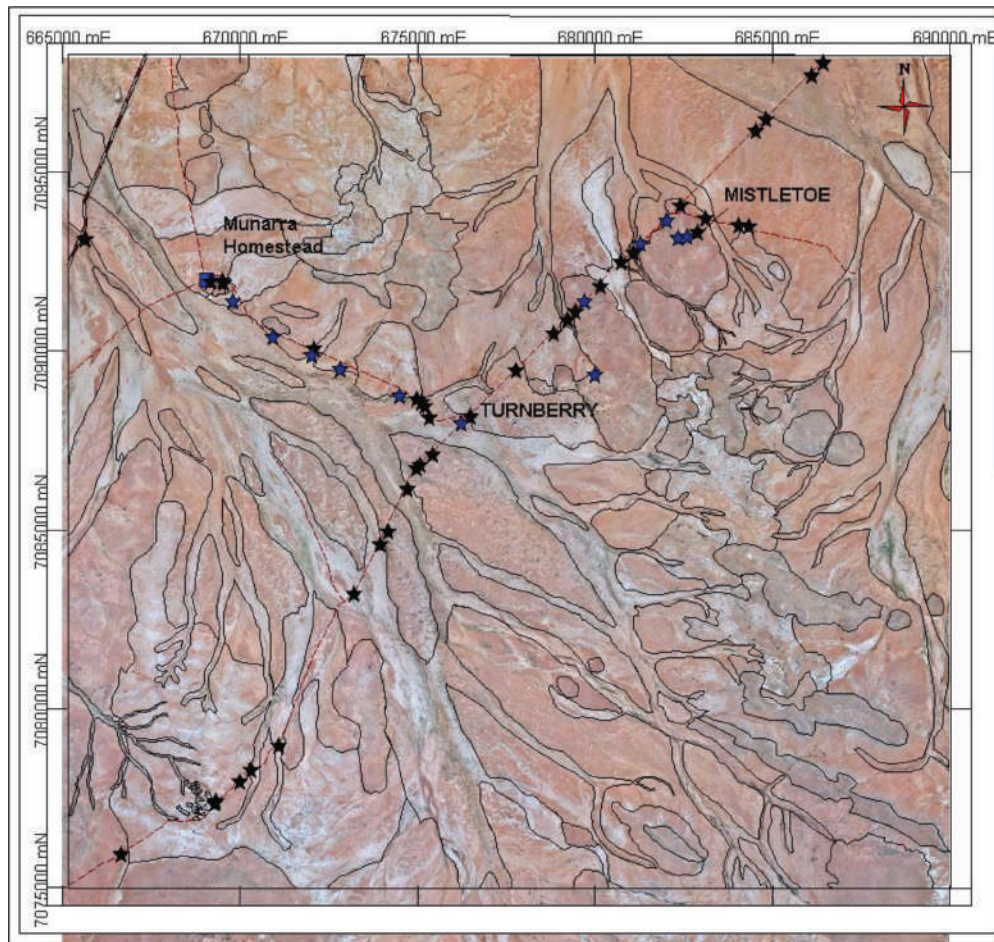
Figure 6: Regolith-landform units field verification points of the Gnaweeda Greenstone Belt, Meekatharra, Western Australia. Star symbols represent field verification point.

Colluvial sheetwash erosional plains (CHep) mainly occupy the Mistletoe study area and at the south east corner of the map. The main components of this unit are ferruginous, quartz and saprolitic lag of various sizes, with some exposure of ferruginous saprolite. *Acacia aneura* is dominant; *Eremophila fraseri* and *Eremophila forrestii* are also common (Fig. 11).

Alluvial sediments fill the channel landscape sequences from northwest to southeast both in the northern and the central part of the map. The materials consist of sand to silt with quartz gravel (Fig. 12a) in drainage channels (Fig. 12b). In the over bank flood plain, the main components are reddish-brown mud to sand. The vegetation is denser, larger, and taller in the channels. The height of *Acacia aneura* (dominant species) in this area can be high up to 10 m or more. *Eremophila fraseri* is common in this

regolith-landform unit. *Eremophila forrestii* generally occurs as an understorey to the high *Acacia aneura* tree (Fig. 12c). Calcrete on alluvial plain (ECap) occurs at the northeastern part of the map.

Insitu regolith mostly occupies the high relief of the landscape. It is characterized by bedrock exposure and residual landforms. Residual erosional plains (Rep) occupy northwestern and eastern part of the map and are characterized by angular quartz lag (1-20 cm) in reddish brown silt sand. It may be derived from granite bedrock (from interpreted geology). Vegetation is sparse and dominated by *Acacia aneura* with a few *Acacia pruinocarpa* (gidgee). Residual sandplain (Rps) includes ferruginous quartzrich sands and silt. It may be derived from sedimentary rock.
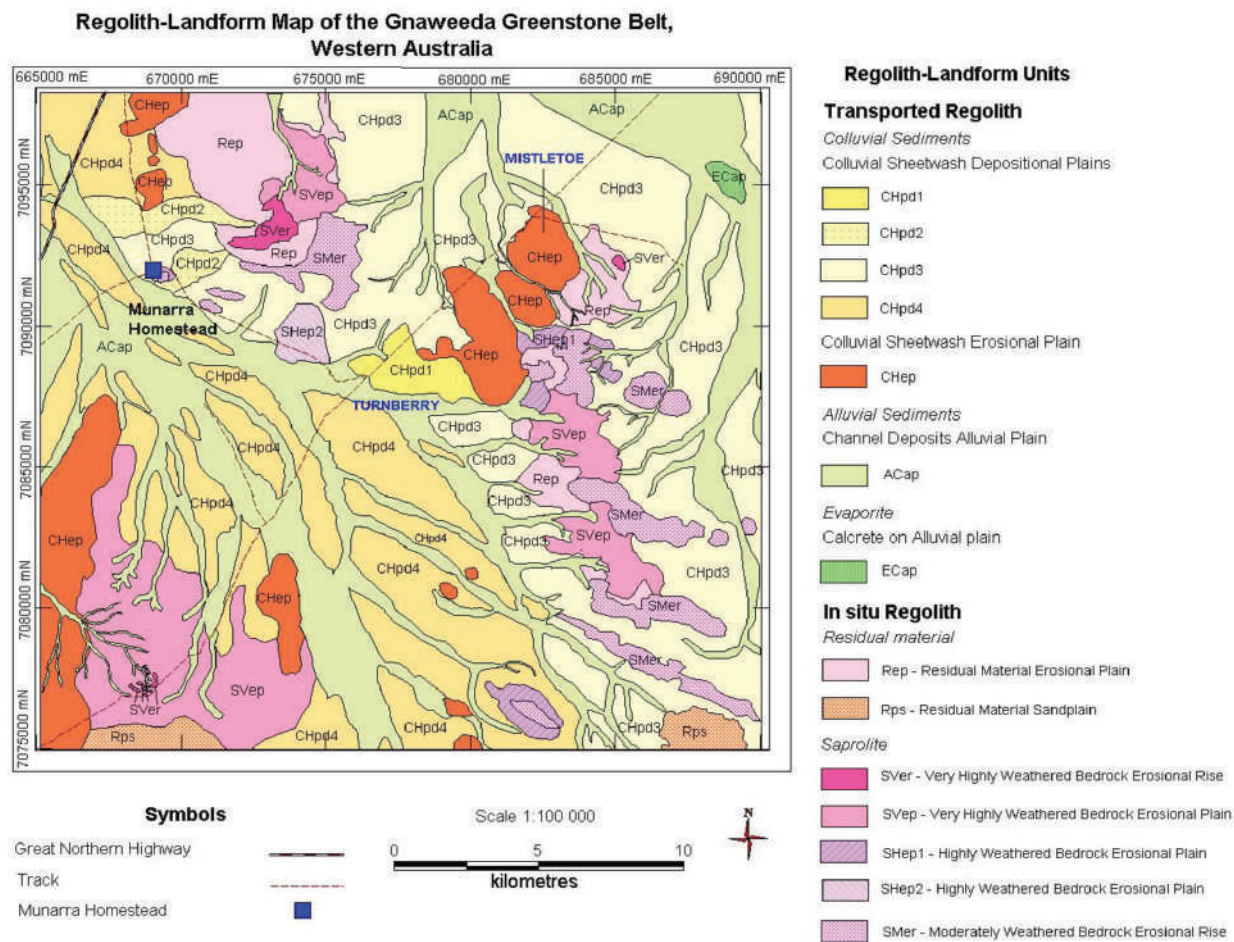
Figure 7: Regolith-landform map of the Gnaweeda Greenstone Belt, Western Australia (UTM GDA94, MGA Zone 50).

Figure 8: Regolith materials and landform for the CHpd1 regolith-landform unit; (a) sand, angular quartz gravel and angular-subangular ferruginous lag (b) a depositional plain (CHpd1) dominated by *Acacia aneura, Eremophila fraseri* and *Eremophila forrestii,* Meekatharra, Western Australia.

Figure 9: View of landscape for the CHpd3 regolith-landform unit. Vegetation is dominated by small size of *Acacia aneura* (2-5 m high), *Eremophila fraseri* and *Eremophila forrestii,* Meekatharra, Western Australia.

(a)   (b)

Figure 10: Surface materials (a) for the CHpd4 regolith-landform unit; ferruginous sand, mud and quartz gravel. (b) Landform setting of the unit, Meekatharra, Western Australia.

(a)   (b)

Figure 11: Surface material for the CHep regolith-landform unit; (a) angular to subrounded ferruginous lag with angular to subangular quartz lag. (b) Landscape view of the unit, Meekatharra, Western Australia.
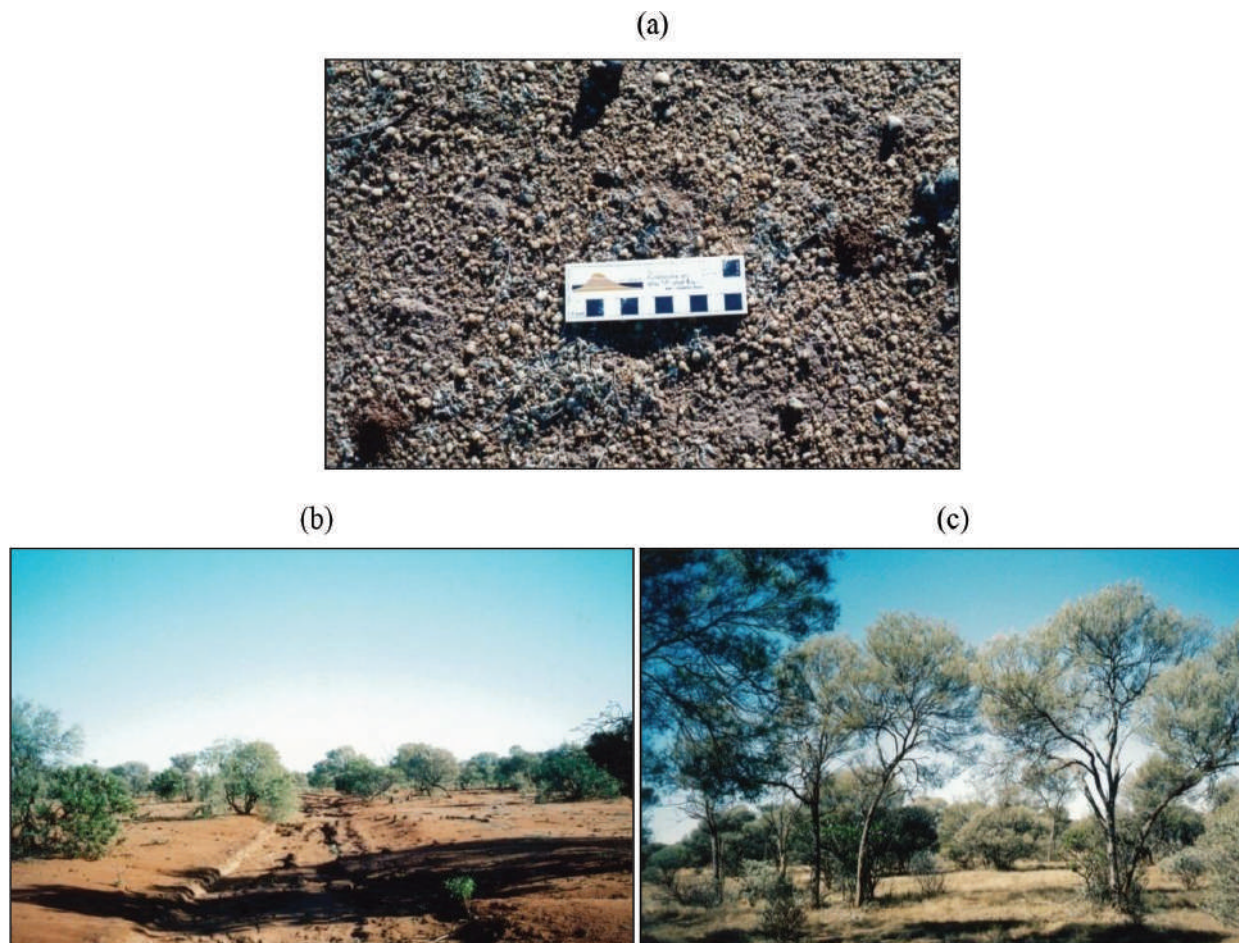
Figure 12: Regolith materials and landscape view for the ACap regolith -landform unit; (a) sand, silt and quartz gravel; (b) channel deposit and (c) high *Acacia aneura* tree with a common of understorey bush, *Eremophila forrestii,* and *Eremophila fraseri, Meekatharra,* Western Australia.

Very highly weathered bedrock erosional rises (SVer) occurred a few spots in the area especially at the southwestern part of the map. This regolith-landform unit is derived from granite rocks with sparse to medium vegetation of *Acacia aneura* and *Eremophila fraseri* (Fig. 13).

Figure 13: Landscape view of a SVer regolith-landform unit; (a) very highly weathered bedrock erosional rises and (b) view on the top of the rises, Meekatharra, Western Australia.

Very highly weathered bedrock erosional plain (SVep) is next to SVer unit and it is also derived from granite rocks. This unit consists of mix of angular quartz (0.5-12 cm) and fragments of granite saprolite (1-20 cm) in brown silt sand soil. Vegetation is sparse and is dominated by *Acacia aneura* (Fig. 14).

(a)

(b)

Figure 14: Surface material for the SVep unit; (a) mix of angular quartz and fragments of granite saprolite. The landform setting is erosional plain (b) with sparse vegetation dominated by *Acacia aneura,* Meekatharra, Western Australia.

Highly weathered bedrocks on erosional plains have been subdivided into two units. Unit SHep1 contains lithic fragments of silicified bedrock with sparse vegetation of *Acacia aneura* and *Eremophila fraseri* (Fig. 15) and another is characterized by subangular quartz gravel (1-7cm) and saprolite on ferruginous sand (SHep2).

Figure 15: View of the landscape for the SHep1 regolith-landform unit. Surface materials include lithic fragments of silicified rock in ferruginous soil. Vegetation is sparse with *Acacia aneura* and *Eremophila fraseri,* Meekatharra, Western Australia.

Moderately weathered silicified bedrock erosional rises (SMer) are distributed at the northwestern and eastern part of the portion of the map. Sparse vegetation is dominated by *Acacia aneura* and spinifex (Fig. 16).

Figure 16: Weathered silicified bedrock (a) with the (b) landform setting (erosional rises) of the unit SMer. *Acacia aneura* and spinifex is common in this unit, Meekatharra, Western Australia.

Conclusions

A regolith-landform map was compiled using ASTER image and aerial photographs with limited field verification points and existing geological information. The regolithlandform map of the Gnaweeda Greenstone Belt provides an overview of regolithlandform features and regolith materials in this area. The similar features in ASTER data and aerial photography of checked units can help to interpolate to regolith-landform units in inaccessible areas. The regolith-landform map shows a relationship with the interpreted geology (Fig. 2). It delineates the weathering products of the two granitoid belts that bound the Gnaweeda Greenstone Belt.

Acknowledgements

References

Bunting, J.A., & McIntyre, J.R. (2003). *Gnaweeda Project, Annual Technical Report on Exploration License 51/926 and 51/927 for the period 31.07.02 to 30.07.03. WAMEX Report A67376.* WA: Department of Mines and Petroleum.

Butt, C.R.M., Lintern, M.J., & Anand, R.R. (1997). Evolution of Regoliths and Landscape in Deeply Weathered Terrain – Implications for Geochemical Exploration. In: A.G. Gubin (Editor), *Proceedings of Exploration 97: Fourth Decennial International Conference on Mineral Exploration* (p. 323-334).

Butt, C.R.M., & Zeegers, H. (1992). Regolith Exploration Geochemistry in Tropical and Subtropical Terrains. *Handbook of Exploration Geochemistry; 4* (pp. 607). Amsterdam: Elsevier.

Craig, M.A. (2001). Regolith mapping for geochemical exploration in the Yilgarn Craton, Western Australia. *Geochemistry Exploration Environment Analysis, 1,* 383-390.

Crawford, R.A., Faulkner, J.A., Sanders, A.J., Lewis, J.D., & Gozzard, J.R. (1996a). *Geochemical mapping of the Glengarry 1:250,000 sheet* (pp. 57). Western Australia: Geological Survey of Western Australia.

Crawford, R.A., Gozzard, J.R., & Sanders, A.J. (1996b). *Glengarry, W.A. Sheet SG 50-12: 1:250,000 Regolith Material Series.* Westerm Australia: Geological Survey.

Eggleton, R.A., (Editor). (2001). *The Regolith Glossary: Surficial Geology, Soils and Landscape* (pp. 144). Canberra and Perth: CRC LEME.

Hill, S.M. (2002). Broken Hill 1:100,000 regolith-landform map: development, features and applications. In: I.C. Roach (Editor), *Regolith and Landscapes in Eastern Australia* (pp. 58-62). CRC LEME.

McIntyre, J.R. (2005). *Gnaweeda Project Information Memorandum.* Unpublished Bullion Minerals Ltd memorandum.

Pain, C. (2008). Regolith description and mapping. In: K.M. Scott and C.F. Pain (Editors), *Regolith Science* (pp. 281-305). CSIRO Publishing.

Pirajno, F., Adamides, N.G., & Ferdinando, D.D. (Cartographer). (1998). Geology of Glengary [map]. 1:100,000. *Western Australia Geological Survey, 1: 100,000 Geological Series Explanatory Notes* (pp. 16)

Ray, G.E., & Reardon, N. (2010). The Gnaweeda Greenstone Gold Property, Murchison Province, Western Australia. *A National Instrument Report 43-101 Technical Report for: Kent Exploration Inc., Archaean Star Resources Inc. and Archaean Star Resources Australia Pty Ltd* (pp.58).

Robertson, I.D.M., & Butt, C.R.M. (1997). Atlas of Weathered Rocks. *Open File Report1* (pp. 35). Perth: CRC LEME.

INSTRUCTIONS TO AUTHORS FOR TGJ

1. Submission of manuscripts.

The Thai Geoscience Journal (TGJ) is an international (Thai and English) journal publishing original research articles dealing with the geological sciences.

Two types of articles are published in the Journal: Research Articles and Reviews. Research Articles are new original articles. Review Articles are those papers that summarize the current state of knowledge on specific fields or topics of geosciences. They analyze and discuss previously published research results, rather than report new results. Copyright of all the contents of Thai Geoscience Journal belong to the Department of Mineral Resources in Thailand.

The manuscript should be sent to the Editor in Chief via tgj.2020@gmail.com.

2. Requirements for electronic file for submission.

1) The manuscript should be prepared in word and pdf files (download from https:// tgjdmr2019. wixsite.com/mysite)

2) Table file (word and pdf) must have a heading.

3) Figure file (JPEG, PNG, TIFF, EPS, PSD or AI); Resolution of all figures must be 300 – 600 dpi. The name of the figure file should be related in the manuscript.

3. Manuscripts Information.

The main document, containing cover sheet, main text, acknowledgement (if applicable), references, figure, table, figure and table captions.

Cover sheet: Cover sheet should contain 1) title, 2) full names and affiliations and the addresses of all authors and 3) postal and e-mail addresses and phone and fax numbers of the Corresponding Author who will take responsibility for the proofs.

Title: A title is to be brief and summarizes the major results of the paper.

Abstract: An abstract should be condensation and concentration of the essential qualities of the paper. All papers, excluding Short Notes, are to be accompanied by an abstract not exceeding 500 words.

Key words: Select keywords (not more than six words or phrases) which identify the most important subjects covered by the paper and arrange them in alphabetical order.

Main text : The main text should contain Introduction, Methods, Results, Discussions, and Conclusions, or something else as appropriate.

Acknowledgements: Brief acknowledgement of funding sources and assistance provided.

References: The references should be in a common citation format as shown below.

Figures and tables: Each figure and table must be mentioned sequentially in the text of the paper. Each figure must have a caption, and each table must have a heading. Captions and headings should be explicit enough that the reader can understand the significance of the illustration or table without reference to the text.

References Format Suggestion
In Text Citation

The APA 6th style requires the references in content, tables and images must specify author-date in-text citation, with the researcher's surname followed by a comma (,) and the year of publication of the document behind the quote. If there are 2-5 authors, cite all names and use & before the last name for the first time, thereafter only the first name followed by et al. but if there are 6 or more authors, cite only the surname of the first author followed by et al. and the year. For examples as followings: (Mogen, 2001), (Jones & Miler, 2008), (Mogen, Jones & Miler, 2008), (Halano et al., 2009)

In Reference Page: Citation Guide in APA 6th Style

List authors in the reference as:
- **For 1 author:** Author, A. A.
- **For 2 authors:** Author, A. A., & Author B. B.
- **For 3-7 authors:** Author, A. A., Author, B. B., Author, C. C., Author, D. D., Author, E. E., Author, F. F., & Author, G. G.
- **For 8 or more authors** (list first six authors, add a three dot, then last author): Author, A. A., Author, B. B., Author, C. C., Author, D. D., Author, E. E., Author, F. F., ... Author, Z. Z.

1. Book

Author, A. A. (Year). *Title of book*. City, Country: Publisher's Name.

Example:

Luffman, J. M., Bulleen, C. V., Liano, A. D., McLeed, P. K., Nash, E. O., & Neuman, C. C. (2004). *Information technology resources management* (2nd ed.). Upper Saddle River, NJ: John & Sons Press.

2. Book Chapter

Author, A. A. (Year). Title of chapter. In A. Editor, & B. Editor (Eds.), *Title of book* (pp. xxx-xxx). Location: Publisher.

Example:

Ogg, J. G., Ogg, G. M., & Gradstein, F. M. (2016). 5 - Cambrian. In J. G. Ogg, G. M. Ogg, & F. M. Gradstein (Eds.), *A Concise Geologic Time Scale* (pp. 41-55). UK: Elsevier.

3. Journal Article

Author1, A. A., & Author2, B. B. (Year). Title of article. *Journal name, volume number* (issue number), pages-pages. doi:xx. xxxxxxxxxx

Example:

Jackson, J. J., & Samuel, T. S. (2001). The impact of climate change on sea levels. *Journal of Environmental Science, 55*(4), 233-277. doi:10.1070/8567-6582.33.5.888

If you are interesting in Geoscience

Please Become

TGJ
THAI GEOSCIENCE JOURNAL

Membership

Free Register NOW!

All articles published by
the Thai Geoscience Journal
are made freely and permanently accessible online
immediately upon publication,
without subscription charges or registration barriers.

Contact

Mineral Resources Research and Development Center
Department Mineral Resources 75/10 Rama VI Road,
Ratchatewi, Bangkok 10400 Phone: +66 2-6219731
Website : https://www.dmr.go.th
E-mail : tgj.2020@gmail.com

Published by

The Reviewer Acceptance form
Thai Geoscience Journal (TGJ)

( ) Accept to be a reviewer Thai Geoscience Journal
( ) Except to be a reviewer Thai Geoscience Journal

Official title ....

Name-Surname ....

Current address ....

Position..Department...

Phone number..E-mail...

Educational background at the degree level

Qualification (Specify the name of the degree and the program of study)	Graduation year	Graduate school / country

Expertise ....

Special interest ....
....

Experience and work history (brief) ....
....
....

The Acceptance form online

Sign ....

(...)

.... / .... / ....

Please reply the acceptance form to Department of Mineral Resources Mineral Resources
E-mail: tgj.2020@gmail.com or **Fax** 0-2621-3731, 0-2621-9554

THAI
GEOSCIENCE
JOURNAL

CONCEPT DESIGN

This logo composes of Abbreviations of Thai Geoscience Journal

T = THAI   G = GEOSCIENCE   J = JOURNAL

Coexistence of 3 abbreviations design in a concept of modernity blend with a Thainess.
Modification of G alphabet in a shape of ammonoid shows relevance to geology
and infinite development of Thai Geoscience Journal.

- **SCOPE AND AIM OF THAI GEOSCIENCE JOURNAL (TGJ):** TGJ is an international (Thai and English) journal publishing original research articles dealing with the geological sciences. It focuses, mainly but not exclusively, on: Sedimentology and Geomorphology, Palaeontology, Quaternary Geology and Environmental Change, Geological Hazards, Environmental Geosciences, Geophysics, Mineral and Petroleum Geology, Tectonics and Structural Geology, Geochemistry and Geochronology, Metamorphic Geology and Volcanic and Igneous Geology. Two types of articles are published in the Journal: Research Articles and Reviews. Research Articles are new original articles, normally not exceeding 25 pages. Review Articles are those papers that summarize the current state of knowledge on specific fields or topics of geosciences. They analyze and discuss previously published research results, rather than report new results. TGJ Aim is to provide valuable geoscience knowledge and information and push more inspiration for readers and researchers to produce treasure research in the future.

- **FEEDBACK AND CONTACT:** We welcome your feedback, comments and suggestions for the development of TGJ.

  Please contact: Dr. Apsorn Sardsud (Editor-in-Cheif, TGJ)
  Department of Mineral Resources of Thailand
  75/10 RamaVI Road Ratchathewee Bangkok 10400

  Phone: +66 (0)2 6219731

  Email: tgj.2020@gmail.com or Fax 0-2621-3731, 0-2621-9554

  website: http://www.dmr.go.th

TGJ Reviewers

CONTENTS